RegMedNet

Powered by fsg

Diabetes

TOP ARTICLES SUPPLEMENT

CONTENTS

Research Article

For reprint orders, please contact: reprints@futuremedicine.com

Regenerative Medicine

Delivery of mesenchymal stem cells in biomimetic engineered scaffolds promotes healing of diabetic ulcers

Aim: We hypothesized that delivery of mesenchymal stem cells (MSCs) in a biomimetic collagen scaffold improves wound healing in a diabetic mouse model. **Materials & methods**: Rolled collagen scaffolds containing MSCs were implanted or applied topically to diabetic C57BL/6 mice with excisional wounds. **Results**: Rolled scaffolds were hypoxic, inducing MSC synthesis and secretion of VEGF. Diabetic mice with wounds treated with rolled scaffolds containing MSCs showed increased healing compared with controls. Histologic examination showed increased cellular proliferation, increased VEGF expression and capillary density, and increased numbers of macrophages, fibroblasts and smooth muscle cells. Addition of laminin to the collagen scaffold enhanced these effects. **Conclusion**: Activated MSCs delivered in a biomimetic-collagen scaffold enhanced wound healing in a translationally relevant diabetic mouse model.

First draft submitted: 19 November 2015; Accepted for publication: 11 February 2016; Published online: 17 March 2016

Keywords: angiogenesis • collagen I • diabetic ulcer • extracellular matrix proteins • laminin • mesenchymal stem cells • tissue engineering • tissue scaffolds • VEGF

Roland Assi[‡,1], Trenton R Foster[‡,1], Hao He[‡,1,2], Katerina Stamati[3], Hualong Bai[1], Yuegao Huang[4], Fahmeed Hyder[4], Douglas Rothman[4], Chang Shu[2], Shervanthi Homer-Vanniasinkam[3], Umber Cheema*[,§,3] & Alan Dardik**[,§,1,5]

[1]Vascular Biology & Therapeutics Program & the Department of Surgery, Yale University School of Medicine, New Haven, CT, USA

[2]Department of Vascular Surgery, The Second Xiangya Hospital of Central South University, Changsha, China

[3]UCL Institute of Orthopaedics & Musculoskeletal Sciences, UCL Division of Surgery & Interventional Sciences, University College London, London, UK

[4]Departments of Diagnostic Radiology & Biomedical Engineering, Yale University, New Haven, CT, USA

[5]Department of Surgery, VA Connecticut Healthcare Systems, West Haven, CT, USA

*Author for correspondence: u.cheema@ucl.ac.uk

**Author for correspondence: Tel.: +1 203 785 7991 alan.dardik@yale.edu

[‡]Co-first authors

[§]Co-senior authors

One of the most important complications of diabetes is the development of lower extremity ulcers. Approximately 2–3% of diabetics develop foot ulcers each year, affecting approximately 15–25% of diabetics during their lifetime [1–5]. The etiology of delayed and poor wound healing in diabetic ulcers is complex and includes poor vascular perfusion, neurological injury and trauma, as well as limited cellular angiogenic potential, a diminished population of mesenchymal stem cells (MSCs) and reduction in the deposition of appropriate extracellular matrix [2,3].

Wound healing requires multiple cell processes, including proliferation, migration, differentiation, matrix deposition and remodeling, angiogenesis, resulting in eventual re-epithelialization of the wound [6]. Current tissue engineering approaches to advanced wound care therapy have been to enhance these processes via delivery of either matrix-based or cell-based scaffolds. Matrix-based scaffolds include Alloderm®, dCell®, Integra® and GraftJacket® that use matrix without cells; cell-based scaffolds include Dermagraft® and MySkin® that do not have significant matrix, and Apligraft® and Epifix that have both cells and matrix [7–9]. Although these products promote wound healing, no treatment paradigm has shown superior long-term efficacy [8].

MSCs are a promising source of cells for multiple regenerative processes, including patches used for myocardial infarction and skin regeneration [10–14]. MSCs give rise to mesodermal lineages including muscle, fat and pericytes and can transdifferentiate into epidermal cells [15,16]; MSCs also enhance angiogenesis via multiple cytokines that ameliorate ischemic environments, including VEGF, MCP-1 and MIP-1α [17,18]. Culturing MSCs in hypoxic conditions enhances their angio-

Future Medicine part of fsg

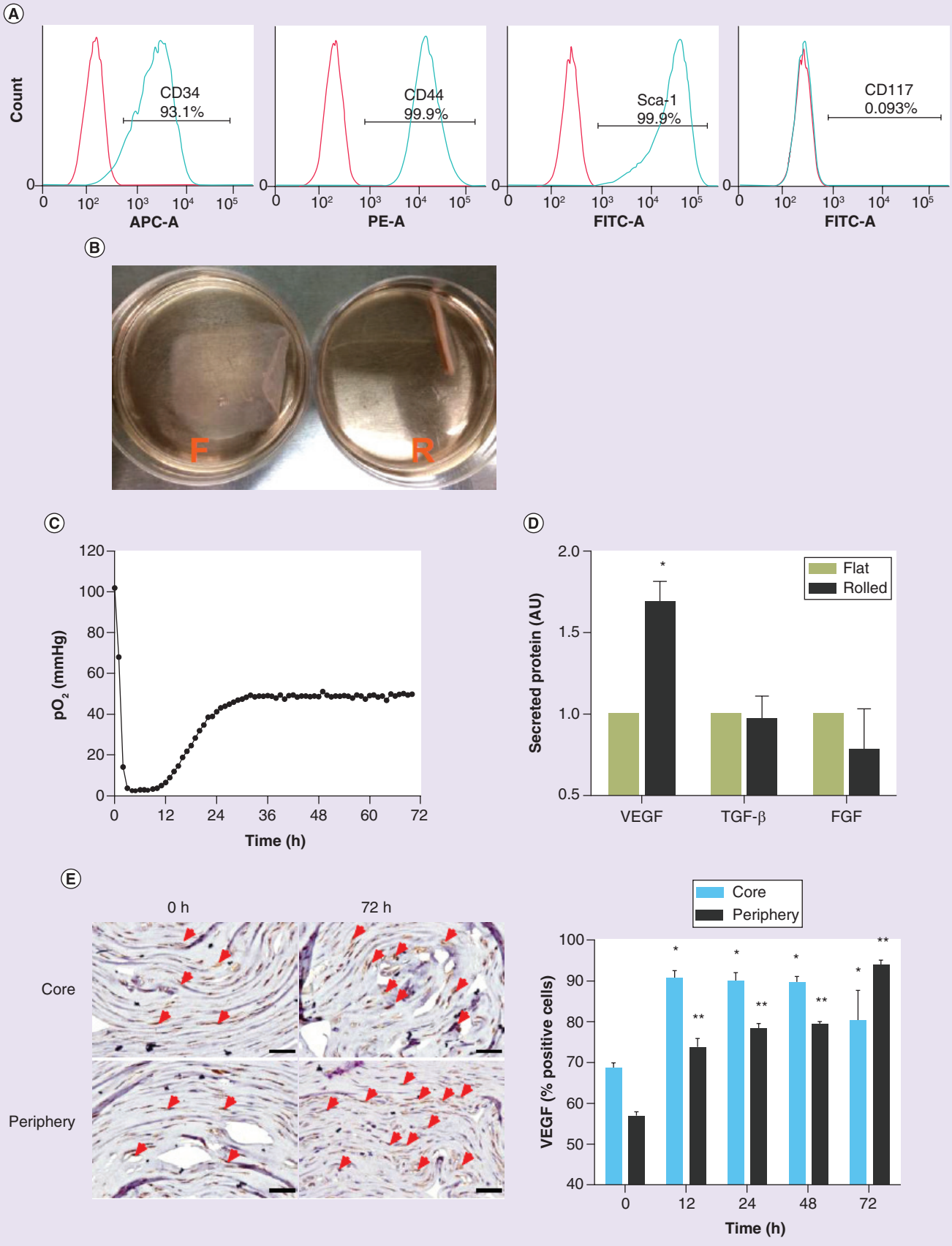
A
Count
CD34
93.1%
CD44
99.9%
Sca-1
99.9%
CD117
0.093%
APC-A
PE-A
FITC-A
FITC-A
B
F
R
C
pO2 (mmHg)
Time (h)
D
Secreted protein (AU)
Flat
Rolled
VEGF
TGF-β
FGF
E
0 h
72 h
Core
Periphery
Core
Periphery
VEGF (% positive cells)
Time (h)

Figure 1. *In vitro* validation of rolled collagen scaffold model (see facing page). (A) FACS analysis confirms identity of murine mesenchymal stem cells with positive expression of CD34, CD44, Sca-1 and lack of expression of CD117. **(B)** The collagen scaffold is created by compressing the collagen into a flat configuration ('F') and then rolling it into a rolled configuration ('R'). **(C)** Graph shows serial measurements of oxygen tension at the core of a rolled collagen scaffold. **(D)** Bar graph shows relative values of growth factor release into the medium after 72-h incubation from a flat or rolled collagen scaffold. VEGF: *p = 0.0006 (*t*-test); n = 8–9. TGF-β: p = 0.9; n = 3. FGF: p = 0.5; n = 3. **(E)** Left panel shows representative immunohistochemical analysis for VEGF in the core (top row) and periphery (bottom row) of the rolled collagen scaffold at 0 h (left column) and 72 h (right column); arrowheads show positive cells. Scale bar, 50 μm. Right panel shows change in percentage of VEGF-positive cells over time; p < 0.0001, ANOVA; *, core is significant at all time points versus time 0 (*post hoc*); **, periphery is significant at all time points versus time 0 (*post hoc*).

genic potential [19], which is not surprising since MSCs reside in the bone marrow niche *in vivo* that has lower oxygen tension compared with typical atmospheric conditions that are used for tissue culture [20].

The extracellular matrix plays a significant role in controlling cell behavior, and the stem cell niche directly and indirectly modulates stem cell functions including self-renewal and differentiation [21]. The bone marrow MSC niche is made up of multiple matrix proteins, including collagen I, collagen IV, laminin and fibronectin. By culturing cells within a 3D scaffold, we can impart some physiological cues that cells would normally be exposed to in tissues. The 3D geometry of a biomimetic scaffold is an important factor that enhances its regenerative capacity, suggesting the importance of mimicking the physical geometry of the native cellular niche [22–24].

We hypothesized that use of a biomimetic scaffold to deliver MSCs will enhance their therapeutic potential. We previously showed that plastic compression of a collagen scaffold to a density approaching that of tissue also creates a hypoxic central core that would be of particular use as a biomimetic scaffold for MSCs [24–26]. We used these compressed collagen scaffolds to deliver MSCs into a mouse model of diabetic wounds to determine their therapeutic potential in this translationally relevant model.

Materials & methods

Cells

Murine bone marrow-derived MSCs were obtained from Cyagen (CA, USA). MSCs were cultured in EGM-2 media (Lonza, Basel, Switzerland). MSC identity was confirmed with FACS analysis of passage 2 MSC using anti-CD34 (BioLegend, CA, USA), anti-CD44 (BD Pharmingen, CA, USA), anti-Sca-1 (BioLegend), and anti-CD117 (BioLegend) using an LSRII flow cytometer (BD Biosciences, CA, USA). Cell passages 2–6 were used for this study.

Collagen scaffolds

Collagen scaffolds were created by adding type 1 rat tail collagen (3 ml of 5% solution; Enzo Life Sciences, NY, USA), phosphate-buffered saline (PBS; 1 ml) and 10× DMEM (0.5 ml; Sigma-Aldrich, MO, USA) and then pH adjusted to 7.0 using dropwise addition of 1 M NaOH according to the supplier directions. For cellular constructs, 2×10^6 MSCs in 0.5 ml solution were added to the collagen gel; for acellular constructs, an equal volume PBS was added (final volume 5 ml). MSC number was determined from previous work showing high cell viability at this seeding density, and the subsequent hypoxia gradient formed by cell consumption of oxygen resulted in an upregulation of the angiogenic growth factor cascade [27]. For laminin containing scaffolds, 25 μg laminin (Corning, MA, USA) was added. The collagen solution was allowed to solidify within a rectangular mold (room temperature, 30 min) and then removed from the mold and compressed between glass plates (5 min). The compressed collagen sheet was then rolled tightly and placed in media (37°C, 72 h).

Core oxygen tension

Fiberoptic fluorescent probes (Oxford Optronix Ltd, Oxford, UK) were used to measure oxygen tension in 3D rolled scaffolds in real time [25]. A probe was embedded into the core of a rolled collagen scaffold, with care taken to achieve 360 transillumination. The scaffold was then placed into sterile media (originally 160 mmHg), and covered with parafilm. Oxygen tension was measured at single-minute intervals.

Growth factor release

Collagen scaffolds were incubated at 37°C for 72 h and then the medium was collected and growth factor concentrations were determined using mouse Quantikine ELISA kits for VEGF, FGF or TGF-β according to the manufacturer's instructions (R&D Systems, MN, USA).

Immunohistochemistry

Sections were heated in citric acid buffer (pH 6.0) at 100°C (10 min) for antigen retrieval. The sections were treated with hydrogen peroxide (0.3%) in methanol for 30 min at room temperature to block endogenous peroxidase activity and incubated with bovine serum albumin (5%) in PBS containing Triton X-100

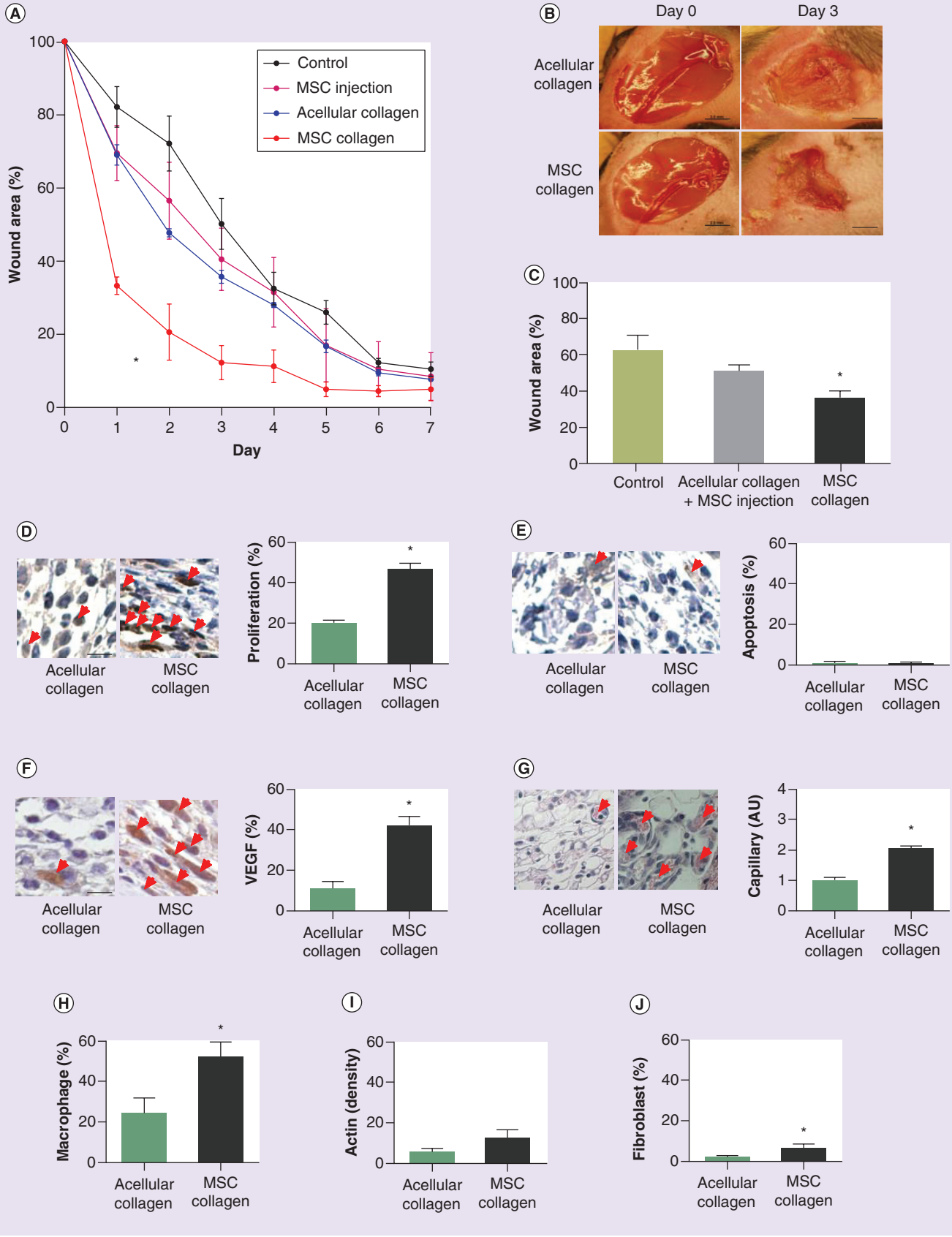
A
Wound area (%)
Day
Control
MSC injection
Acellular collagen
MSC collagen
*
B
Day 0
Day 3
Acellular collagen
MSC collagen
C
Wound area (%)
Control
Acellular collagen + MSC injection
MSC collagen
*
D
Acellular collagen
MSC collagen
Proliferation (%)
*
E
Acellular collagen
MSC collagen
Apoptosis (%)
F
Acellular collagen
MSC collagen
VEGF (%)
*
G
Acellular collagen
MSC collagen
Capillary (AU)
*
H
Macrophage (%)
*
I
Actin (density)
J
Fibroblast (%)
*

Figure 2. Delivery of mesenchymal stem cells in a rolled collagen scaffold enhances wound healing in a diabetic mouse leg wound model (see facing page). **(A)** Line graph shows wound size over time. *p < 0.0001 (two-way ANOVA). Control: n = 6; MSC injection: n = 2; acellular collagen: n = 4; MSC collagen: n = 3. **(B)** Photographs show representative images of wounds, days 0 and 3. Scale bar: 2 mm. **(C)** Bar graph shows mean wound area at day 1 in a replicate experiment with additional control group to include acellular + MSC. p = 0.0041 (ANOVA). *p = 0.0037 versus control (*post hoc*) and p = 0.0347 versus acellular + MSC injection (*post hoc*). Control: n = 4; acellular + MSC injection: n = 12; MSC: n = 6. **(D)** Representative images and bar graph showing percentage of cells positive for Ki-67 adjacent to acellular and MSC scaffolds. *p = 0.0001 (*t*-test); n = 4. **(E)** Representative images and bar graph showing percentage of cells positive for cleaved caspase-3 adjacent to acellular and MSC scaffolds. p = 0.6 (*t*-test); n = 4. **(F)** Representative images and bar graph showing VEGF-positive cells adjacent to acellular and MSC scaffolds. *p = 0.04 (*t*-test); n = 3–4. **(G)** Representative images and bar graph showing relative number of capillaries adjacent to acellular and MSC scaffolds. *p < 0.0001 (*t*-test); n = 4. **(D–G)** Scale bars: 10 μm. **(H)** Bar graph showing F4/80-positive cells adjacent to acellular and MSC scaffolds. *p = 0.04 (*t*-test); n = 3–4. **(I)** Bar graph showing smooth muscle actin-positive cells adjacent to acellular and MSC scaffolds. p = 0.2 (*t*-test); n = 3. **(J)** Bar graph showing vimentin-positive cells adjacent to acellular and MSC scaffolds. *p = 0.003 (*t*-test); n = 3. Red arrows show positive cells.
MSC: Mesenchymal stem cell.

(0.05%; T-PBS) for 1 h at room temperature to block nonspecific protein-binding sites. Sections were then incubated in T-PBS at 4°C with the primary antibodies: anti-VEGF (rabbit; 1:100; Santa Cruz Biotechnology, TX, USA), Ki67 (rabbit: 1:200; Abcam, MA, USA), anti-caspase 3 (rabbit: 1:1000; Cell signaling, MA, USA), F4/80 (rat: 1:100; Abcam), α-SMA (rabbit: 1:50; Abcam), vimentin (rabbit: 1:500; Abcam). After overnight incubation, the sections were incubated with either secondary anti-rabbit antibody Dako EnVision™ + Dual Link System-HRP (Dako, CA, USA) or secondary anti-rat antibody (Dako) for 1 h at room temperature and treated with Dako Liquid DAB+ Substrate Chromogen System (Dako) to visualize the reaction products. Finally, the sections were counterstained with Dako Mayer's Hematoxylin (Lillie's Modification) Histological Staining Reagent (Dako). Photomicrographs were then obtained of the slides and positive staining cells were manually counted and reported as a percentage of positive cells.

Diabetic hind limb wound model

All animal studies were performed in strict compliance with Federal guidelines and approved by Yale University's Institutional Animal Care and Use Committee. Male C57BL/6 mice (8–12 weeks; 20–30 g; Jackson Laboratory, ME, USA) were used for induction of diabetes with streptozotocin [28]. In brief, mice were injected daily for 7 days with streptozotocin (50 mg/kg IP; Tocris Biosciences, Bristol, UK). After at least 1 week, hyperglycemia was confirmed with a glucometer; only mice with blood glucose greater than 300 mg/dl were used.

Mice were anesthetized with ketamine (100 mg/kg) and xylazine (10 mg/kg). One of the lower extremities was removed of hair using a chemical depilatory (Nair, NJ, USA). A full-thickness skin wound (6 mm diameter) was then made over the anterior thigh of the lower extremity. A subcutaneous pocket was created with blunt dissection immediately adjacent to and proximal to the wound, and a collagen scaffold (3 mm length, containing 2×10^5 cells) was inserted into the subcutaneous pocket. Control mice received either no collagen scaffold, an acellular collagen scaffold, and/or an injection of a matched number of MSCs (2×10^5) without a scaffold. For mice treated with an MSC injection, the injection was made through the wound into the subcutaneous space; a subcutaneous pocket was not dissected to prevent creating additional surgical trauma as well as avoiding leakage of MSCs out of the injection site. Photographs of the wounds were taken daily using a dissecting microscope and the wound area analyzed (Image J software, NIH). At the completion of study, mice were euthanized and the wounds and surrounding tissues were harvested and processed. Paraffin embedded sections were prepared and stained using immunohistochemistry for markers of proliferation, apoptosis, VEGF, actin and markers of macrophages and fibroblasts. The percentage of positive cells was determined using manual counting in four high power fields. Capillaries were identified on H&E stained slides by their typical tubular morphology and the presence of intraluminal red blood cells; quantification was performed by averaging the capillary density in four manually counted high power fields.

MSC labeling & detection *in vivo*

MSCs were labeled with Molday ION Rhodamine B (12.5 ng/ml; Biopal, MA, USA) for 18 h prior to incorporation into the collagen scaffold. Immediately after collagen incorporation, the mice (n = 3 for non-labeled control and labeled groups, respectively) were artificially ventilated (70% N_2O and 30% O_2) and kept under 2% isoflurane anesthesia. The mice were then positioned in a custom-built MRI compatible holder. The spin-echo MR datasets were obtained using 11.7 T horizontal-bore spectrometer (Agilent,

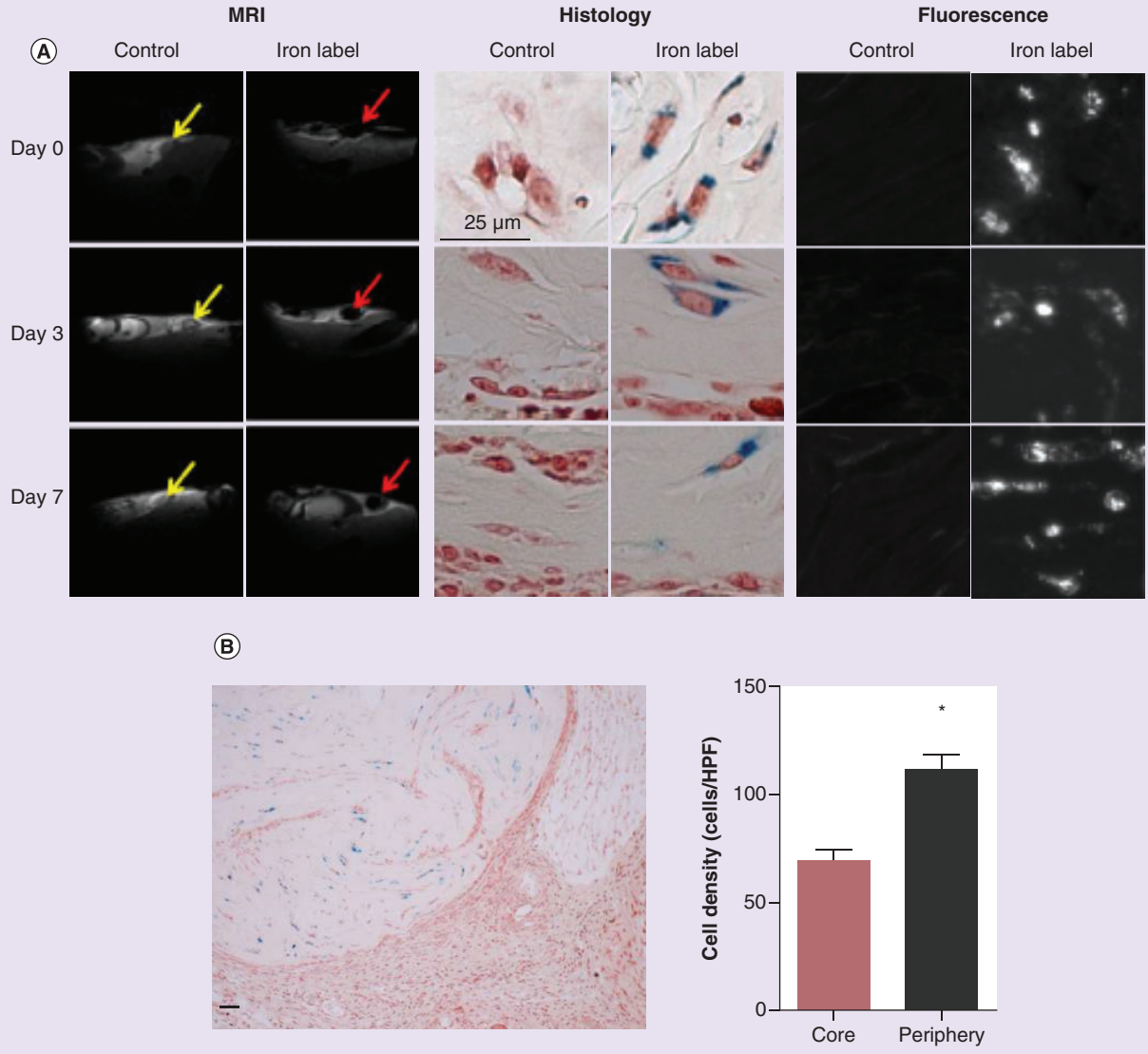

Figure 3. Retention of mesenchymal stem cells within the collagen scaffold *in vivo*. (A) Representative images showing detection of nanoparticle-labeled mesenchymal stem cells *in vivo*; first two columns, MRI; middle two columns, histology; right two columns, fluorescence. Top row, day 0; middle row, day 3; bottom row, day 7. Red arrows identify signal attenuation from labeled mesenchymal stem cells, yellow arrows show corresponding region in control mice. Histology scale bar: 25 µm. **(B)** Left panel, representative image showing presence of labeled cells in the collagen scaffold, and no labeled cells in adjacent tissue; red arrow shows unlabeled cells at periphery of the collagen scaffold. Right panel, bar graph showing cell density in the core and periphery of the collagen scaffold. *p = 0.002 (*t*-test). n = 4.
HPF: High power field.

CA, USA) with a ^{1}H RF surface coil of 1.5 cm diameter positioned on top of the wound of the thigh. Axial slices of 128 × 128 image matrix and 1-mm thickness were acquired using a field of view of 25.6 mm^2 (in plane resolution of 200 × 200 µm), a recycle time of 1500 ms and echo time of 9 ms (gradient echo). The resulting MR images were processed in Matlab (MathWorks Inc., MA, USA). Longitudinal MR scannings were performed on the same slice of the wounds for the same animal at day 0, 3 and 7 for both nonlabeled control and labeled mice. Rhodamine fluorescence was detected using fluorescence microscopy. Iron oxide was detected using Prussian blue staining.

Splinted back wound model

The splinted excisional wound model was created as previously described [29]. In brief, diabetic mice were anesthetized and removed of hair over their back using a chemical depilatory. A full-thickness skin wound (5 mm diameter) was created on the back. The colla-

gen scaffold was divided into four pieces (7.5 mm each containing 5×10^5 cells), and each piece implanted into a subcutaneous pocket adjacent to the wound in four equally spaced directions (total of 2×10^6 cells implanted per mouse). Control mice received equivalent-sized acellular collagen scaffolds. A silicone ring (6 mm inner diameter, 0.5 mm thick) was sutured into place surrounding the wound and a Tegaderm dressing (3M, St Paul, MN, USA) was placed over the splinted wound. Photographs of the wounds were taken daily using a dissecting microscope and the wound area analyzed (Image J software, NIH). At the completion of study, mice were euthanized and the wounds and surrounding tissues were harvested and processed as described above.

Topical application of collagen scaffolds

Acellular and MSC-containing collagen scaffolds were created as described. Some scaffolds were then immediately unrolled back into a flat configuration (nonhypoxic) or kept in rolled configuration (physiological hypoxia) for the 72-h incubation *in vitro* (37°C). At the end of 72 h, all scaffolds were unrolled into flat configuration. The flat scaffolds were then secured on top of splinted back wounds of diabetic mice using eight evenly spaced nylon sutures at the wound edge; no scaffolds were implanted in mice receiving topical scaffolds. Photographs of the wounds were taken daily using a dissecting microscope and the wound area analyzed (Image J software). At the completion of study, mice were euthanized and the wounds and surrounding tissues were harvested and processed as described above.

Statistical analysis

Results are presented as mean value ± SEM. A two-tailed *t*-test or analysis of variance was used for comparison between groups. Results were considered significant when $p < 0.05$. The Tukey's *post hoc* test was used for correction of results that were significant by ANOVA. GraphPad Prism 6 software (La Jolla, CA, USA) was used for statistical analysis and creation of graphs.

Results

A collagen scaffold increases VEGF secretion from MSC *in vitro*

In order to determine whether a biomimetic scaffold enables MSC survival and function *in vitro*, MSCs were embedded into rolled collagen scaffolds as previously described [30]. FACS analysis confirmed that the murine MSC expressed CD34, CD44 and Sca-1, but not CD117, prior to implantation (Figure 1A), as expected from the supplier documentation [31]. MSCs were embedded in compressed collagen gels, which were either left as flat sheets or rolled, to provide a complex 3D geometry (Figure 1B) with a central hypoxic core (Figure 1C). The hypoxia generated through cell consumption of O_2 in rolled scaffolds resulted in a higher level of VEGF secretion into the medium, but this hypoxic environment did not promote the secretion of TGF-β or FGF (Figure 1D), suggesting that the geometrically complex scaffolds provided MSCs with a microenvironment promoting secretion of the angiogenic factor VEGF. VEGF-positive MSCs were detectable at baseline; within 12 h MSCs in the core of the rolled scaffold were nearly uniformly VEGF-positive, whereas MSCs at the periphery required approximately 72 h to develop near uniform VEGF positivity (Figure 1E). These results suggest that the hypoxic core environment of the rolled scaffold stimulates MSC production of VEGF that likely stimulates the MSCs in the periphery of the scaffold to increase VEGF synthesis and secretion.

Activated MSC in collagen scaffolds increase wound healing *in vivo*

Since MSCs have increased VEGF upregulation and release in rolled scaffolds, compared with flat scaffolds, *in vitro*, we determined whether delivery of MSCs in a rolled scaffold enhances wound healing in a diabetic mouse leg wound model. Preoperative age, weight and the rate of diabetes achieved after streptozotocin therapy were similar between all groups (data not shown). The basal rate of wound healing was significantly reduced in diabetic mice compared with nondiabetic mice ($p < 0.0001$, ANOVA; $n = 4$; data not shown). In diabetic mice, rolled scaffolds without or with MSCs were implanted subcutaneously just proximal to the wound at the time of wound creation. Control diabetic mice healed the leg wounds within approximately 7 days. Wounds to which MSCs were delivered in a rolled scaffold showed significant improvement in wound healing by day 1 compared with mice receiving either collagen scaffolds without MSCs, or MSC injected directly into the wound (Figures 2A & B), suggesting that the combination of a relevant cell type delivered in a biomimetic scaffold was critical to enhance wound healing. Mice receiving rolled scaffolds with MSCs not only healed more quickly compared with mice receiving both acellular collagen scaffolds and MSCs directly injected into the wound, but closed the wound area by a significant margin (64% closure vs 49% with MSC injection vs 37% with acellular scaffold on day 1, $p = 0.004$; Figure 2C). Examination of the tissue immediately adjacent to the collagen scaffolds showed that there was increased numbers of proliferating cells (Figure 2D) with no change in apoptotic cells (Figure 2E) in scaffolds containing MSC compared with acellular scaffolds. Since MSC-containing scaffolds

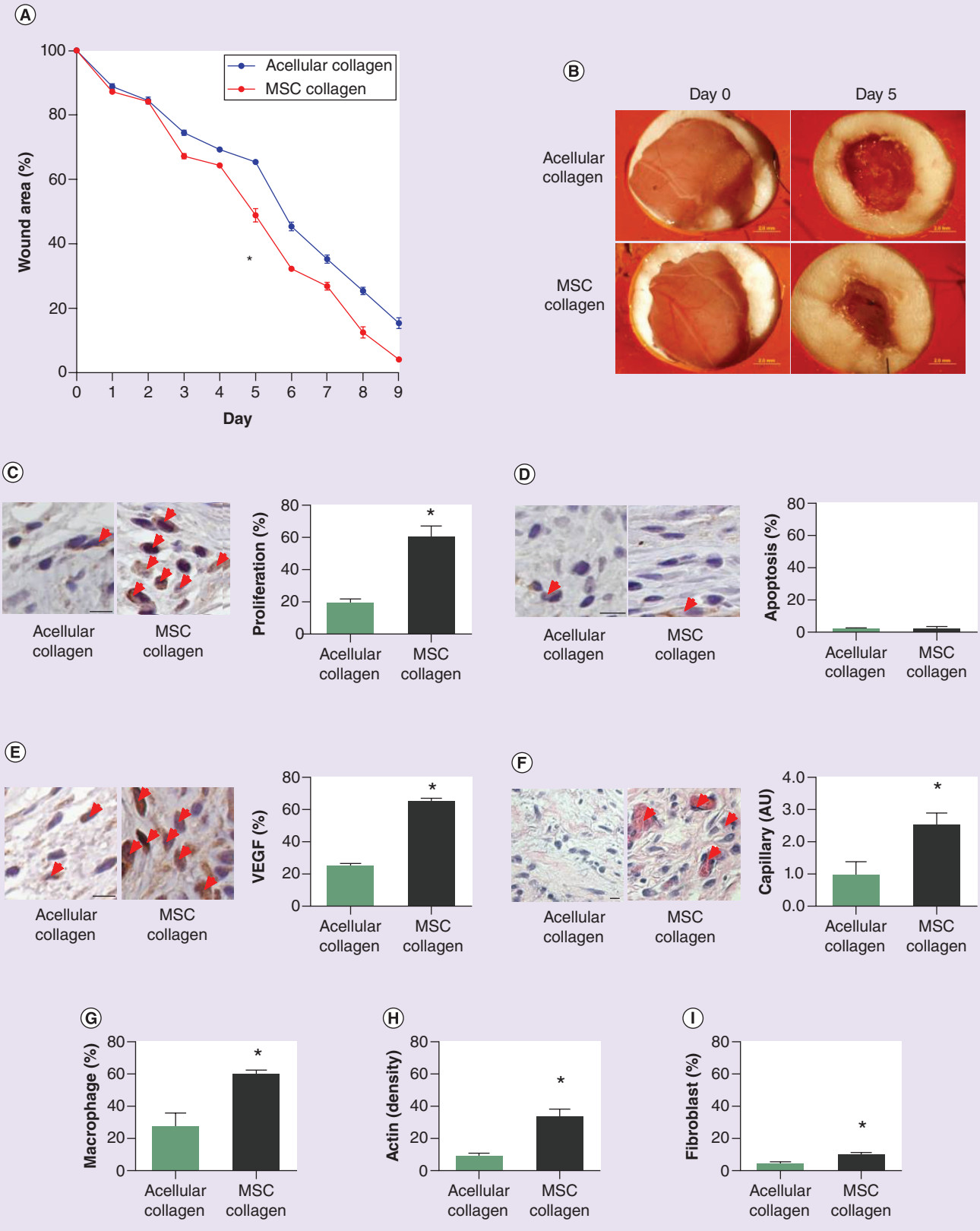
A
Acellular collagen
MSC collagen
Wound area (%)
Day
B
Day 0
Day 5
Acellular collagen
MSC collagen
C
Acellular collagen
MSC collagen
Proliferation (%)
D
Apoptosis (%)
E
VEGF (%)
F
Capillary (AU)
G
Macrophage (%)
H
Actin (density)
I
Fibroblast (%)

Figure 4. Delivery of mesenchymal stem cells in a rolled collagen scaffold enhances wound healing in a diabetic mouse splinted back wound model (see facing page). (A) Line graph shows wound size over time. *p < 0.0001 (two-way ANOVA); n = 6. **(B)** Photographs show representative images of wounds, days 0 and 5. Scale bar 2 mm. **(C)** Representative images and bar graph showing percentage of cells positive for Ki-67 adjacent to acellular and MSC scaffolds. *p = 0.003 (*t*-test); n = 3. **(D)** Representative images and bar graph showing percentage of cells positive for cleaved caspase-3 adjacent to acellular and MSC scaffolds. p = 0.8 (*t*-test); n = 3. **(E)** Representative images and bar graph showing VEGF-positive cells adjacent to acellular and MSC scaffolds. *p < 0.0001 (*t*-test); n = 4. Scale bars **(C–F)**, 10 μm. **(F)** Representative images and bar graph showing relative number of capillaries adjacent to acellular and MSC scaffolds. *p = 0.02 (*t*-test); n = 5–6. **(G)** Bar graph showing F4/80-positive cells adjacent to acellular and MSC scaffolds. *p = 0.02 (*t*-test); n = 3. **(H)** Bar graph showing smooth muscle actin-positive cells adjacent to acellular and MSC scaffolds. *p = 0.01 (*t*-test); n = 3. **(I)** Bar graph showing vimentin-positive cells adjacent to acellular and MSC scaffolds. *p = 0.003 (*t*-test); n = 3. Red arrows show positive cells. MSC: Mesenchymal stem cell.

secrete more VEGF *in vitro* in the rolled configuration compared with flat scaffolds (Figure 1D), we examined VEGF secretion *in vivo*; there were increased numbers of VEGF-positive cells in the tissue adjacent to MSC-containing scaffolds compared with acellular scaffolds (Figure 2F). Similarly there were more capillaries adjacent to MSC-containing scaffolds compared with acellular scaffolds (Figure 2G). There were more cells that were F4/80-positive, consistent with macrophages as well as vimentin-positive, consistent with fibroblasts, and a trend toward increased numbers of smooth muscle actin (SMA)-positive cells, consistent with myofibroblasts, near MSC-containing scaffolds compared with acellular scaffolds (Figures 2H–J). These data show that MSCs in a rolled scaffold enhance wound healing *in vivo*, in multiple ways, of which enhancing wound vascularization is one such mechanism. These findings are consistent with our original hypothesis that by creating a biomimetic physiological environment for the MSCs, we enhance their wound healing capability.

Since there was increased cell proliferation and enhanced wound healing in diabetic mice with wounds treated with MSC-containing scaffolds, we determined whether MSCs persist in the scaffold *in vivo* after implantation. MSCs were labeled with nanoparticles containing both iron and rhodamine prior to implantation. MRI was used to detect the labeled cells *in vivo*. Iron-labeled cells were detectable in the collagen scaffold immediately after implantation as well as on postoperative days 3 and 7 (Figure 3A; first two columns). The MRI data from iron labeled mice showed a specific darkening (red arrow in Figure 3A) that was absent in the control mice (yellow arrow in Figure 3A). Similarly, iron-labeled cells were also detectable with histology through day 7 (Figure 3A; middle two columns). In addition, the rhodamine-labeled cells were directly detectable through day 7 (Figure 3A; last two columns). Since labeled MSCs were detectable in the collagen scaffold *in vivo* postoperatively, and proliferating cells were present adjacent to the scaffold (Figure 2D), we examined scaffolds to determine if any unlabeled cells were also present. Unlabeled cells were present in the scaffold, with more unlabeled cells in the periphery of the scaffold compared with the core of the scaffold (Figure 3B). These results suggest that cells migrate into the scaffold after implantation, for example, biomimetic scaffolds promote cell survival *in vivo*.

Activated MSCs increase wound healing in a splinted back wound model

Since the diabetic mouse wound healing model is thought to measure both wound healing as well as wound contraction, and human wounds generally heal with little contraction, we determined whether MSC-containing scaffolds promote wound healing in the splinted back wound model, as this model prevents wound contraction [32]. Rolled collagen scaffolds without and with MSCs were implanted subcutaneously adjacent to splinted back wounds in diabetic mice. Wounds treated with MSC-containing scaffolds had increased wound healing compared with acellular rolled scaffolds as early as postoperative day 4 (36 vs 31%, day 4; 51 vs 35%, day 5; 68 vs 55%, day 6; p < 0.0001; Figures 4A & B). Similar to the diabetic leg wounds treated with MSC-containing scaffolds, splinted diabetic back wounds treated with MSC-containing scaffolds had adjacent increased proliferation without increased apoptosis, increased VEGF-positive cells and capillaries and increased numbers of F4/80-, SMA- and vimentin-positive cells (Figures 4C–I). These results suggest that MSC-containing scaffolds promote wound healing in splinted diabetic back wounds, for example, they promote wound healing in a clinically relevant model.

Laminin improves wound healing efficiency

Since laminin promotes MSC function in tissue-engineered constructs [33], and we have previously shown that laminin promotes vascular network formation in 3D collagen scaffolds [34], we determined the effects of laminin in the splinted diabetic mouse back wound model. Relative to mice treated with acellular laminin-containing collagen scaffolds, mice treated with MSC in laminin-containing collagen scaffolds

showed an increased rate of wound healing (64 vs 31%, day 4; 52 vs 22%, day 5; $p < 0.0001$; Figures 5A & B). Wounds treated with MSC + laminin-containing collagen scaffolds showed increased proliferation without increased apoptosis, increased VEGF-positive cells and capillaries and increased numbers of F4/80-, SMA- and vimentin-positive cells in comparison to wounds treated with acellular laminin-containing collagen scaffolds (Figures 5C–I).

Interestingly, wounds that were treated with MSCs in laminin-containing collagen scaffolds (Figure 5A) had an even further increased rate of wound healing in comparison to treatment with MSCs in collagen scaffolds without laminin (Figure 4A; $p < 0.0001$, ANOVA). Furthermore, wounds that were treated with MSCs in laminin-containing collagen scaffolds had increased VEGF-positive cells (83 vs 65%; $p = 0.002$, *t*-test), increased numbers of F4/80-positive cells (76 vs 60%; $p = 0.0007$, *t*-test) and a dramatically increased number of vimentin-positive cells (70 vs 11%; $p < 0.0001$, *t*-test) compared with treatment with MSCs in collagen scaffolds without laminin. These results show that addition of laminin to the collagen scaffold augments the rate of diabetic wound healing, suggesting that the biomimetic scaffold promotes MSC survival and/or function *in vivo*.

MSC delivered topically increase wound healing

Since biomimetic scaffolds containing MSCs heal diabetic leg wounds as well as diabetic splinted back wounds, we determined if scaffolds that were unrolled prior to topical application would be similarly successful, for example, the improved MSCs function would retain its efficacy in a clinically useful model. Topical application of collagen scaffolds containing MSCs that were cultured in rolled configuration for 72 h *in vitro* and then unrolled prior to implantation *in vivo* ('rolled *in vitro*') showed improved wound healing compared with acellular scaffolds (Figure 6A, red line vs black line; $p < 0.0001$, ANOVA). Wounds treated with topical scaffolds containing MSCs had increased proliferation without increased apoptosis, increased VEGF-positive cells and capillaries, and increased numbers of F4/80-, SMA- and vimentin-positive cells in comparison to wounds treated with acellular collagen scaffolds (Figures 6C–I). These results show that rolled biomimetic scaffolds contain MSCs with enhanced survival and/or function that retain the ability to enhance wound healing even when applied topically to the wound, for example, without the continued hypoxic or biomimetic environment.

Since these results suggest the importance of the cells being in the rolled scaffold configuration during the *in vitro* culture period to promote MSCs survival and/or function, we hypothesized that MSCs cultured in flat configuration would lose the enhancement of MSCs survival and/or function. Therefore, MSCs were seeded in scaffolds and rolled, but immediately unrolled and cultured *in vitro* for 72 h in flat configuration prior to topical application to the wound. These scaffolds ('flat *in vitro*') showed reduced rates of wound healing compared with scaffolds that were cultured in rolled configuration *in vitro* (Figure 6A, blue line vs red line; $p < 0.0001$, ANOVA). Furthermore, unrolling the scaffolds immediately after creation and culturing in a flat configuration resulted in reduced VEGF-positive cells (63 vs 82%; $p < 0.05$, ANOVA; Figure 6E), reduced capillary formation (1.7 vs 2.5%; $p < 0.05$, ANOVA; Figure 6F) and reduced numbers of vimentin-positive cells (16 vs 37%; $p < 0.05$, ANOVA; Figure 6I) compared with wounds treated with scaffolds cultured in the rolled configuration. These results confirm that culture of MSCs in a biomimetic scaffold in the rolled configuration promotes MSC survival and/or function to enhance wound healing and that is retained with topical application to the wound.

Discussion

We show that MSC-seeded collagen scaffolds rapidly develop a hypoxic core that increases VEGF secretion (Figure 1), and that delivery of MSCs in a biomimetic collagen scaffold increases wound healing in the diabetic mouse leg model (Figure 2). Interestingly, MSCs can be found up to 1 week after implantation *in vivo*, suggesting that the collagen scaffold promotes MSC survival (Figure 3). Use of the splinted back wound model also shows improved wound healing with MSCs (Figure 4), suggesting the translatability of this strategy to human diabetic patients. Addition of laminin to the scaffold improves wound healing, confirming the importance of the scaffold in reproducing the MSCs niche environment (Figure 5). Finally we show that MSCs conditioned in collagen scaffolds can be delivered topically to enhance diabetic wound healing, and that the rolled configuration of the biomimetic scaffold is important to promoting MSC survival and/or function (Figure 6). These results show that biomimetic scaffolds can promote stem cell survival and function, enabling a new therapeutic modality for diabetic wounds.

There has been a recent appreciation for the use of 3D scaffolds to aid regeneration and healing of diseased tissues. Recent work includes the use of acellular patches made of extracellular matrix, mainly collagen type I, to aid the regeneration process in infarcted cardiac tissue; these patches provided superior healing compared with polymeric patches [35]. Similarly

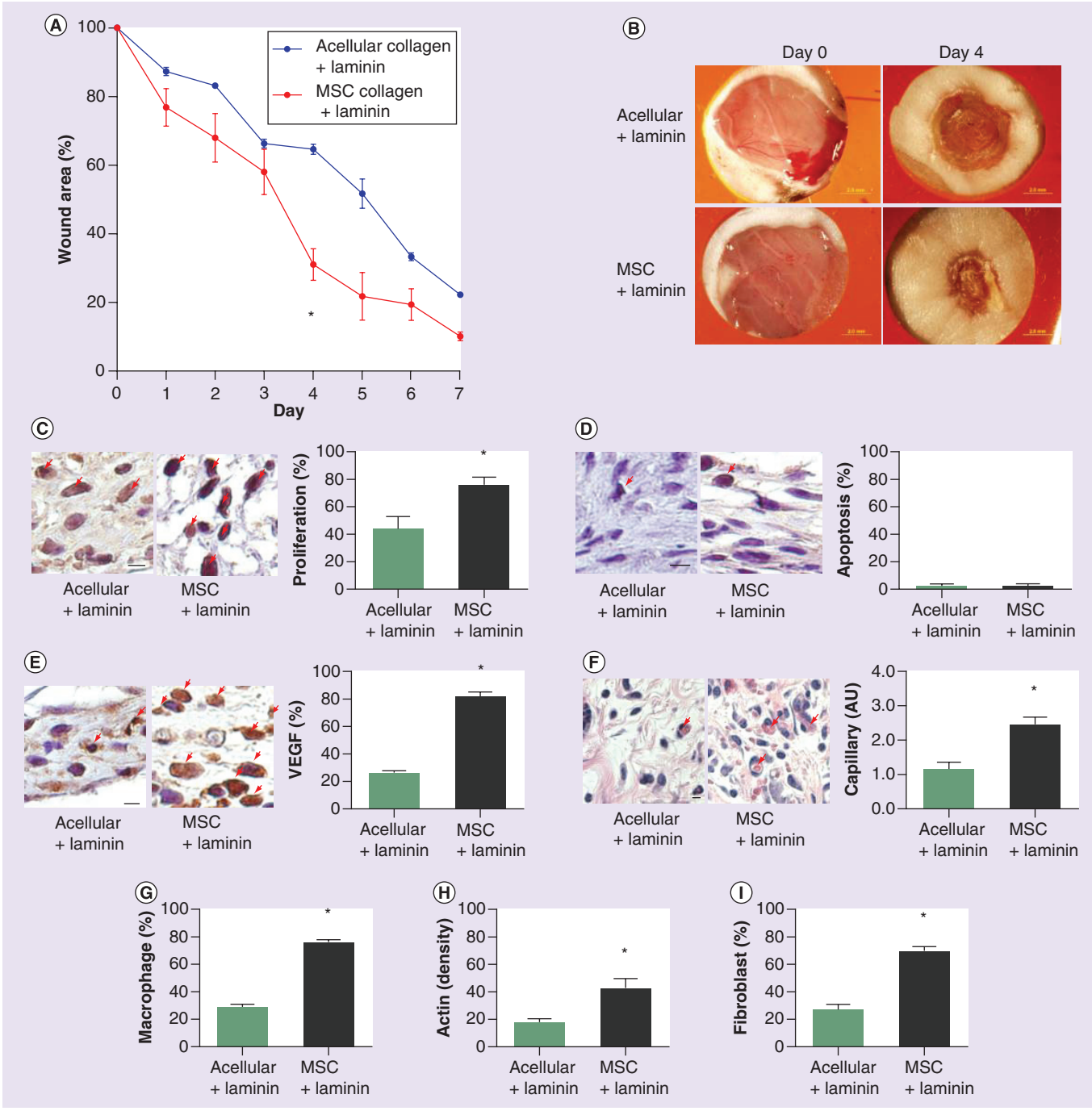

Figure 5. Addition of laminin to the rolled collagen scaffold further enhances wound healing in a diabetic mouse splinted back wound model. **(A)** Line graph shows wound size over time.*p < 0.0001 (two-way ANOVA); n = 3. **(B)** Photographs show representative images of wounds, days 0 and 4. Scale bar: 2 mm. **(C)** Representative images and bar graph showing percentage of cells positive for Ki-67 adjacent to acellular + laminin and MSC + laminin collagen scaffolds. *p = 0.02 (*t*-test); n = 3. **(D)** Representative images and bar graph showing percentage of cells positive for cleaved caspase-3 adjacent to acellular + laminin and MSC + laminin collagen scaffolds; p = 0.8 (*t*-test); n = 3. **(E)** Representative images and bar graph showing VEGF-positive cells adjacent to acellular + laminin and MSC + laminin collagen scaffolds; *p < 0.0001 (*t*-test); n = 3. **(F)** Representative images and bar graph showing relative number of capillaries adjacent to acellular + laminin and MSC + laminin collagen scaffolds. *p = 0.02 (*t*-test); n = 3. Scale bars **(C–F)**, 10 μm. **(G)** Bar graph showing F4/80-positive cells adjacent to acellular + laminin and MSC + laminin collagen scaffolds. *p < 0.0001 (*t*-test); n = 3. **(H)** Bar graph showing smooth muscle actin-positive cells adjacent to acellular + laminin and MSC + laminin collagen scaffolds. *p = 0.01 (*t*-test); n = 3. **(I)** Bar graph showing vimentin-positive cells adjacent to acellular + laminin and MSC + laminin collagen scaffolds. *p = 0.0005 (*t*-test); n = 3. Red arrows show positive cells.
MSC: Mesenchymal stem cell.

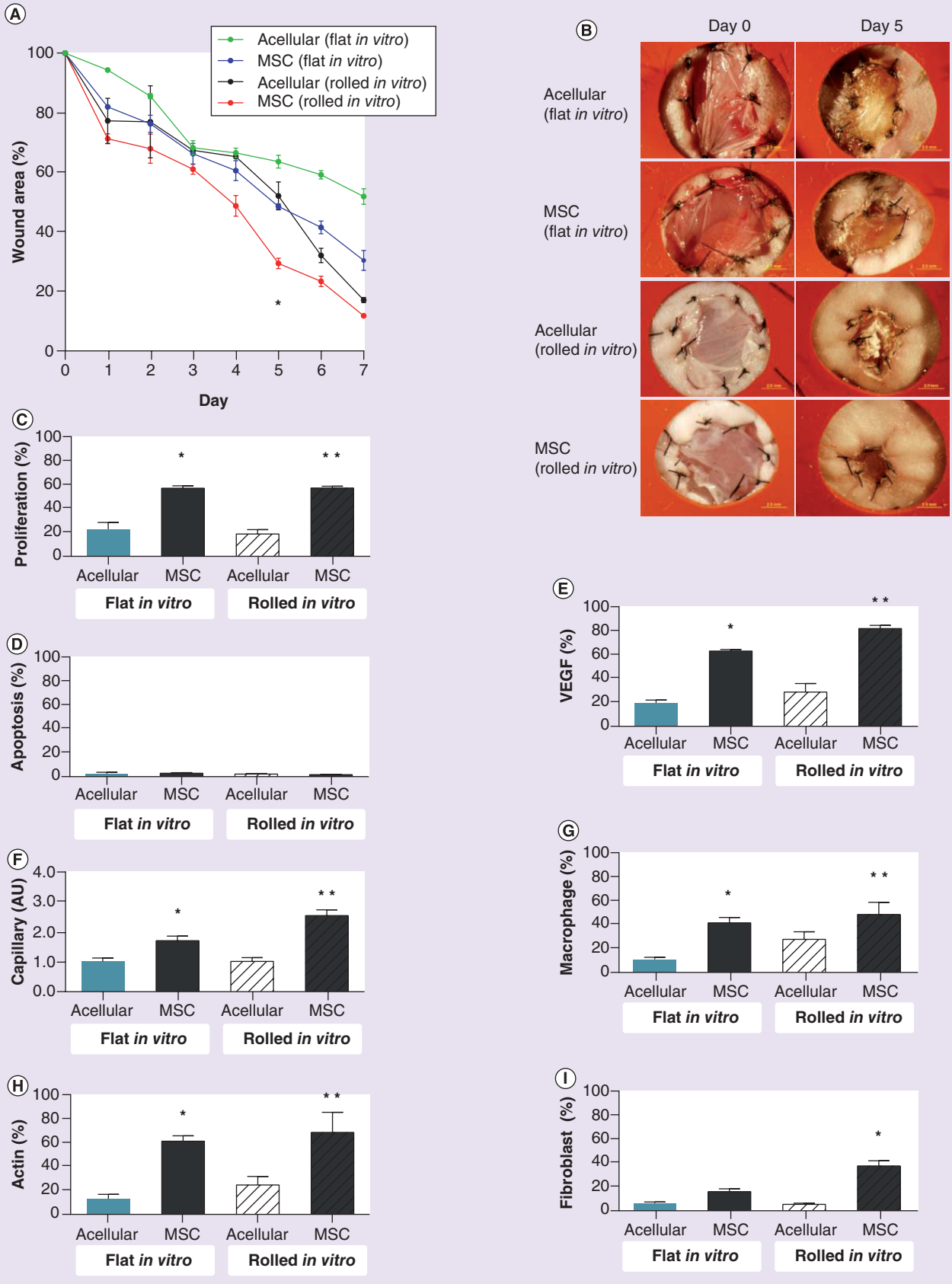
A
Acellular (flat *in vitro*)
MSC (flat *in vitro*)
Acellular (rolled *in vitro*)
MSC (rolled *in vitro*)
Wound area (%)
Day
B
Day 0
Day 5
Acellular (flat *in vitro*)
MSC (flat *in vitro*)
Acellular (rolled *in vitro*)
MSC (rolled *in vitro*)
C
Proliferation (%)
D
Apoptosis (%)
E
VEGF (%)
F
Capillary (AU)
G
Macrophage (%)
H
Actin (%)
I
Fibroblast (%)
Acellular
MSC
Flat *in vitro*
Rolled *in vitro*

Figure 6. Topical application of collagen scaffolds containing mesenchymal stem cells enhances wound healing in a diabetic mouse splinted back wound model. (A) Line graph shows wound size over time. *p < 0.0001 (two-way ANOVA); n = 3. **(B)** Photographs show representative images of wounds, days 0 and 5. Scale bar: 2 mm. **(C)** Bar graph showing percentage of cells positive for Ki-67 adjacent to acellular and MSC collagen scaffolds applied topically; p < 0.0001 (one-way ANOVA); n = 3. *p < 0.05 (*post hoc*) MSC flat versus acellular rolled and acellular flat. **p < 0.05 (*post hoc*) MSC rolled versus acellular rolled and acellular flat. **(D)** Bar graph showing percentage of cells positive for cleaved caspase-3 adjacent to acellular and MSC collagen scaffolds applied topically. p = 0.7 (one-way ANOVA); n = 3. **(E)** Bar graph showing percentage of VEGF-positive cells adjacent to acellular and MSC collagen scaffolds applied topically. p < 0.0001 (one-way ANOVA); n = 3. *p < 0.05 (*post hoc*) MSC flat versus acellular rolled and acellular flat. **p < 0.05 (*post hoc*) MSC rolled versus MSC flat, acellular rolled and acellular flat. **(F)** Bar graph showing relative number of capillaries adjacent to acellular and MSC collagen scaffolds applied topically. p = 0.0003 (one-way ANOVA); n = 3. *p < 0.05 (*post hoc*) MSC flat versus acellular rolled and acellular flat. **p < 0.05 (*post hoc*) MSC rolled versus MSC flat, acellular rolled and acellular flat. **(G)** Bar graph showing F4/80-positive cells adjacent to acellular and MSC collagen scaffolds applied topically. p = 0.01 (one-way ANOVA); n = 3. *p < 0.05 (*post hoc*) MSC flat versus acellular flat. **p < 0.05 (*post hoc*) MSC rolled versus acellular flat. **(H)** Bar graph showing smooth muscle actin-positive cells adjacent to acellular and MSC collagen scaffolds applied topically. p = 0.009 (one-way ANOVA); n = 3. *p < 0.05 (*post hoc*) MSC flat versus acellular flat. **p < 0.05 (*post hoc*) MSC rolled versus acellular flat and acellular rolled. **(I)** Bar graph showing vimentin-positive cells adjacent to acellular and MSC collagen scaffolds applied topically. p < 0.0001 (one-way ANOVA); n = 3. *p < 0.05 (*post hoc*) MSC rolled versus MSC flat, acellular flat and acellular rolled.
MSC: Mesenchymal stem cell.

a 3D vicryl graft was used to deliver adipose-derived stromal vascular fraction cells to improve cardiac function after infarct [36]. We used a biomimetic scaffold to optimize MSC angiogenic potential, enhancing wound healing in diabetic mice. Our approach was to control three physiological parameters to optimize the biomimetic nature of the environment based on the MSC niche environment *in vivo*. These parameters included biomimetic matrix composition, tissue-like matrix density and physiological oxygen environment. The matrix material tested was either collagen I only or collagen I with laminin. Matrix density was controlled and increased to approximately 10%, which is approaching tissue density, by the process of plastic compression [24]. Cell-embedded scaffolds were rolled in a spiral configuration to create a hypoxic gradient maximally at the scaffold core; we have previously shown that this scaffold configuration stimulates multiple cell types to increase VEGF synthesis and secretion [25]. Our data suggest that use of the proper matrix components, at physiological density and configuration, promotes MSC survival and function to promote wound healing. Interestingly, diabetes is associated with diminished subpopulations of MSCs, suggesting that diabetic ulcers may be amenable to therapies that restore MSC numbers and/or function [37,38].

The stem cell niche provides a microenvironment conducive for stem cell survival and maintenance of multipotency. Within the bone marrow, the physiological site of the MSCs niche environment, reported levels of physiological pO_2 range between 0 and 7% [20,39]. MSCs within rolled collagen scaffolds generated physiological hypoxia due to the formation of O_2 consumption gradients [25]. The level of O_2 within the core of our constructs dipped below 1% for the first 12 h of culture, which is nearing pathological hypoxia (Figure 1C). We hypothesize that changes in MSC O_2 metabolism then result in a lower consumption of O_2, allowing stabilization of O_2 levels at 50 mmHg (6.6%) from 24 h onward (Figure 1C), since this low O_2 environment does not result in loss of cell viability of implanted scaffolds (Figure 3). Indeed, we were able to detect persistent MSCs *in vivo* even after 1 week (Figure 3). Interestingly, after 72 h of hypoxia, subsequent exposure of the MSCs to the ambient environment with topical application retains efficacy of wound healing (Figure 6), suggesting that the hypoxic cellular activation is not transient.

Addition of laminin to the collagen scaffold promotes wound healing as well as increases the number of VEGF-positive cells, macrophages and fibroblasts near the implanted scaffold (Figure 5), suggesting that the biomimetic scaffold promotes MSC survival and/or function *in vivo*. We have also shown that inclusion of laminin increases cell expression of integrin α6 and VEGFR2 as well as VEGF uptake [34]. These data suggest that the matrix composition of the scaffold to which the cells are attached is critical for optimal cell function and wound healing. Other groups have shown that MSCs cultured in defined matrix scaffolds can direct lineage commitment, particularly true of laminins [40]. The importance of the topographical and mechanical properties of scaffolds in which cells are cultured is a driver of multiple cell functions [41]. However, the optimal niche composition and physical organization for MSCs remains to be defined [42]. For example, the role of hydroxyapatite in promoting MSC survival and function is yet to be determined.

We also show that topical application of the unrolled flat MSC-containing scaffold improves wound healing in the splinted back wound model (Figure 6). These results suggest that delivering MSCs with a biomimetic

scaffold may be translatable to human patients with diabetic wounds, either via subcutaneous implantation near the wound (Figures 2, 4 & 5) or topically on the wound (Figure 6). Since the subcutaneous implants were in the rolled configuration and the topical application was in the flat configuration, these results suggest that the hypoxia-activated MSCs are the key therapeutic agent, rather than the scaffold, for example, the critical aspect of the biomimetic scaffold is its ability to activate MSCs to promote cellular survival and/or function. One limitation of this study is the relatively small n used in each of the individual *in vivo* experiments; however, the reproducibility of the results using multiple delivery parameters suggests, in toto, that the biomimetic scaffold improves MSC function sufficiently to promote wound healing *in vivo*. Furthermore, the consistently improved rate of early wound healing shown in all the experiments may be translatable to clinically meaningful results for patients.

Conclusion

In summary, we show that delivery of MSCs in biomimetic scaffolds through implantation or by topical application promotes wound healing in a translationally relevant diabetic mouse model. These results suggest that a tissue engineering approach is a viable approach to this difficult and complex clinical problem. These results also suggest that a biomimetic scaffold can mimic a stem cell niche environment, promoting stem cell survival and/or function *in vivo*, potentially increasing their therapeutic application.

Financial & competing interests disclosure

This work was supported in part by Yale-UCL Medtech Initiative Flagship Project Vascular Engineering award (to A Dardik, U Cheema, S Homer-Vanniasinkam), NIH Grants R56-HL095498 and R01-HL-095498 (to A Dardik), a Yale Department of Surgery Ohse award (to A Dardik), as well as through the resources and use of facilities at the Veterans Affairs Connecticut Healthcare System (West Haven, CT, USA). The authors have no other relevant affiliations or financial involvement with any organization or entity with a financial interest in or financial conflict with the subject matter or materials discussed in the manuscript apart from those disclosed.

No writing assistance was utilized in the production of this manuscript.

Ethical conduct of research

The authors state that they have obtained appropriate institutional review board approval or have followed the principles outlined in the Declaration of Helsinki for all human or animal experimental investigations. In addition, for investigations involving human subjects, informed consent has been obtained from the participants involved.

Executive summary

Tissue-engineered collagen scaffolds activate mesenchymal stem cells

- Collagen scaffolds, with or without laminin, can be used to both activate stem cells and to deliver them for therapeutic applications.
- Stem cells cultured in collagen scaffolds release detectable levels of angiogenic mediators including VEGF.
- Collagen scaffolds may mimic the natural stem cell niche environment promoting stem cell survival and/or function.

Activated mesenchymal stem cells in collagen scaffolds increase wound healing *in vivo*

- Lower extremity wounds remain an important clinical problem for patients with diabetes.
- Activated mesenchymal stem cells (MSCs) implanted adjacent to a wound promote healing in diabetic mouse hindlimb wound and splinted back wound models.

Topical application of activated MSCs promotes wound healing

- Activated MSCs placed topically on a wound promote healing in a diabetic mouse splinted back wound model.
- Topical application of activated stem cells with a collagen scaffold is a viable and translationally relevant model for stem cell treatment of wounds.
- Tissue-engineering approaches may yield solutions to management of diabetic wounds.

References

Papers of special note have been highlighted as:
• of interest; •• of considerable interest

1 American Diabetes Association. Economic costs of diabetes in the U.S. in 2012. *Diabetes Care* 36(4), 1033–1046 (2013).

2 Cavanagh PR, Lipsky BA, Bradbury AW, Botek G. Treatment for diabetic foot ulcers. *Lancet* 366(9498), 1725–1735 (2005).

3 Leung PC. Diabetic foot ulcers – a comprehensive review. *Surgeon* 5(4), 219–231 (2007).

4 Martins-Mendes D, Monteiro-Soares M, Boyko EJ *et al.* The independent contribution of diabetic foot ulcer on lower extremity amputation and mortality risk. *J. Diabetes Complications* 28(5), 632–638 (2014).

5 Tecilazich F, Dinh T, Veves A. Treating diabetic ulcers. *Expert Opin. Pharmacother.* 12(4), 593–606 (2011).

6 Chen M, Przyborowski M, Berthiaume F. Stem cells for skin tissue engineering and wound healing. *Crit. Rev. Biomed. Eng.* 37(4–5), 399–421 (2009).

7 Markeson D, Pleat JM, Sharpe JR, Harris AL, Seifalian AM, Watt SM. Scarring, stem cells, scaffolds and skin repair. *J. Tissue Eng. Regen. Med.* 9(6), 649–668 (2013).

8 Mulder G, Tenenhaus M, D'Souza GF. Reduction of diabetic foot ulcer healing times through use of advanced treatment modalities. *Int. J. Low Extrem. Wounds* 13(4), 335–346 (2014).

9 Pushpoth S, Tambe K, Sandramouli S. The use of AlloDerm in the reconstruction of full-thickness eyelid defects. *Orbit* 27(5), 337–340 (2008).

10 Balaji S, Keswani SG, Crombleholme TM. The role of mesenchymal stem cells in the regenerative wound healing phenotype. *Adv. Wound Care (New Rochelle)* 1(4), 159–165 (2012).

11 Blumberg SN, Berger A, Hwang L, Pastar I, Warren SM, Chen W. The role of stem cells in the treatment of diabetic foot ulcers. *Diabetes Res. Clin. Pract.* 96(1), 1–9 (2012).

• **Reviews current therapies to manage diabetic ulcers with a discussion of the evidence supporting use of bone marrow-derived stem cells as a potential treatment modality.**

12 Jiang XY, Lu DB, Chen B. Progress in stem cell therapy for the diabetic foot. *Diabetes Res. Clin. Pract.* 97(1), 43–50 (2012).

13 Sorrell JM, Caplan AI. Topical delivery of mesenchymal stem cells and their function in wounds. *Stem Cell Res. Ther.* 1(4), 30 (2010).

•• **Reviews evidence supporting topical delivery of mesenchymal stem cells to promote wound healing.**

14 Wang S, Qu X, Zhao RC. Clinical applications of mesenchymal stem cells. *J. Hematol. Oncol.* 5, 19 (2012).

15 Jackson WM, Nesti LJ, Tuan RS. Concise review: clinical translation of wound healing therapies based on mesenchymal stem cells. *Stem Cells Transl. Med.* 1(1), 44–50 (2012).

16 Sasaki M, Abe R, Fujita Y, Ando S, Inokuma D, Shimizu H. Mesenchymal stem cells are recruited into wounded skin and contribute to wound repair by transdifferentiation into multiple skin cell type. *J. Immunol.* 180(4), 2581–2587 (2008).

17 Boomsma RA, Geenen DL. Mesenchymal stem cells secrete multiple cytokines that promote angiogenesis and have contrasting effects on chemotaxis and apoptosis. *PLoS ONE* 7(4), e35685 (2012).

18 Wu Y, Chen L, Scott PG, Tredget EE. Mesenchymal stem cells enhance wound healing through differentiation and angiogenesis. *Stem Cells* 25(10), 2648–2659 (2007).

19 Leroux L, Descamps B, Tojais NF *et al.* Hypoxia preconditioned mesenchymal stem cells improve vascular and skeletal muscle fiber regeneration after ischemia through a Wnt4-dependent pathway. *Mol. Ther.* 18(8), 1545–1552 (2010).

20 Stamati K, Mudera V, Cheema U. Evolution of oxygen utilization in multicellular organisms and implications for cell signalling in tissue engineering. *J. Tissue Eng.* 2(1), 2041731411432365 (2011).

21 Gattazzo F, Urciuolo A, Bonaldo P. Extracellular matrix: a dynamic microenvironment for stem cell niche. *Biochim. Biophys. Acta* 1840(8), 2506–2519 (2014).

22 Critser PJ, Kreger ST, Voytik-Harbin SL, Yoder MC. Collagen matrix physical properties modulate endothelial colony forming cell-derived vessels *in vivo*. *Microvasc. Res.* 80(1), 23–30 (2010).

23 Gower RM, Shea LD. Biomaterial scaffolds for controlled, localized gene delivery of regenerative factors. *Adv. Wound Care (New Rochelle)* 2(3), 100–106 (2013).

24 Mudera V, Morgan M, Cheema U, Nazhat S, Brown R. Ultra-rapid engineered collagen constructs tested in an *in vivo* nursery site. *J. Tissue Eng. Regen. Med.* 1(3), 192–198 (2007).

25 Cheema U, Brown RA, Alp B, MacRobert AJ. Spatially defined oxygen gradients and vascular endothelial growth factor expression in an engineered 3D cell model. *Cell Mol. Life Sci.* 65(1), 177–186 (2008).

•• **Describes the mechanism of collagen scaffold activation of cell function by decreasing oxygen concentration in the scaffold core.**

26 Cheema U, Rong Z, Kirresh O, Macrobert AJ, Vadgama P, Brown RA. Oxygen diffusion through collagen scaffolds at defined densities: implications for cell survival in tissue models. *J. Tissue Eng. Regen. Med.* 6(1), 77–84 (2012).

27 Cheema U, Alekseeva T, Abou-Neel EA, Brown RA. Switching off angiogenic signalling: creating channelled constructs for adequate oxygen delivery in tissue engineered constructs. *Eur. Cell Mater.* 20, 274–280 (2010).

28 Chaudhry ZZ, Morris DL, Moss DR *et al.* Streptozotocin is equally diabetogenic whether administered to fed or fasted mice. *Lab. Anim.* 47(4), 257–265 (2013).

29 Chen JS, Longaker MT, Gurtner GC. Murine models of human wound healing. *Methods Mol. Biol.* 1037 265–274 (2013).

• **Describes the technical details of the murine excisional model of wound healing including the splinted wound model.**

30 Egana JT, Fierro FA, Kruger S *et al.* Use of human mesenchymal cells to improve vascularization in a mouse model for scaffold-based dermal regeneration. *Tissue Eng. Part A* 15(5), 1191–1200 (2009).

31 Cyagen. User Manual: OriCellTM strain C57BL/6 mouse mesenchymal stem cells. www.cyagen.com/media/uploads

32 Galiano RD, Michaels Jt, Dobryansky M, Levine JP, Gurtner GC. Quantitative and reproducible murine model of excisional wound healing. *Wound Repair Regen.* 12(4), 485–492 (2004).

33 Hashimoto J, Kariya Y, Miyazaki K. Regulation of proliferation and chondrogenic differentiation of human mesenchymal stem cells by laminin-5 (laminin-332). *Stem Cells* 24(11), 2346–2354 (2006).

34 Stamati K, Priestley JV, Mudera V, Cheema U. Laminin promotes vascular network formation in 3D *in vitro* collagen

scaffolds by regulating VEGF uptake. *Exp. Cell Res.* 327(1), 68–77 (2014).

•• **Describes how the microenvironment within the collagen scaffold can be altered by addition of laminin to improve endothelial cell function.**

35 Robinson KA, Li J, Mathison M *et al.* Extracellular matrix scaffold for cardiac repair. *Circulation* 112(9 Suppl.), I135–143 (2005).

36 Leblanc AJ, Nguyen QT, Touroo JS *et al.* Adipose-derived cell construct stabilizes heart function and increases microvascular perfusion in an established infarct. *Stem Cells Transl. Med.* 2(11), 896–905 (2013).

37 Januszyk M, Sorkin M, Glotzbach JP *et al.* Diabetes irreversibly depletes bone marrow-derived mesenchymal progenitor cell subpopulations. *Diabetes* 63(9), 3047–3056 (2014).

38 Rennert RC, Sorkin M, Januszyk M *et al.* Diabetes impairs the angiogenic potential of adipose-derived stem cells by selectively depleting cellular subpopulations. *Stem Cell Res. Ther.* 5(3), 79 (2014).

39 Lekli I, Gurusamy N, Ray D, Tosaki A, Das DK. Redox regulation of stem cell mobilization. *Can. J. Physiol. Pharmacol.* 87(12), 989–995 (2009).

40 Swift J, Ivanovska IL, Buxboim A *et al.* Nuclear lamin-A scales with tissue stiffness and enhances matrix-directed differentiation. *Science* 341(6149), 1240104 (2013).

41 Dalby MJ, Gadegaard N, Oreffo RO. Harnessing nanotopography and integrin-matrix interactions to influence stem cell fate. *Nat. Mater.* 13(6), 558–569 (2014).

42 Schraufstatter IU, Discipio RG, Khaldoyanidi S. Mesenchymal stem cells and their microenvironment. *Front Biosci. (Landmark Ed.)* 16, 2271–2288 (2011).

Research Article

For reprint orders, please contact: reprints@futuremedicine.com

Regenerative Medicine

Selected renal cells modulate disease progression in rodent models of chronic kidney disease via NF-κB and TGF-β1 pathways

Aim: Identification of mechanistic pathways for selected renal cell (SRC) therapeutic bioactivity in rodent models of chronic kidney disease. **Materials & methods:** *In vivo* and *in vitro* functional bioassays applied to investigate regenerative outcomes associated with delivery of SRC to diseased rodent kidney. **Results:** *In vivo*, SRC reduces chronic infiltration by monocytes/macrophages. SRC attenuates NF-κB and PAI-1 responses while simultaneously promoting host tubular cell expansion through trophic cues. *In vitro*, SRC-derived conditioned media attenuates TNF-α-induced NF-κB response, TGF-β-mediated PAI-1 response and increases expression of transcripts associated with cell cycle regulation. Observed bioactive responses were from vesicle and nonvesicle-associated factors, including specific miRNAs. **Conclusion:** We identify a paracrine mechanism for SRC immunomodulatory and trophic cues on host renal tissues, catalyzing long-term functional benefits *in vivo*.

Keywords: cell therapy • chronic kidney disease • fibrosis • inflammation • mechanism of action • miRNA • NF-κB • PAI-1 • paracrine • regeneration • selected renal cell • stem cell • tissue engineering • vesicle

Andrew T Bruce[1,2], Roger M Ilagan[1,2], Kelly I Guthrie[1,2], Elias Rivera[2,3], Sumana Choudhury[2,4], Namrata Sangha[2,5], Thomas Spencer[2,6], Timothy A Bertram[2,6], Deepak Jain[2,6], Russell W Kelley[2,7] & Joydeep Basu*[,2,6]

[1]Regenerative Medicine, United Therapeutics, 55 TW Alexander Drive, Research Triangle Park, NC 27709, USA
[2]Tengion, Inc., 3929 Westpoint Blvd, Ste G, Winston-Salem, NC 27103, USA
[3]Infinium Pathology Consultants LLC, 1805 Wild Fern Dr., Oak Ridge, NC 27310, USA
[4]Gene Therapy Center, Vector Core, University of North Carolina at Chapel Hill, NC 27617, USA
[5]Wake Forest Institute for Regenerative Medicine, Medical Centre Boulevard, Winston-Salem, NC 27157, USA
[6]RegenMedTX LLC, 3929 Westpoint Blvd, Ste G, Winston-Salem, NC 27103, USA
[7]Burroughs Wellcome Fund, 21 TW Alexander Drive, Research Triangle Park, NC 27709, USA
*Author for correspondence:
Tel.: +1 336 722 5855
Fax: +1 336 722 2436
jbasu2@yahoo.com

Chronic kidney disease (CKD) represents a significant and increasing healthcare issue in North America and the rest of the world. Observed rates of increase are due principally to development of renal failure secondary to noninsulin-dependent diabetes and hypertension [1]. Modern strategies for management of the CKD patient population are based on pharmaceuticals for amelioration of the primary disease (i.e., glycemic control agents and antihypertensive agents) that serve to modulate development of secondary renal damage and disease. Ultimately, however, dialysis or whole organ transplantation is indicated as a proxy for renal filtration functionality. Patients presenting with advanced CKD are also controlled through pharmaceuticals to restore other key aspects of renal bioactivity, including erythropoiesis catalyzed by erythropoietin (EPO), and secretion of vitamin D from tubule-specific vitamin D hydroxylase [2]. Whole kidney transplantation remains the standard of care, but the CKD patient population advancing to end-stage renal disease (ESRD) requiring dialysis or transplant is much greater than the number of acceptable donor kidneys [3]. To this end, regenerative medicine and tissue-engineering methodologies may provide additional therapeutic possibilities for CKD patients.

Rescue of renal functionality with cell-based methodologies has been explored clinically for acute renal failure (ARF) with extracorporeal filtration units containing renal tubular cells [4], and by transfer of allogeneically sourced mesenchymal stem cells (MSCs) through the renal artery [5,6]. These approaches mediate short-term recovery of defined renal functionalities. Preclinical studies involving delivery of different cell populations immediately before or after establishment of ARF include: intrarenal or systemic delivery of MSC [7], fetal cells or tissue rudiments [8–11] and endothelial progenitor cells (EPC) [12,13]. Preclinical studies of cell-based therapies for CKD are limited, with few sys-

Future Medicine part of fsg

tematic investigations of the therapeutic potential of cell-based treatments after onset of chronic injury. Therapeutic bioactivity has been observed in rodent models of Alport syndrome following treatment with bone marrow cells [14], in rodent models of partial nephrectomy or ischemia-reperfusion injury following systemic injection with fetal kidney cells [15], and in swine models of unilateral renal artery stenosis following treatment with autologously sourced EPC [13].

Typically, strategies currently under consideration for cell therapy of the kidney in response to onset of CKD have focused on leveraging the potential paracrine-mediated therapeutic properties of MSC, embryonic stem cells and related cell populations (reviewed by [16]). However, from a manufacturing and product development perspective, primary cell types are preferable when compared with stem and progenitor cell populations, owing to considerable streamlining of isolation, expansion, maintenance and characterization conditions (reviewed by [17,18]). To this end, numerous studies on regeneration of renal architecture and function following acute kidney injury point to tubular epithelial cells as central in restoration of renal functionality [19,20].

Tubular cells can be separated from other kidney cell types on the basis of differential buoyant density [21]. This predominant population of tubular cells is reproducibly separable from remnant cells as a well-defined band (B2) with buoyant density between 1.045 and 1.063 g/ml and is characterized as an epithelial cell-enriched population comprised of tubular and aquaporin 2-positive collecting duct cells [21]. Upon delivery to 5/6-nephrectomized (5/6N_x) rats 4–7 weeks postinjury, B2 cells stimulated tissue regeneration and stabilized renal filtration functions for 6 months post-treatment, leading to 100% survival in treated rats versus 0% survival in untreated rats. B2 cells were therefore leveraged to form the principal component of selected renal cells (SRCs; see the 'Materials & methods' section for additional details). B1 and B5 cell populations, representing additional defined bands with distinct buoyant densities, were observed to be therapeutically inert in rodent CKD models, and are additionally leveraged as non-SRC cellular controls in the current report [21–23]. These cell populations (B1–B5) have been phenotypically characterized in detail at the morphological, transcriptomic and immunohistochemical (IHC) levels [21–23] and are composed of principally E-cadherin (ECAD$^+$), Pan-cadherin$^+$, cytokeratin 8/18/19 (CK8/18/19$^+$), gamma glutamyl transpeptidase (GGT1$^+$) cells and oxygen responsive EPO$^+$ (erythropoietin) subpopulations [21–23].

From a mechanism of action (MOA) perspective, although engraftment of SRC within the treated kidney has been demonstrated out to 6 months postimplantation [21–23], this is likely not the only therapeutic mechanism at play for preserving nephron function and delaying overt tissue inflammation and fibrosis. The ability to augment renal function with SRC might reflect a combination of the potential of the engrafted cell to salvage cellular compartments and the autocrine, paracrine and perhaps endocrine factors that are transiently and/or constitutively transferred to a recipient diseased cell from the donor cell population. Additionally, we note that SRC have not been observed to engraft at sites other than the targeted kidney.

The development of tubulointerstitial fibrosis during the progression of CKD is associated with TGF-β1-mediated epithelial–mesenchymal transition (EMT) of tubular epithelial cells [24]. Progressive fibrosis is a hallmark of CKD and is a clear feature of the 5/6N_x model. The accumulation of fibrotic extracellular matrix (ECM) proteins, which include fibronectin (FN) and type I collagen, has long been associated with persistent expression of TGF-β1 by injured or distressed cells [25]. Plasmin-dependent proteolysis of ECM proteins, through the increased expression of PAI-1, can further promote the development of fibrotic lesions [26]. It has been demonstrated that TGF-β1 and PAI-1 interact within a positive feedback loop that may, in the absence of intervention, trigger pathologies associated with uncontrolled deposition and inadequate degradation of ECM [27]. Molecular analyses of diseased rodent kidney tissue at the time of necropsy (3 and 6 months after treatment) demonstrate that treatment with B2 attenuated expression of TGF-β1, PAI-1 and FN [21–23]. These observations taken together suggest that B2 cells are communicating to host cells through paracrine factors. This hypothesis is supported, in part, by the observation that the reduction in profibrotic markers is maintained even 6 months after implantation, despite the relatively low number of donor cells as detected by PCR-based analysis of *SRY* in those same tissues [21–23].

In this manuscript, we extend our previously published observations by hypothesizing a paracrine-mediated MOA for observed therapeutic bioactivity of SRC in preclinical rodent models of CKD (5/6N_x Lewis rats and ZSF1 diabetic nephropathy model, see the 'Materials & methods' section below). Specific histological observations of antifibrotic and anti-inflammatory outcomes secondary to SRC delivery in rodent CKD kidneys led us to investigate at a molecular level the NF-κB and TGF-β1-mediated PAI-1 signaling pathways known to drive tissue inflammation and fibrosis during onset of CKD [27]. We further hypothesize that these SRC-derived paracrine factors may function through extracellular vesicle-mediated communication mechanisms. To this end, we used molecular histologic techniques to show SRC can attenuate the NF-κB and PAI-1 responses known to drive tissue

inflammation and fibrosis, while simultaneously promoting host tubular cell expansion through trophic cues. As an indicator of renal-specific and NF-κB-mediated inflammatory status, urine CCL2/MCP-1 and CCL5/RANTES protein levels were measured by ELISA [28] and observed to at least partially be modulated in response to SRC. Consistent with these *in vivo* outcomes, we demonstrate that SRC-derived conditioned media (CM) can attenuate the TNF-α-induced NF-κB response, TGF-β1-mediated PAI-1 response and increase expression of transcripts associated with cell cycle regulation in established renal cell lines. Observed bioactive responses were from vesicle and nonvesicle-associated factors present in SRC-CM. These *in vitro* findings recapitulate our *in vivo* analysis of rat SRC-treated kidneys: robust inhibition of NF-κB activation and PAI-1 expression and increased number of proliferative cells in targeted tissues is observed following direct SRC injection. Taken together, these data identify a paracrine mechanism by which SRC may provide immunomodulatory and trophic cues to diseased host renal tissues.

Materials & methods

Animal models of CKD

Materials generated from rodent models of CKD were derived from studies previously described [21–23,29]. For characterizing the pathogenesis of CKD, 30 female Lewis rats underwent a two-step 5/6N_x procedure as previously described [29]. ZSF1 rats were provided by Charles Rivers Laboratories and are a hybrid strain generated from the zucker diabetic fatty rat (ZDF-1; *Lepr*$^{+/fa}$) and the spontaneously hypertensive heart failure rat (SHHF/Mcc, *Lepr*$^{+/cp}$). The ZSF1 rat strain provides an experimental model for translating the potential utility of cell-based therapies for preventing or delaying renal disease progression secondary to Type 2 diabetes. The metabolic syndrome and the progressive diabetic nephropathy (DN) in the ZSF1 culminate from morbid obesity, severe hyperglycemia, hyperinsulemia and hyperlipidemia, hypertension and cardiovascular complications that also increase the risk of congestive heart failure [30,31]. An overview of study design is presented in Tables 1 & 2. Clinical parameters associated with entry criteria and evaluation of therapeutic outcomes are described in detail in [21–23,29] and will not be repeated here. While the ZSF1 model may survive up to 63 weeks of age, a more typical survival time is 48 weeks of age [30,31]. Within the first 8 weeks of life, ZSF1 rats present with the hallmark indicators of metabolic syndrome which includes Type 2 diabetes and initial signs of renal functional impairment, and by 32 weeks of age, ZSF1 kidney structure and function have declined significantly and are consistent with

Table 1. Summary of Lewis 5/6N_x experimental design.

1 week		4–7 weeks		8–24 weeks	Ref.
Model generation two-step 5/6N_x	**Establishment of disease state**	**Entry into study**	**Treatment**	**Clinical outcomes**	
Day 0, left kidney 2 poles removed Day 7, right kidney removed	sCREAT and BUN monitored weekly standard chow/water *ad libitum*	Criteria: ↑ sCREAT ≥200% ↑ BUN >200% >2 consecutive weeks	Randomization	Slowed progression by improving functional renal mass; 6-month survival	[22]

Test:
– Intrarenal delivery of 5 × 10^6 SRC (B2 + B4 cells) delivered to cortex of remnant kidney (n = 3)
Controls:
– Intra-renal delivery of 5 × 10^6 non-SRC (B1 + B5 cells) delivered to cortex of remnant kidney (n = 2)
– Nephrectomy (n = 3)
– Hemi-nephrectomy (n = 3)

BUN: Blood Urea Nitrogen; sCREAT: Serum creatinine; SRC: Selected renal cell.

Table 2. Summary of ZSF1 experimental design.

1–17 weeks			18 weeks		31 weeks	32–63 weeks	Ref.
Establishment of disease state	Entry into study	Treatment				Clinical outcomes	
Metabolic syndrome of obesity, diabetes mellitus, hypertension; fed diabetogenic diet	Criteria: 65% functional eGFR	Randomization	Test: – Intraparenchymal delivery of 2.5 × 10^6 SRC in 100 µl volume in each of the anterior and posterior poles of both kidneys (n = 7) Controls: – Obese no treatment (n = 5) – Lean no treatment (n = 5)	Diet changed to maintenance diet plus insulin		Improved nephron function by increasing filtration ↓ sCre and BUN, increased tubular transport ↓ sCal sPhos and improved ability to concentrate urine ↑ uOsmol; improved survival	[23]

SRC: Selected renal cell; eGFR: Estimated glomerular filtration rates; sCre: Serum Creatinine; sCal: Serum calcium; sPhos: Serum phosphate; uOsmol:Urine osmolality.

DN [30,31]. By 18 weeks of age, ZSF1 renal function is significantly impaired under the study conditions described herein. Using defined estimated glomerular filtration rate (eGFR) staging criteria, ZSF1 rats possessed approximately 65% remaining eGFR function at the time of SRC implant. We measured survival of the ZSF1 rats under the conditions described herein up to 63 weeks of age (45 weeks on study). Only one of five untreated ZSF1 rats survived the study (80% mortality) compared with six of seven surviving animals in the treated group (1/7; <15% mortality). All of the lean animals were alive at the end of study. See [23] for additional details. Our attempts to intervene at a later time point (more chronic model) have been complicated by poor survival rates of these notably sicker animals following surgery. 18 weeks of age represents a reasonable compromise between development of clinically relevant disease criteria while maintaining acceptable survival outcomes postsurgery. Ethical considerations pertinent to the treatment of all research animals used in this study were evaluated by the Institutional Animal Care and Use Committee (IACUC) at the site of this research.

SRC renal cell culture & transplantation

The preparation of selected bioactive primary renal cells from whole rat kidney has been previously described in detail [21–23,29]. Briefly, whole kidneys were harvested from 5-week-old male Lewis rats (Hilltop Labs, PA, USA) and kidney tissue was dissociated enzymatically in a buffer containing 4.0 units/ml dispase (Stem Cell Technologies, Inc., BC, Canada) and 300 units/ml collagenase IV (Worthington Biochemical, NJ, USA). Red blood cells and debris were removed by centrifugation through 15% iodixanol (Optiprep®, Axis Shield, MA, USA). Primary renal cells were seeded onto tissue culture-treated polystyrene plates (NUNC, NY, USA) and cultured in 50:50 media, a 1:1 mixture of high glucose Dulbecco's Modified Eagle Medium (DMEM):keratinocyte serum-free medium (KSFM) containing 5% fetal bovine serum, 2.5 µg EGF, 25 mg bovine pituitary extract, 1× ITS (insulin/transferrin/sodium selenite medium supplement) and antibiotic/antimycotic (all from Invitrogen, CA, USA). Prior to postculture cell separation, primary renal cell cultures were transferred from atmospheric oxygen conditions (21%) to a more physiologically relevant low-oxygen (2%) environment for 24 h, to improve cell separation efficiency. Separation of primary renal cell cultures, prepared as 75 × 10^6 cells in 2 ml unsupplemented KSFM (uKSFM), was performed by centrifugation through a four-step iodixanol (OptiPrep; 60% w/v in uKSFM) density gradient-layered specifically for rodent (16, 13, 11 and 7%) in 15 ml conical polypropylene tubes and

Table 3. Renal biomarker profiles for 5/6 nephrectomized rodent models of chronic kidney disease treated with selected renal cells at 12 weeks on study.

Clinical biomarker (12 weeks post-T_x)	Sham nephrectomy (n = 5)	Nephrectomy (5/6) (n = 8)	SRC treatment (n = 3)	p-value
Glomerular function				
Serum creatinine (mg/dl)	0.4 ± 0.0	1.13 ± 0.15	0.70 ± 0.10	$p < 0.01$ and $p \geq 0.001$
BUN (mg/dl)	18.0 ± 1.41	45.71 ± 5.41	36.33 ± 7.77	$p < 0.05$ and $p \geq 0.01$
Tubular function				
Serum albumin (g/dl)	4.22 ± 0.08	2.84 ± 0.10	3.30 ± 0.10	$p < 0.001$
A:G ratio (A/G)	1.19 ± 0.04	0.80 ± 0.04	1.05 ± 0.12	$p < 0.01$ and $p \geq 0.001$

Means ± standard deviation, see also [22].
BUN: Blood urea nitrogen; SRC: Selected renal cell; T_x: treatment.

centrifuged at 800 g for 20 min at room temperature (without brake). After centrifugation, cellular subfractions were extracted from the gradient via pipette and collected as four distinct bands (B1–B4) and a pellet (B5). All bands were washed three-times with sterile phosphate buffered saline prior to use. Therapeutically bioactive renal cells were produced by combining B2 and band 4 (B4) from the density gradient centrifugation step at a ratio of 97% B2 to 3% B4. This results in a population of tubular cell-enriched cells previously demonstrated to significantly stabilize serum creatinine and blood urea nitrogen (BUN) and improve survival in the rodent 2-step 5/6N_x of CKD [21–23]. B1/B5 has been previously demonstrated to be therapeutically inert and functioned as a non-SRC cellular control [21–23]. B1 cells are predominantly distal tubular and collecting duct cells with trace amounts of other cell types. B5 contains vascular, endocrine and glomerular cells [21–23]. Recipient female Lewis 5/6N_x rats or male ZSF1 obese rats (all from Charles Rivers Laboratories) were anesthetized, and the kidneys for treatment were exposed by a ventral medial-lateral incision. Cell suspensions (100 µl) were loaded into a 1 cc syringe fitted with a half inch 23G needle (Becton Dickinson, RTP, NC, USA) and injected directly into the kidney parenchyma at a depth of 3–5 mm as previously described [21–23,29]. 5/6N_x Lewis rats received a single dose into the remnant kidney, while ZSF1 obese rats received four doses, one at each pole of each kidney.

SRC product potency

Assays for SRC product potency were based on functional characterization of B2-associated glutamyl transpeptidase (GGT1) activity and megalin:cubilin-mediated albumin transport as described in [22]. Specificity of albumin transport was demonstrated by blockage with RAP, a known competitive inhibitor of megalin:cubilin-mediated albumin uptake, and by absence of transport in the nontubular B4 subpopulation as described in [22].

Conditioned media

CM was derived from cultures of human SRC collected and centrifuged at 3500 g for 30 min at 4°C to remove debris and supernatant collected. To identify bioactive components, CM was subjected to ultracentrifugation at 200,000 g for 2 h at 4°C. The ultracentrifuge pellet (containing secreted vesicles) was resuspended in basal media (DMEM:KSFM alone) at 1/5 of the original volume. Supernatant media (here termed vesicle-free media [VFM]) was collected and further fractionated using Viva-spin™ semipermeable polyethersulfone membrane concentrators (GE Healthcare, NY, USA) with molecular weight cutoffs (MWCO) at 5, 10, 50 and 100 kDa.

Cell culture experiments & transfections

The human proximal tubule cell line, HK2 (ATCC) was maintained in 1:1 mixture of high glucose DMEM and KSFM containing 5% (v/v) fetal bovine serum, 2.5 µg EGF, 25 mg bovine pituitary extract, 1× ITS (insulin/transferrin/sodium selenite medium supplement) and 1× antibiotic/antimycotic (all from Life Technologies). HK2 cells were transfected using NF-κB reporter plasmid construct, pGL4.32[*luc2P*/NF-κB-RE/Hygro] (Promega, WI, USA) using Lipofectamine™-2000 transfection reagent (Life Technologies) and single clonal colonies subcultured through several passages in selective growth media containing 100 µg/ml Hygromycin B (Life Technologies) to generate a stable cell line. Transcriptional activation of the NF-κB reporter was determined using ONE-Glo™ luciferase reagent (Promega). For proliferation experiments, near-confluent

Table 4. Renal biomarker profiles for ZSF1 obese rats treated with selected renal cells at 16 or 24 weeks post-treatment, as percentage of baseline.

Clinical biomarker (16 or 24 weeks post-T_x)	ZSF (obese; n = 5)	ZSF (obese) + SRC (n = 5)	p-value
Glomerular function			
Serum creatinine (μmol/l)	53 ± 2.7	44.2 ± 1.8	0.014
BUN (mmol/l)	11.42 ± 0.75	8.21 ± 0.61	0.029
Tubular function			
Calcium (mmol/l)	3.02 ± 0.04	2.87 ± 0.03	0.020
Phosphorus (mmol/l)	2.23 ± 0.08	1.97 ± 0.06	0.030
Loop of Henle and collecting duct			
Urine osmolality (mOsmol/kg)	681 ± 48.7	901 ± 41.6	0.007
Urine specific gravity	1.034 ± 0.001	1.040 ± 0.001	0.001

See also [23].
BUN: Blood urea nitrogen; SRC: Selected renal cell.

monolayers of HK2 cells were serum starved in basal media (DMEM:KSFM) for 2 h prior to 24- and 48-h exposures to SRC-CM. CM was prepared as described above. CM was collected from rat and human cultures of SRC under serum- and supplement-free conditions and utilized for *in vitro* assays. Commercially available human-derived renal mesangial cells (HRMC) were used as surrogates for host-response tissues in the *in vitro* assays since mesangial cells express PAI-1 in injured/diseased kidneys. Vesicular particles shed by cells into the culture media were collected by high-speed centrifugation and total RNA was extracted from the pellet with TRIzol reagent (Invitrogen, CA, USA). RNA content of vesicles was screened using PCR-based arrays of known miRNA sequences with a focus on miRNAs known to be involved in fibrosis and inflammation (Qiagen, CA, USA). miRNA was synthesized (Invitrogen) for transfection using Lipofectamine-2000 according to manufacturer's instructions.

Quantitative RT-PCR

Total RNA was extracted from cells and tissues using the RNeasy-Plus Mini Kit/QIA-shredder (Qiagen). cDNA was synthesized from 700 ng total RNA using SuperScript® VILO™ cDNA Synthesis Kit (Life Technologies). Gene amplification was performed with ABI-Prism 7300 real-time PCR system using the following TaqMan® primer/probe sets (Life Technologies): rat *CCL5* (Rn00579590_m1), rat *CD68* (Rn01495634_g1), rat *CD3* (Rn01417940_m1), rat *PPIB* (Rn00574762_m1), rat Serpine (Rn00561717_ml), human *CCND1* (Hs00765553_m1), human *FOS* (Hs00170630_m1), human *PPIA* (Hs99999904_m1). Relative gene-expression was calculated using comparative cycle threshold (ΔΔCt) method with *PPIB* (rat tissues) or *PPIA* (human cells) as endogenous control. Values were calibrated to experimental controls (e.g., unmanipulated rats, unilateral N_x rats, basal media-treated cells).

Western blot

Kidney tissues were snap-frozen in liquid nitrogen and homogenized using mortar and pestle prior to lysis. Cell culture samples were processed directly without snap freezing. Nuclear and cytoplasmic fractions were isolated using the NE-PER extraction kit following manufacturer's protocol (Thermo Fisher Scientific, MA, USA). Western blotting was performed as described in [29]. Membranes were probed overnight at 4°C in 2% (w/v) nonfat milk in TBST with the following antibodies: 1:5000 anti-βActin (A5441, Sigma-Aldrich, MO, USA), 1:500 anti-IκBα (ab32518, Abcam, MA, USA), 1:250 anti-CD3 (ab5690, Abcam), 1:500 anti-CD68 (ab31630, Abcam), 1:250 anti-PTEN (ab32199, Abcam), 1:1000 anti-PCNA (ab29, Abcam), 1:500 anti-p65 (ab7970, Abcam), 1:20 anti-PAI-1 (612025 BD), 1:40 anti-FN (MAB1918, R&D), 1:1000 anti-p50 (ab32360, Abcam), 1:200 anti-Lamin B1 (ab16048, Abcam). For each western blot, n = 3 independent experiments were performed, with n = 3 replicates per protein of interest. Quantitation of western blots was performed with NIH Image J software [32].

Enzyme-linked immunosorbent assays

Protein concentration of kidney tissue lysates was determined by Bradford assay and normalized to final concentration of 25 μg/ml. Urine samples were diluted 1:200 for CCL2/MCP–1 and 1:1.5 for CCL5/RANTES. CCL2 and CCL5 concentrations were determined by ELISA following manufacturer's instructions (Ray-Biotech, GA, USA). Absorbance at 450 nm was determined on the FLUO-star Omega microplate reader (BMG Labtech, Offenburg, Germany).

Immunohistochemistry

Rat kidneys were fixed in formalin, processed for paraffin embedding, sectioned and stained by immunohistochemistry following standard protocols (Premier Labs, CO, USA). Primary antibodies used for immunohistochemistry were: anti-p65 (ab7970, Abcam), anti-CD3 (A0452, Dako, CA, USA), anti-CD68 (MCA341R, AbD Serotec) and anti-Ki67 (M7248, Dako). Quantitative image analysis was performed on anti-p65 (ab7970, Abcam) and anti-PAI-1 (ab28207, Abcam) stained sections from SRC-treated and untreated 5/6N_x and ZSF1 obese rats at end of study following standard protocols with Scanscope XT (Aperio, IL, USA), completed slides were scanned into digital images (apparent magnification 20×). Image analysis was performed with modified version of Aperio's positive pixel count algorithm (Premier Labs).

Immunofluorescence & image analysis

Cell immunofluorescence was as previously described [22,23]. Quantification of NF-κB bioactivity was based on scoring the number of positive nuclei. Image quantification was performed using IN Cell Analyzer, Multi-Target Analysis (MTA) software (GE Healthcare).

Statistical analysis

For gene- and protein-expression data in rat tissues/human cells, data are presented as average of three animals/replicates (except n = 2 for cell treatment group), with standard error of mean calculated for each group. Statistical significances between experimental groups were determined by unpaired, two-tailed student's *t*-tests. For urinary cytokine expression (CCL2, CCL5), multivariate models were constructed with JMP version 7.0 software (SAS Institute, NC, USA) to determine statistical significance of treatment effects. Effect of SRC-CM on translocation of NF-κB was tested using logistic regression analysis with JMP version 7.0 software (SAS Institute). Chi-square analyses were performed comparing the frequency of the 'high' and total ('high' + 'low') activation in basal media versus SRC-CM, with and without TNF-α stimulation.

Results

SRC product potency

Functional assays confirmed that the observed expression of GGT1 and cubilin resulted in active proteins [22]. Nitroaniline was produced by active GGT1 in B2 cells, and fluorescently tagged albumin was actively transported into cubilin-positive B2 cells [22]. Taken together, these data confirm SRC product potency prior to *in vivo* cell transplantation studies.

Progressive NF-κB activation & interstitial inflammation are features in the development of CKD in the 5/6 nephrectomy model

To understand the temporal dynamics of the 5/6N_x model of CKD and to evaluate involvement of NF-κB signaling in disease progression, we conducted a time-course analysis of 5/6N_x Lewis rats and assayed kidney tissue at 1, 2, 4, 6 and 8 weeks postsurgery. Unmanipulated control kidneys were collected at the beginning of the study. We observed a time-dependent increase in both expression and nuclear localization of NF-κB p65 subunit, particularly during the chronic phase of disease progression (2–8 weeks postnephrectomy), see histological outcomes summarized in Table 4.

In histological sections of remnant kidneys, few cells showed evidence of nuclear p65 at 2 weeks postnephrectomy; however, increase of cytoplasmic (inactive) p65 in distal tubular cells was observed (Figure 1A). At 6 weeks post-nephrectomy, robust p65 nuclear localization was observed in tubular epithelial cells and glomerular cells (Figure 1A). Significantly higher expression of p65 was observed in glomerular cells of 5/6N_x rats compared with the tubular compartment (Figure 1A). Increased NF-κB activity was confirmed semiquantitatively by p65 western blot analysis on cytoplasmic and nuclear extracts taken at selected time points during the 8-week study (Figure 1E). Data were quantified by calculating the ratio: intensity p65 (nucleus)/intensity p65 (cytoplasm) relative to the control sample (set as 1). As shown in Figure 1E, this ratio increased to 6.7 at 1-week postnephrectomy and increased further to 9.4 by 6-week postnephrectomy, confirming a significant transfer of cytoplasmic p65 to the nucleus in response to injury.

Beginning at the 2-week time point, *CCL5* gene-expression was increased four- to six-fold over unmanipulated controls and these levels were maintained throughout the remainder of the study (Figure 1B). Concomitant with the increase in CCL5 expression, a time-dependent increase in $CD68^+$ macrophages and $CD3^+$ T lymphocytes in the interstitial space was observed (Figure 1A). Increased presence of macrophages and T lymphocytes was assessed quantitatively by RT-PCR (Figure 1C) and by western blot (Figure 1D). Expression of CD68 relative to β-actin increased from 0.19 to 1.31 at 1-week postinjury before dropping to 0.49 at 8 weeks postinjury. Expression of CD3 increased much more slowly, with a relative expression level of 0.63 at 4 weeks postinjury, rising to 2.24 by 8 weeks postinjury.

Transplanted SRC attenuate NF-κB & PAI-1 activation & reduce macrophage & T-cell infiltration in the 5/6 nephrectomy model

Clinical outcomes associated with SRC treatment of 5/6N_x rodents are summarized in Table 3. Statistically

significant improvement in glomerular function was observed at 12 weeks post-treatment, with serum creatinine dropping from 1.13 ± 0.15 to 0.70 ± 0.10 mg/dl. BUN dropped from 45.71 ± 5.41 to 36.33 ± 7.77 mg/dl. In addition, statistically significant improvement in tubular function was observed at 12 weeks post-treatment, with serum albumin levels rising from 2.84 ± 0.10 to 3.30 ± 0.10 g/dl. A:G ratio (albumin:globulin) rose from 0.80 ± 0.04 to 1.05 ± 0.12. No untreated animals survived the entire 6 month time-course. IHC analysis at time of death revealed intense, widespread expression and nuclear localization of p65 throughout

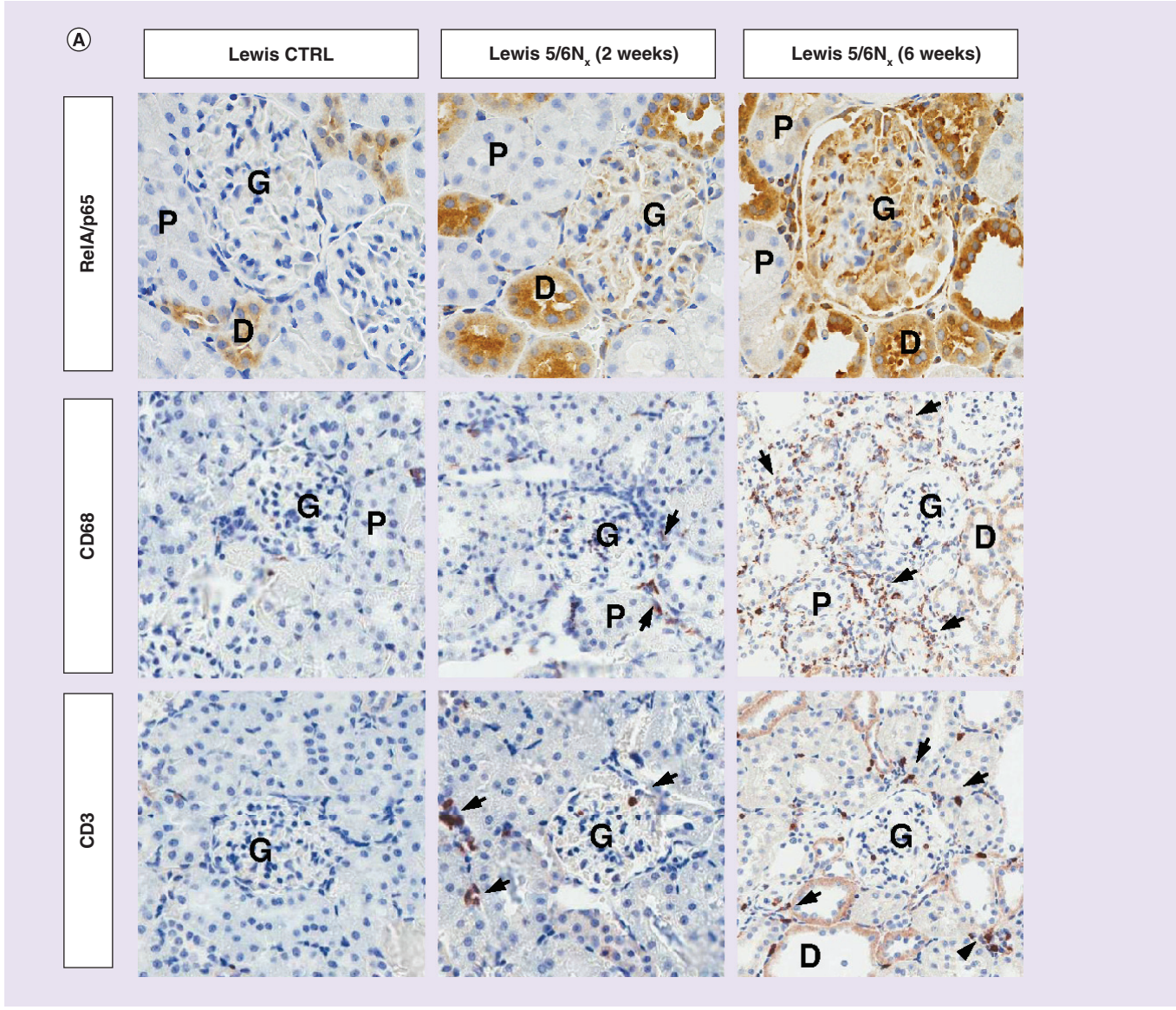

Figure 1. Immunohistological and molecular characterization of 5/6 nephrectomy Lewis rat model. Immunohistochemical staining for NF-κB subunit p65 in unmanipulated CTRL rats compared with animals subjected to 5/6 nephrectomy procedure (**[A]** top row). Nuclear staining (arrows) indicates NF-κB-activated cells. Infiltration of macrophages and T lymphocytes as identified by CD68 and CD3 immunostaining (arrows), respectively, is observed in nephrectomized animals at 2 and 6 weeks postprocedure (**[A]** middle and bottom rows). Whole tissue lysates were assayed for CCL5 by quantitative real-time PCR **(B)**. Increased presence of CD68 and CD3 expressing cells was confirmed by quantitative real-time PCR (**[C]**). Semiquantitative western blot analysis on whole kidney lysates at 1, 2, 4, 6 and 8 weeks postnephrectomy **(D)** demonstrates increased IκBα stability as well as increased presence of macrophages and T lymphocytes (CD68, CD3) with disease progression. Analysis of cytoplasmic ('C') and nuclear ('N') lysates from kidney tissues at 1, 2, 4, 6 and 8 weeks postnephrectomy **(E)** reveals progressive nuclear localization of the p65 subunit. LB1 is used as a nuclear fraction loading control. For western blots in **(D)**, band densities were quantified relative to internal control (β-actin) and are expressed below each band. For western blot in **(E)**, band densities were quantified by calculating the ratio N/C (nuclear p65/cytoplasmic p65). The N/C ratio for the control was set at 1 and all treatment conditions expressed relative to control.
CTRL: Control; D: Distal-convoluted tubule; G: glomerulus; N_x: Nephrectomy; P: Proximal-convoluted tubule.

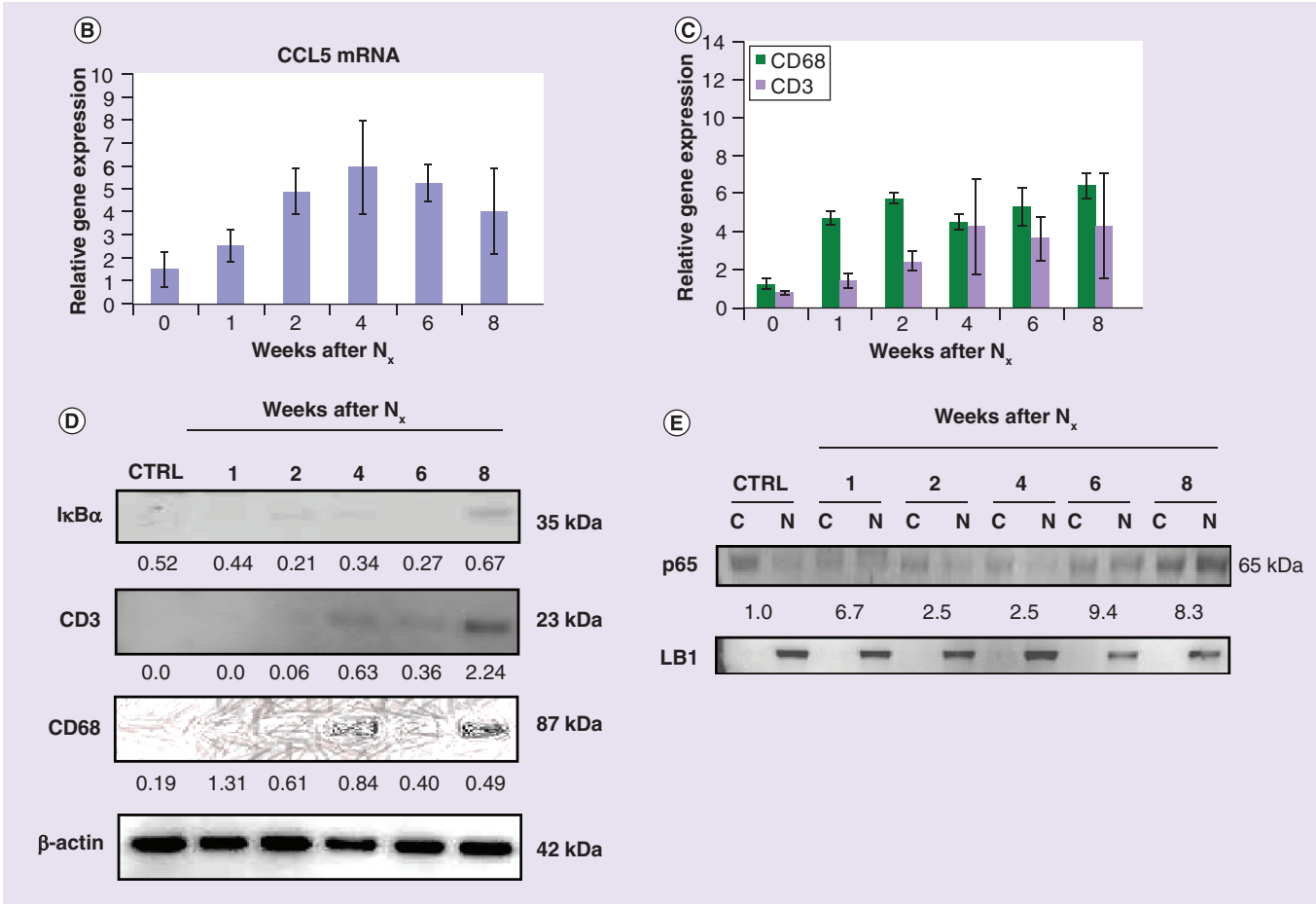

Figure 1. Immunohistological and molecular characterization of 5/6 nephrectomy Lewis rat model (cont.).

kidney tissue (Figure 2A). In addition, extensive infiltration of $CD68^+$ and $CD3^+$ leukocytes was observed (Figure 2A). Nuclear localization of p65 subunit was not widely observed in healthy, unilaterally nephrectomized animals and $CD68^+$ and $CD3^+$ cells were scarce in those tissues (Figure 2A). SRC-treated tissues displayed decreased p65 nuclear localization and reduced numbers of both $CD68^+$ and $CD3^+$ leukocytes, while B1/B5 (non-SRC cell control) treated animals resembled untreated disease state (Figure 2A). Quantitative IHC analysis at time of death of untreated animals in Lewis 5/6N_x confirmed upregulation of NF-κB p65 and *PAI-1* expression. Treatment with SRC significantly reduced both NFkB-p65 and *PAI-1* expression levels (Figure 2B & C & Table 3). These observations were confirmed by gene-expression and western blot on whole lysates from representative tissue samples (Figure 2D & E). Quantitative western analysis of relative (to β-actin) *PAI-1* expression showed a significant reduction from 148.2 in nephrectomized animals at <100 days on study to 31.2 upon SRC treatment at <100 days on study. FN (another marker of fibrosis) levels were also reduced in SRC-treated animals (Figure 2E) at <100 days on study, with relative expression levels falling from 108 to 44 upon SRC treatment. Similar results were observed >100 days on study: relative *PAI-1* expression fell from 106.1 to 28.5 upon SRC treatment and relative FN expression levels dropped from 108.6 to 68.1.

Additional evidence demonstrating attenuation of NF-κB signaling in SRC-treated animals was provided by gene-expression and western blot analysis of nuclear localization of NF-κB p65. Compared with untreated 5/6N_x controls and B1/B5-treated animals, SRC-treated tissues had reduced levels of nuclear p65 (Figure 2H). Quantitation of nuclear p65/cytoplasmic p65 was performed relative to hemi-N_x control animals. As observed previously (Figure 1E), response to full 5/6N_x is associated with significant cytoplasmic to nuclear transfer of p65, with relative expression levels increasing to 4.2 (Figure 2H) but reduced to 0.4 upon treatment with SRC. Treatment with B1/B5 only resulted in reduction to a relative expression level of 2.2. In addition, treatment with SRC reduced relative expression of CD3 from 0.70 (pre-treatment) to 0.22, comparable to the hemi-N_x control expres-

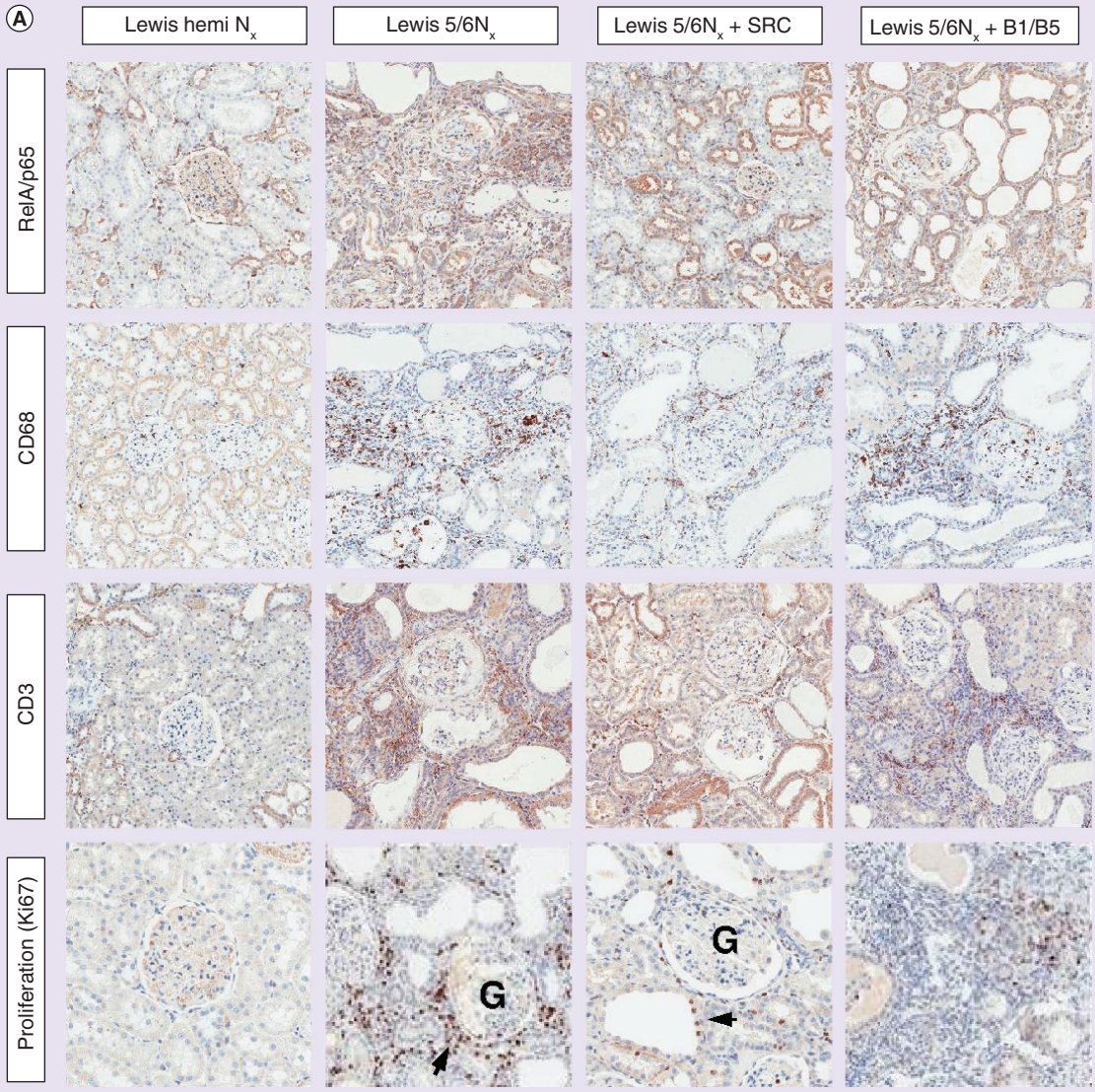

Figure 2. Transplantation of selected renal cell into 5/6 nephrectomy model attenuates NF-κB activity and alters inflammatory profile of kidney. Kidney tissue was harvested 6 month post-transplantation or at time of death, in rats treated with SRC or B1/B5 cells. Hemi-N_x and 5/6N_x animals were carried as healthy and diseased controls, respectively. Immunohistochemistry for the NF-κB p65 subunit, CD68, CD3 was performed to assess the inflammatory state of tissues **[A]**, top three rows). Cellular proliferation in tissues was determined by Ki67 immunostaining **[A]**, bottom row). Tissue protein levels of NF-κB p65 subunit and PAI-1 at end-of-study were significantly reduced in 5/6N_x + SRC animals **[B]**, magnification 20× and 200× in-lay) compared with untreated controls by quantitative immunohistochemistry **[C]**, quantitation of PAI-1 and NF-κB p65 staining, n = 3). Tissue lysates (n = 3, except n = 2 for B1/B5 treatment) were assayed for *CCL5* expression by quantitative real time-PCR **(F)** and *CCL2* expression by ELISA **(G)**. Error bars represent standard error of mean in each experimental group. Quantitative real time-PCR was conducted on kidney tissue harvested at necropsy and relative gene-expression values plotted against time (days) on study. 5/6N_x animals (red squares) demonstrated more robust expression of PAI-1 relative to those treated with bioactive renal cells (blue diamonds) and sham-operated controls (green triangles) **(D)**. Representative western blot analysis of kidney samples taken at 3 and 6 months post-treatment. Treated tissues of 5/6N_x rats (N_x + SRC) showed reduced accumulation of PAI-1 and FN protein, normalized to β-actin by the formula: (intensity PAI1 or FN/intensity β-actin) ×100 **(E)**. Western blot analysis confirmed increased nuclear localization of NF-κB p65 **(H)** in diseased and B1/B5-treated rats compared with healthy and SRC-treated rats. Reduction of nuclear p65 corresponded with decreased IκBα, CD3 and CD68 **(I)**. For western blot in 1H, band densities were quantified by calculating the ratio N/C (nuclear p65/cytoplasmic p65). The N/C ratio for the control (hemi-Nx) was set at 1 and all treatment conditions expressed relative to control. In **(I)**, quantitation of band density shown as (intensity marker/intensity β-actin).
C: Cytoplasm; Hemi: Unilateral; N: Nucleus; N_X: Nephrectomy; Sham: Sham surgery; SRC: Selected renal cell.

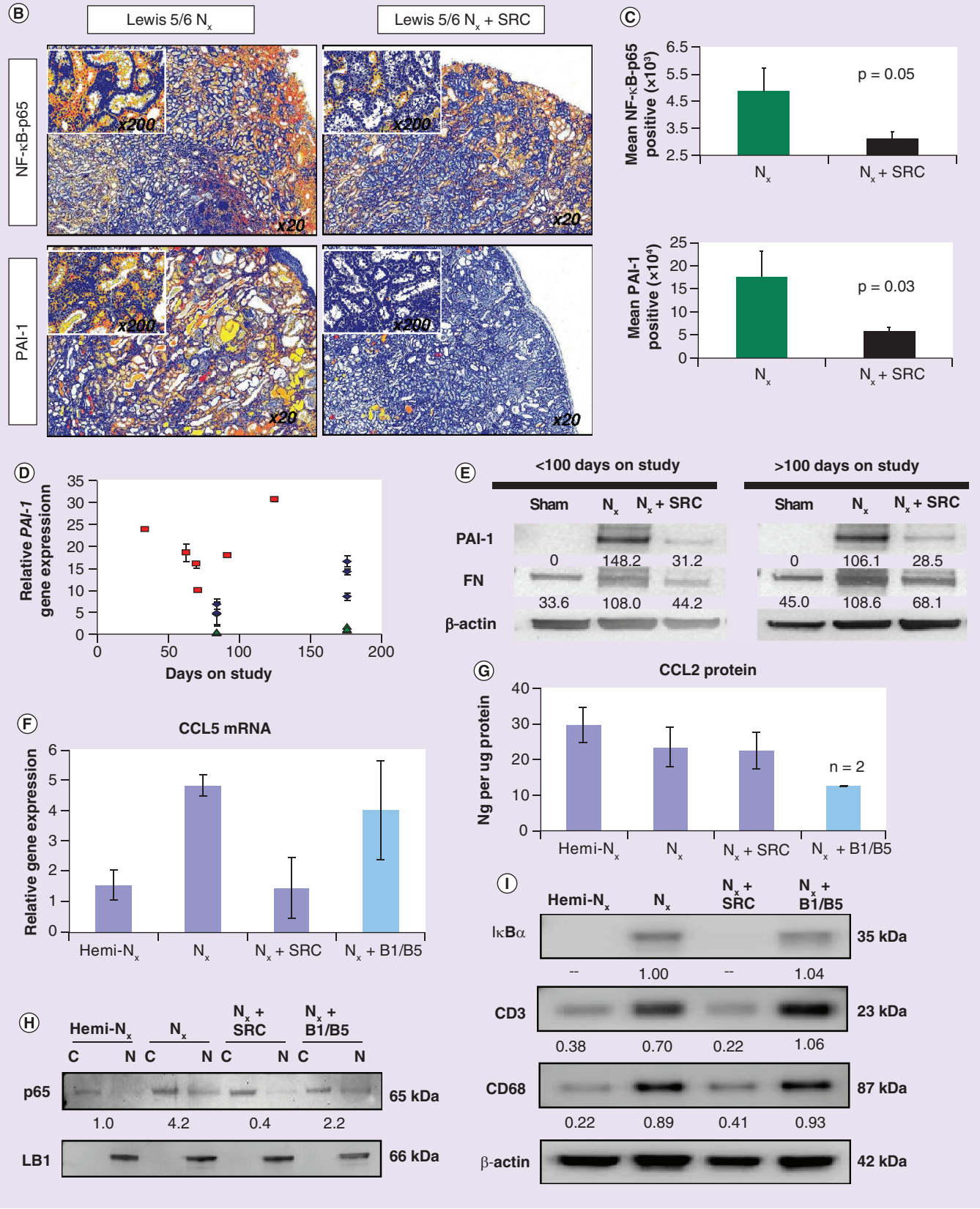

Figure 2. Transplantation of selected renal cell into 5/6 nephrectomy model attenuates NF-κB activity and alters inflammatory profile of kidney (cont.).

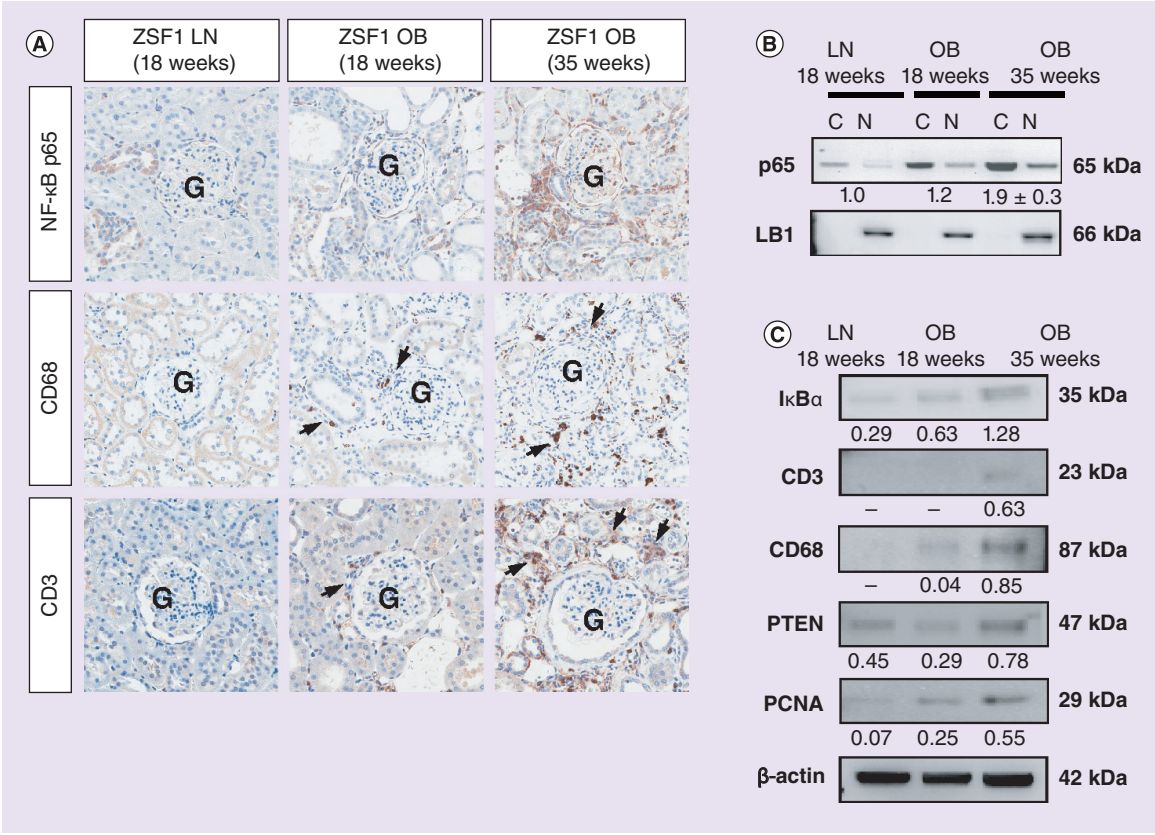

Figure 3. Immunohistochemical and molecular characterization of ZSF1 rat model. Kidney tissues from lean, 18-week-old ZSF1 rats were compared with obese ZSF1 rats at 18 and 35 weeks of age. Immunostaining for p65, CD68 and CD3 demonstrate increased inflammatory states in diseased animals, which increases over time (**[A]**, arrows). Western blot analysis for nuclear p65 **(B)**, as well CD68 and CD3 in whole lysates, confirms those observations **(C)**. IκBα, PTEN and PCNA also increase in diseased tissues and are dependent on age **(C)**. For western blot in **(B)**, band densities were quantified by calculating the ratio N/C (nuclear p65/cytoplasmic p65). The N/C ratio for the control (LN, 18 weeks) was set at 1 and all treatment conditions expressed relative to control. In **(C)**, quantitation of band density shown as (intensity marker/intensity β-actin).
C: Cytoplasm; G: Glomerulus; LN: Lean; N: Nucleus; OB: Obese.

sion level of 0.38. By contrast, treatment with B1/B5 resulted in an increase of CD3 relative expression levels to 1.06 (Figure 2I). Similarly, SRC treatment reduced expression of CD68 from 0.89 to 0.41 (relative to β-actin), comparable to the hemi-N_x control expression level of 0.22, whereas treatment with B1/B5 caused an increase in CD68 relative expression to 0.93 (Figure 2I). Finally, CCL5 gene-expression levels in SRC-treated rats were comparable to untreated healthy controls (Figure 2F), while CCL2 expression remained unaltered (Figure 2G).

Transplanted SRC promote tubular cell proliferation in 5/6N_x rats

Rodent tissues were evaluated by immunohistochemistry for the cell cycle marker Ki67. SRC treatment increased the number of proliferating cells specifically in the tubular epithelia (Figure 2A). By comparison, few $Ki67^+$ epithelial cells were observed in untreated and B1/B5-treated kidneys. However, several proliferative cells were observed in the interstitial compartment (Figure 2A), see also Table 3.

Transplanted SRC attenuate NF-κB signaling & PAI-1 expression in ZSF1 model of DN

Clinical outcomes associated with SRC treatment of ZSF1 rodents are summarized in Table 4. Statistically, significant improvement in glomerular function was observed at 16 weeks post-treatment, with serum creatinine dropping from 53 ± 2.7 to 44.2 ± 1.8 μmol/l. BUN dropped from 11.42 ± 0.75 to 8.21 ± 0.61 mmol/l. In addition, statistically significant improvement in tubular function was observed at 24 weeks post-treatment, with excreted calcium levels dropping from 3.02 ± 0.04 to 2.87 ± 0.03 mmol/l. Excreted phosphorus dropped from 2.23 ± 0.08 to 1.97 ± 0.06 mmol/l. Finally, biomarkers associated with function of the Loop of Henle and collecting ducts

also showed statistically significant improvement at 16 weeks post-treatment, with urine osmolality increasing from 681 ± 48.7 to 901 ± 41.6 mOsmol/kg and urine specific gravity increasing from 1.034 ± 0.001 to 1.040 ± 0.001. Baseline indices for all renal biomarkers in the ZSF1 model are reported in [23].

To ascertain the involvement of NF-κB signaling in progression of CKD in a different rodent model, we conducted molecular analysis on tissues derived from ZSF1 lean (i.e., nondiseased) and obese (i.e., diseased) rats. IHC analysis of kidneys revealed that by 18 weeks of age, obese rat kidney tissues are more highly activated for NF-κB pathways compared with lean littermates based on the increased expression and nuclear localization of the p65 subunit (Figure 3A). By 35 weeks of age, obese rats demonstrated more robust NF-κB activation compared with 18-week-old obese rats, reflecting the progressive nature of DN (Figure 3A). Western blot analysis was performed on cytoplasmic and nuclear extracts from 18-week-old lean, 18-week-old obese and 35-week-old obese rat kidneys to semiquantitatively assess the activation levels of NF-κB. Transfer of p65 from cytoplasm to nucleus was observed during development of the diabetic condition in the ZSF1 rodent: By 35 weeks, the ratio p65(nucleus)/p65(cytoplasm) in the obese animal had increased to 1.9 relative to the lean rodent at 18 weeks (Figure 3B). This was accompanied by increases in the relative expression levels of IκBα (increased from 0.29 in lean rodents at 18 weeks to 1.28 in obese rodents at 35 weeks), CD3 (increased from 0 in lean rodents at 18 weeks to 0.63 in obese rodents at 35 weeks), CD68 (increased from 0 in lean rodents at 18 weeks to 0.85 in obese rodents at 35 weeks), PTEN (increased from 0.45 in lean rodents at 18 weeks to 0.78 in obese rodents at 35 weeks) and PCNA (increased from 0.07 in lean rodents at 18 weeks to 0.55 in obese rodents at 35 weeks) (Figure 3C). This analysis confirmed that expression and nuclear localization of p65 as well as other proinflammatory markers including IαBα increased in obese rats over time.

IHC analysis on 18-week-old lean, 18-week-old obese and 35-week-old obese rat kidneys for expression of CD68 and CD3 showed an increased presence of monocytes/macrophages and T lymphocytes in the peritubular and periglomerular spaces in obese kidney tissues compared with lean control tissues (Figure 3A). The number of leukocytes increased over time in diseased animals. Tissue levels of PAI-1 were measured at end stage of disease using quantitative IHC analysis of ZSF1 obese untreated and SRC-treated animals. As observed in 5/6N$_x$ rats, SRC treatment was associated with reduction in expression of urinary CCL5 (but not urinary CCL2), NF-κBp65 and PAI-1 (Figures 4A & B & 5A & B).

CM from human SRC can attenuate NF-κB activation *in vitro* independent of vesicle-mediated cell signaling

To mimic the disease state, HK2 cells were cultured for 30 min with TNF-α to drive NF-κB activation. We tested NF-κB activation by exposing HK2 cells to 10 ng/ml TNF-α under serum- and supplement-free conditions and assayed for nuclear localization of p65 by immunofluorescence (Figures 6A & B & 7A).

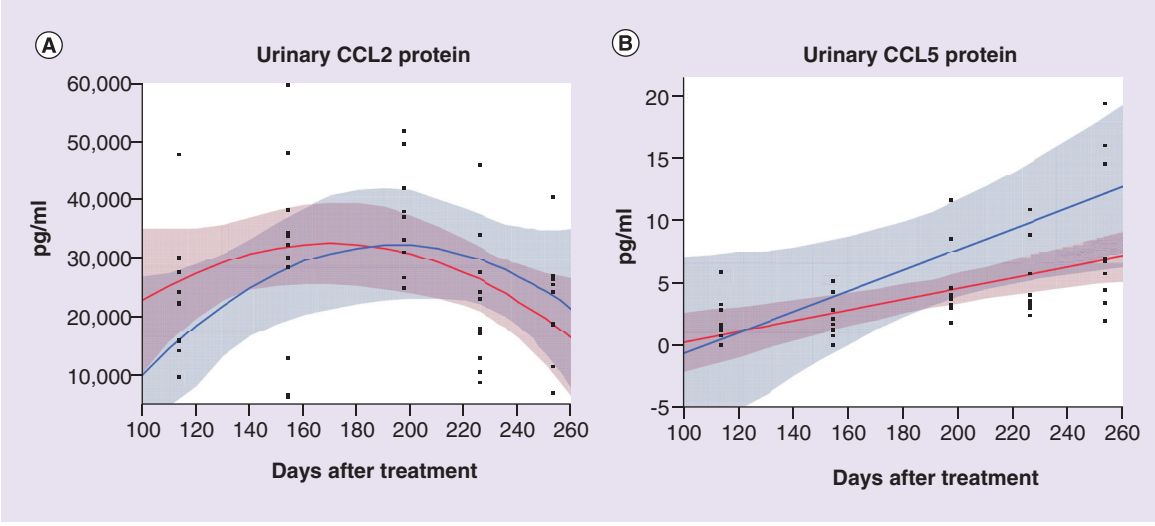

Figure 4. Urinary cytokines in ZSF1 rats treated with selected renal cell. Urinary **(A)** CCL2 and **(B)** CCL5 as a measure of tissue-level inflammatory states of the kidney were assayed by ELISA at regular intervals over the course of the study. Based on these data, multivariable models were generated by JMP version 7.0 software, with the blue-shaded regions representing modeled cytokine excretion (CCL2, CCL5) in untreated ZSF1 obese rats (n = 5) and the red-shaded region representing modeled cytokine excretion in selected renal cell-treated ZSF1 obese rats (n = 7).

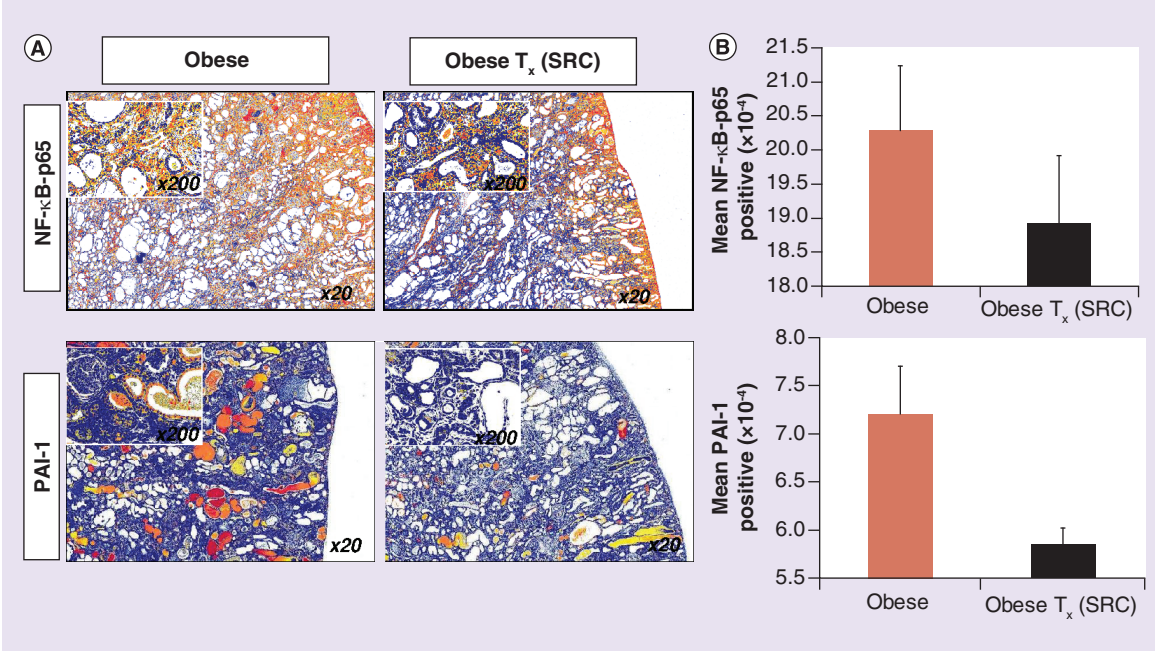

Figure 5. Immunohistochemical analysis of ZSF1 rats treated with selected renal cell. Tissue protein levels at end of study of NF-κB-p65 subunit and PAI-1 were significantly reduced in ZSF1-obese-treated animals (**[A]**, magnification 20× and 200× in-lay) compared with untreated controls by quantitative immunohistochemistry (**[B]**, n = 3).
SRC: Selected renal cell; T_x: Treatment.

Preincubating HK2 cells with CM derived from unfractionated renal primary cells for 2 h was effective in attenuating TNF-α-induced p65 nuclear localization response (Figure 7A). Nuclear-localized p65 in HK2 cells (sum of low and high activation) under basal control conditions was observed in approximately 30% of culture and increased to approximately 50% upon TNF-α stimulation. SRC-CM reduced p65 nuclear localization (sum of low and high activation) in unstimulated cells to approximately 12%, but did not alter percentage of total p65 nuclear localization after addition of TNF-α (activation remaining at approximately 50%). However, SRC-CM reduced total percentage of highly activated cells from 32% (basal media with TNF-α) to 16% (SRC-CM + TNF-α) (Figure 7B). Western blot analysis confirms primary renal cell-derived CM attenuated TNF-α-mediated NF-κB activation, shown by reduced presence of both p65 and p50 subunits in nuclear lysates (Figure 7C).

In vitro experiments were repeated using an HK2 line containing NF-κB reporter construct with luciferase gene-expression under control of five tandem repeats of NF-κB response elements (Promega). Here, TNF-α induced robust dose-dependent luciferase expression after 4 h of incubation (Figure 8A). Cells preincubated with SRC-CM for 24 h prior to activation showed significant reduction in basal luciferase activity (Figure 8A) and this suppressive activity was maintained at TNF-α exposures of 0.1, 1.0 and 10 ng/ml. To identify bioactive component(s) of SRC-CM responsible for NF-κB attenuation capacity, media was subjected to ultracentrifugation at 200,000 g. Supernatant media was depleted of large particles (including secreted vesicles) while still containing soluble proteins and metabolites. This VFM was sufficient to reduce NF-κB activation *in vitro* at a magnitude comparable to noncentrifuged SRC-CM (Figure 8A). Components of the 200,000 g pellet were resuspended in serum- and supplement-free media, concentrating the components by a factor of five. This pellet was unable to attenuate NF-κB activity (Figure 8A). These data indicate that NF-κB suppressor(s) contained within SRC-CM are not directly associated with secreted vesicles.

In order to further identify bioactive component(s), vesicle-free CM was fractionated by passing samples through semipermeable polyethersulfone membranes with MWCO at 5–100 kDa. This strategy was employed to narrow down sizes of bioactive particle(s) present in CM. Each flow-through fraction was tested for capacity to inhibit NF-κB reporter activity *in vitro*. 100 and 50 kDa filtrates retained suppressive activity on TNF-α-induced NF-κB (data not shown). However, 10 and 5 kDa membranes did not eliminate NF-κB-suppressive

component (Figure 8B), indicating that the bioactive component is smaller than 5 kDa.

Secreted vesicles in CM from rat & human SRC can attenuate PAI-1 expression *in vitro*

CM from rat and human SRC attenuated expression of PAI-1 from cultured HRMC induced (+) and uninduced (-) with TGF-β1 (Figure 9A & B). To identify bioactive component(s) of SRC-CM responsible for PAI-1 attenuation capacity, media was subjected to ultracentrifugation at 200,000 g. CM supernatant collected postcentrifugation was less effective at attenuating PAI-1 expression relative to control CM (Figure 9A & B), suggesting that the CM component responsible for observed attenuation of PAI-1 protein is associated with an insoluble cellular element.

To evaluate this hypothesis, we have examined the miRNA profile of secreted vesicles isolated from human and rodent SRC-CM against PCR arrays of established miRNAs. A detailed characterization of the SRC-CM miRNA profile will be published elsewhere [Basu *et al.* (2016), Manuscript in Preparation]. In the current manuscript, we analyze miRNAs specifically and directly linked to the PAI-1/NF-κB signaling pathway.

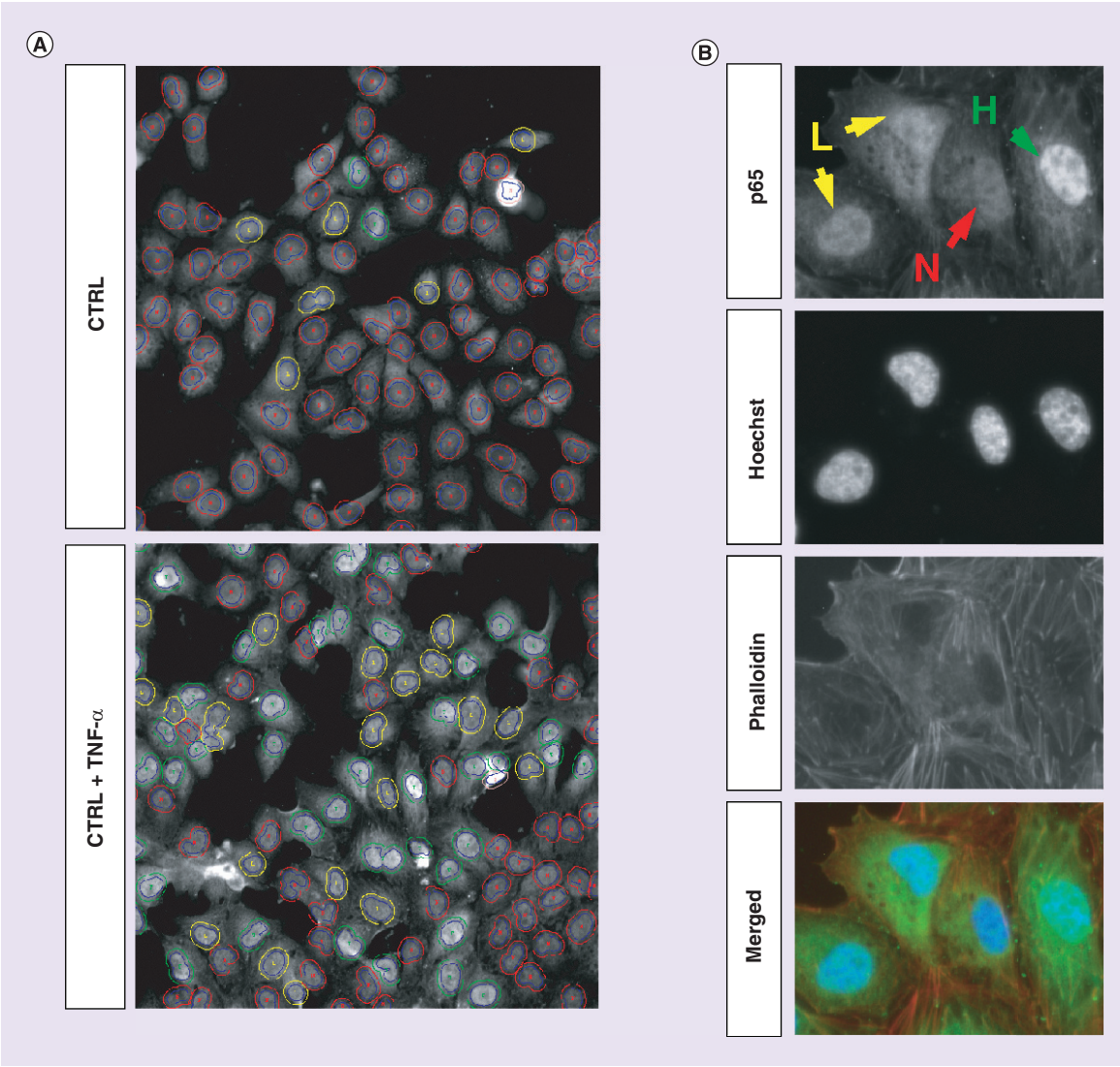

Figure 6. Quantification of p65 nuclear localization. (A) Cells that were untreated or treated with 10 ng/ml TNF-α were assessed for NF-κB activation by p65 immunofluorescence. Grayscale images were taken at 200× magnification, and analyzed with a classifier filter based on nuclear intensity. Nuclear boundaries (blue lines) were defined by Hoescht dye. Red lines identify 'N', yellow lines identify 'L' and green lines identify 'H'. **(B)** Higher power view of representative cells that were categorized as 'N' (red), 'L' (yellow) and 'H' (green). Cells were counterstained with Hoescht dye to define nuclear boundaries and Alexa-Fluor 594-phallodin to better visualize individual cells **(B)**.
CTRL: Control; H: High activation; L: Low activation; N: No activation.

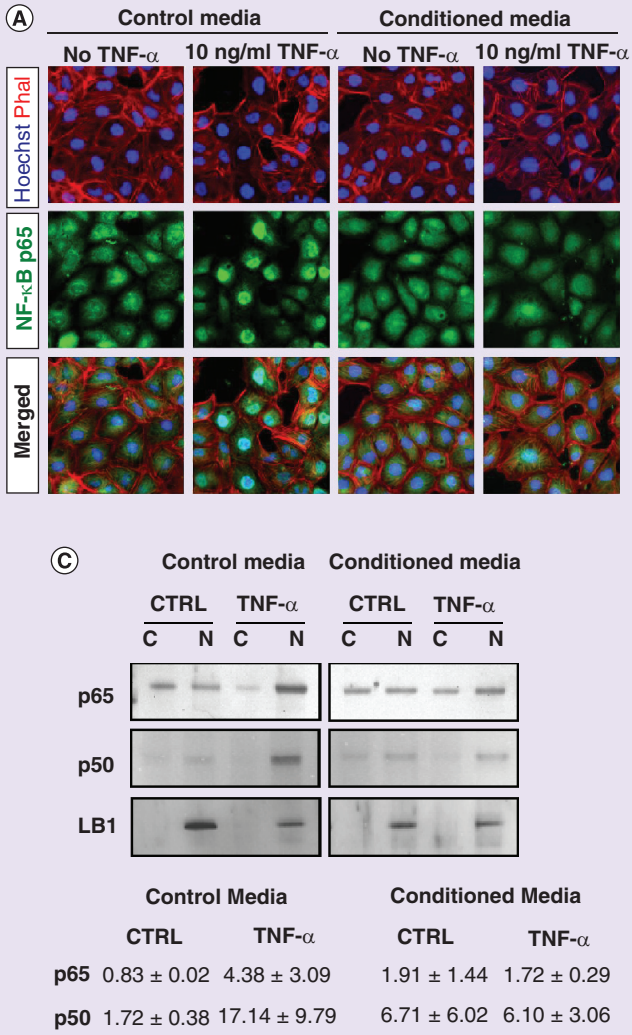

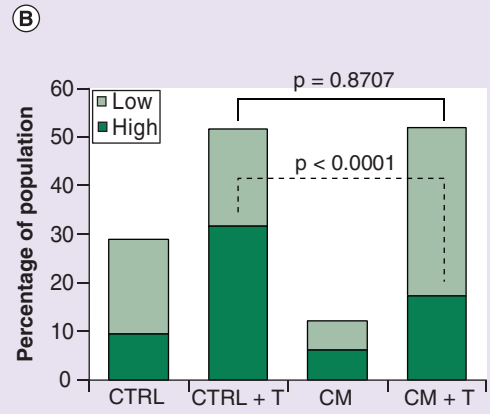

	No activation (<110 units)		Low activation (110–130 units)		High activation (>130 units)	
CTRL	213/299	71.2%	59/299	19.7%	27/299	9.0%
CTRL TNF-α	174/362	48.1%	72/362	19.9%	116/362	32.0%
CM	258/293	88.1%	18/293	6.1%	17/293	5.8%
CM TNF-α	135/274	49.3%	94/274	34.3%	45/274	16.4%

Figure 7. Extracellular factors attenuate NF-κB activation in target epithelial cells. (A) Immunofluorescence assay to determine nuclear localization of p65 (Alexa-Fluor 488, green) in HK2 cells that were unstimulated or stimulated with 10 ng/ml TNF-α for 30 min. Cells were counterstained with Hoechst (blue) and Alexa-Fluor 594-phalloidin (red). Cells were pretreated with basal media or CM from selected renal cell for 2 h prior to TNF-α induction. **(B)** All cells from three fields of view for each condition were classified into three categories (high activation, low activation and no activation) based on staining intensity for p65 and plotted as percentages of the total cell populations. **(C)** Western blot analysis confirms that pretreating HK2 cells with selected renal cell-CM can reduce nuclear localization of p65 as well as NF-κB-p50 subunit. LaminB1 was used as a nuclear fraction ('N') loading CTRL and was not detected in cytoplasmic extracts ('C'). Quantitation of the blot is through the formula intensity (p65/p50 N)/intensity (p65/p50 C).
C: Cytoplasm; CM: Conditioned media; CTRL: Control; N: Nucleus; T: TNF-α.

miR-449a, a possible regulator of PAI-1 [33,34], was identified for additional functional evaluation. Other miRNAs of interest include miR-21 (RNA target: Pellino-1), miR-146a (RNA target: IRAK/TRAF6), miR-30b-5p (both regulators of PAI-1), miR-124 and miR-151 (RNA target: NF-κB). To evaluate the potential functional role of miR-449a, HRMC were transfected with miR-449a and exposed to 5 ng/ml TGF-β1 for 24 h. The expression of PAI-1 and β-actin by was evaluated by western blot. As shown in Figure 9C, transfection of synthetic miR-449a reduced TGF-β-induced expression of PAI-1 protein (from a relative expression level of 1.68 to 1.09, Figure 9C).

Nonvesicle components of SRC-CM induce tubular cell proliferation

Near-confluent monolayers of HK2 cells were cultured with SRC-CM or basal control media for 24 and 48 h and assayed by qRT-PCR for cell cycle genes Cyclin D1, and *FOS*. SRC-CM increased Cyclin D1 gene-expression approximately twofold after 48 h of culture compared with basal media con-

trols (Figure 10A). *FOS* gene-expression was increased approximately twofold at 24 h, but returned to a level comparable to control media after 48 h of culture (Figure 10B). To determine if trophic factors were vesicle-associated components, we depleted SRC-CM by ultracentrifugation at 200,000 g. As before, pelleted vesicles were resuspended in basal media and concentrated fivefold. Direct comparison between vesicle-rich and vesicle-depleted SRC media shows proliferation (assessed by Cyclin D1 and *FOS*) is enhanced in target epithelia by nonvesicular factors (Figure 10A & B).

Discussion

We have previously established the therapeutic effects of autologous native renal cells isolated from kidney tissue as primary cultures in progressive models of CKD; a summary of the overall study design is presented in Tables 1 & 2, and specific clinical outcomes in these rodent models are described in detail in [21–23,29], and will not be repeated here. However, specific mechanistic pathways and networks leading to observed disease-related outcomes within these models remain undefined, with concomitant ambiguity regarding MOA of SRC-based therapies under evaluation. Two-step 5/6 nephrectomy (5/6N$_x$) in rodents reproducibly generates terminally progressive renal failure with characteristic systemic and histological parameters of CKD (e.g., hypertension, reduced glomerular filtration rate, elevated serum creatinine and BUN, glomerular and tubulointerstitial fibrosis, hyperlipidemia, hyperphosphatemia and anemia) [21–23]. These clinically relevant features of the 5/6N$_x$ model combined with technical reproducibility and commercial availability provide the basis for its selection as a disease model for CKD. In addition, diabetes is the most important risk factor for CKD and ESRD. We have previously evaluated function, structure and lifespan of the ZSF1 diabetic rodents and demonstrated clinically relevant functional outcomes from SRC-cell therapy [23]. Extension in ZSF1 rodent survival following SRC treatment was accompanied by significant improvements to renal structure and function in multiple renal tissue niches [23].

Direct injection of these bioactive renal cell subpopulations in the rat 5/6N$_x$ model of CKD resulted in extended survival and enhancement of renal function for 6 month post-treatment [22]. That study also presented evidence that a potential MOA by which regenerative outcomes in the treated tissue occurred was consistent with mechanistic models currently under consideration for the therapeutic action of adult-derived stem cells [16,35–36]. Such MOAs leverage paracrine factors secreted by bioactive adult-derived cells to catalyze the mobilization of resident, host-derived stem cell populations, to ameliorate fibrosis and inflammation, to facilitate angiogenesis and neo-vascularization,

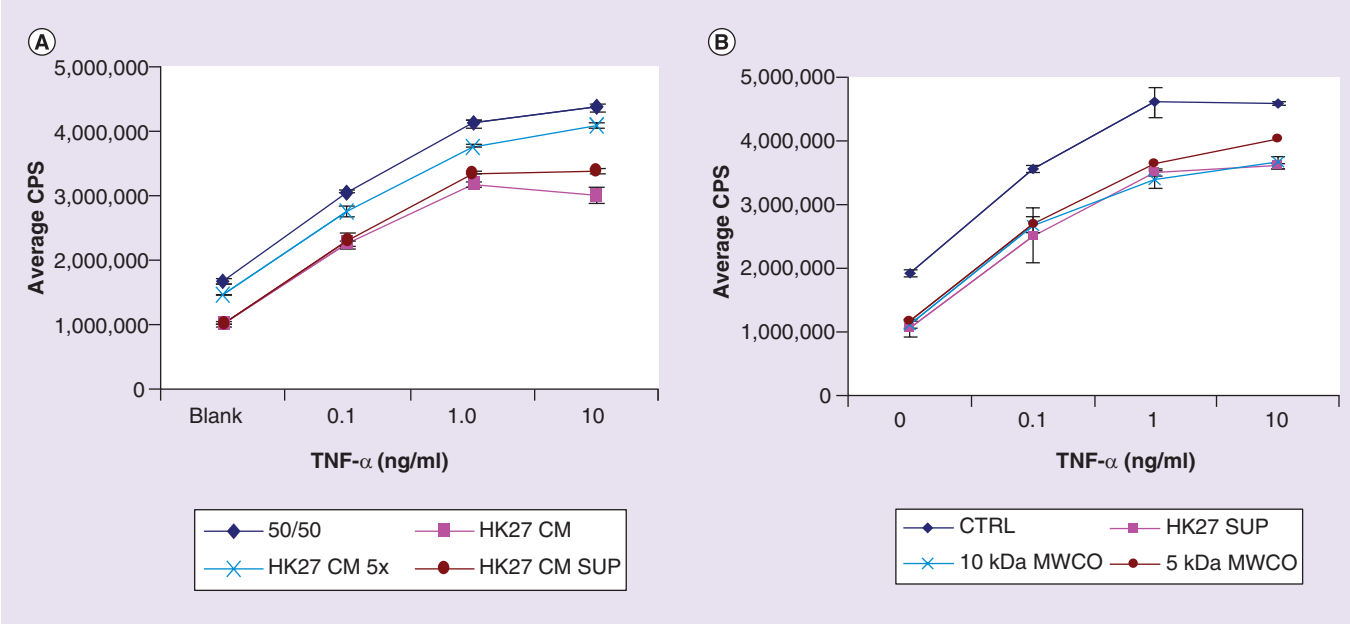

Figure 8. Nonvesicle components of selected renal cell-conditioned media inhibit TNF-α-mediated NF-κB activation. (A) HK2 cells transfected with an NF-κB luciferase reporter construct were pretreated for 16 h with basal media or CM from selected renal cell then subsequently stimulated with TNF-α for 4 h. The NF-κB inhibitory component is associated with the nonvesicular components of the CM. **(B)** Size exclusion based on MWCO of 10 and 5 kDa revealed that the NF-κB inhibitory component is smaller than 5 kDa. Error bars represent the standard deviation of three experimental replicates.
CM: Conditioned media; CPS: Counts per second; CTRL: Control; MWCO: Molecular weight cutoffs; SUP: Supernatant.

and to modulate the immune response. Evidence for the mobilization of resident stem cell populations in rodent 5/6N_x CKD models following SRC treatment has been provided by studies showing activation of key markers associated with host stem cell populations upon SRC implant [29]. Engraftment of delivered SRC has been established up to 6 months postimplantation only in the targeted kidney [21–23]. Consistent with paracrine-based models of MSC bioactivity and experimental evidence that SRC produce factors that can potentially alter the balance between fibrosis and regenerative pathways in diseased kidney tissue are the secretomic profiles of bioactive renal cell populations [37]. Both SRC in 2D culture and 3D culture

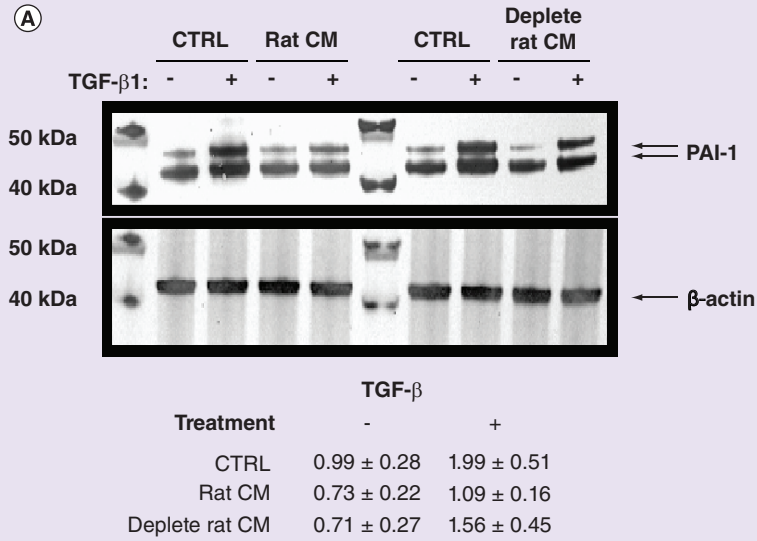

Treatment	-	+
CTRL	0.99 ± 0.28	1.99 ± 0.51
Rat CM	0.73 ± 0.22	1.09 ± 0.16
Deplete rat CM	0.71 ± 0.27	1.56 ± 0.45

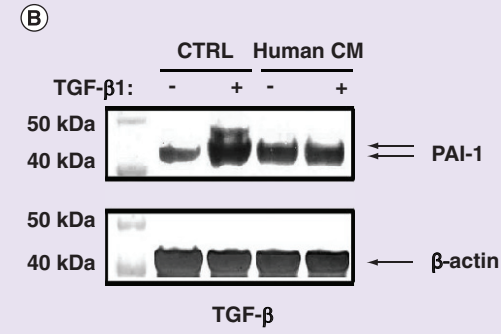

Treatment	-	+
Control media	0.89 ± 0.15	1.84 ± 0.13
Human conditioned	0.71 ± 0.15	1.35 ± 0.13

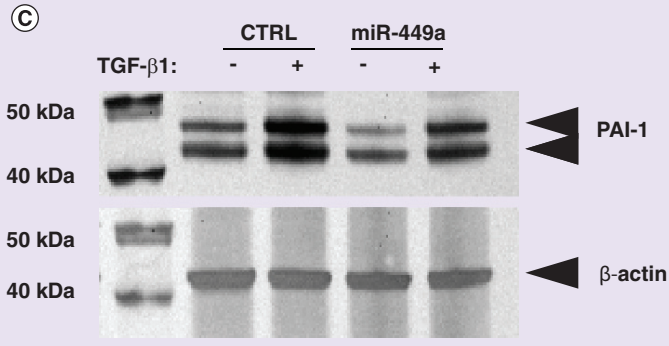

Treatment	-	+
CTRL	0.46 ± 0.23	1.68 ± 0.26
miR-449a	0.50 ± 0.30	1.09 ± 0.07

Figure 9. Vesicle components of selected renal cell-conditioned media attenuate PAI-1 induced by TGF-β1 signaling. *In vitro* experiments were designed to mimic the treatment effect of selected renal cell (SRC) observed *in vivo*. Human-derived renal mesangial cells (HRMC) control express increased levels of PAI-1 in the presence (+) of 5 ng/ml TGF-β1. **(A)** CM from rat SRC modulates PAI-1 expression in cultured HRMC induced (+) and uninduced (-) with TGF-β1. **(B)** HRMC cocultured with CM derived from human SRC attenuates TGF-β1-induced PAI-1 protein expression. Secreted vesicles from human and rat SRC-CM were collected by high-speed centrifugation and assayed for miRNA content using PCR-based arrays of known sequences. miR-449a, a putative regulator of PAI-1 was identified. HRMC were transiently transfected with miR-449a or not (CTRL). **(C)** 24-h post-transfection HRMC were either exposed to 5 ng/ml TGF-β1 (+) or not (-) for an additional 24 h. Total protein was prepared and assayed for PAI-1 and β-actin by western blot. miR-449a reduced basal and induced PAI-1 protein expression. For **(A–C)**, quantitation of band density shown as (intensity PAI-1/intensity β-actin).
CM: Conditioned media; CTRL: Control.

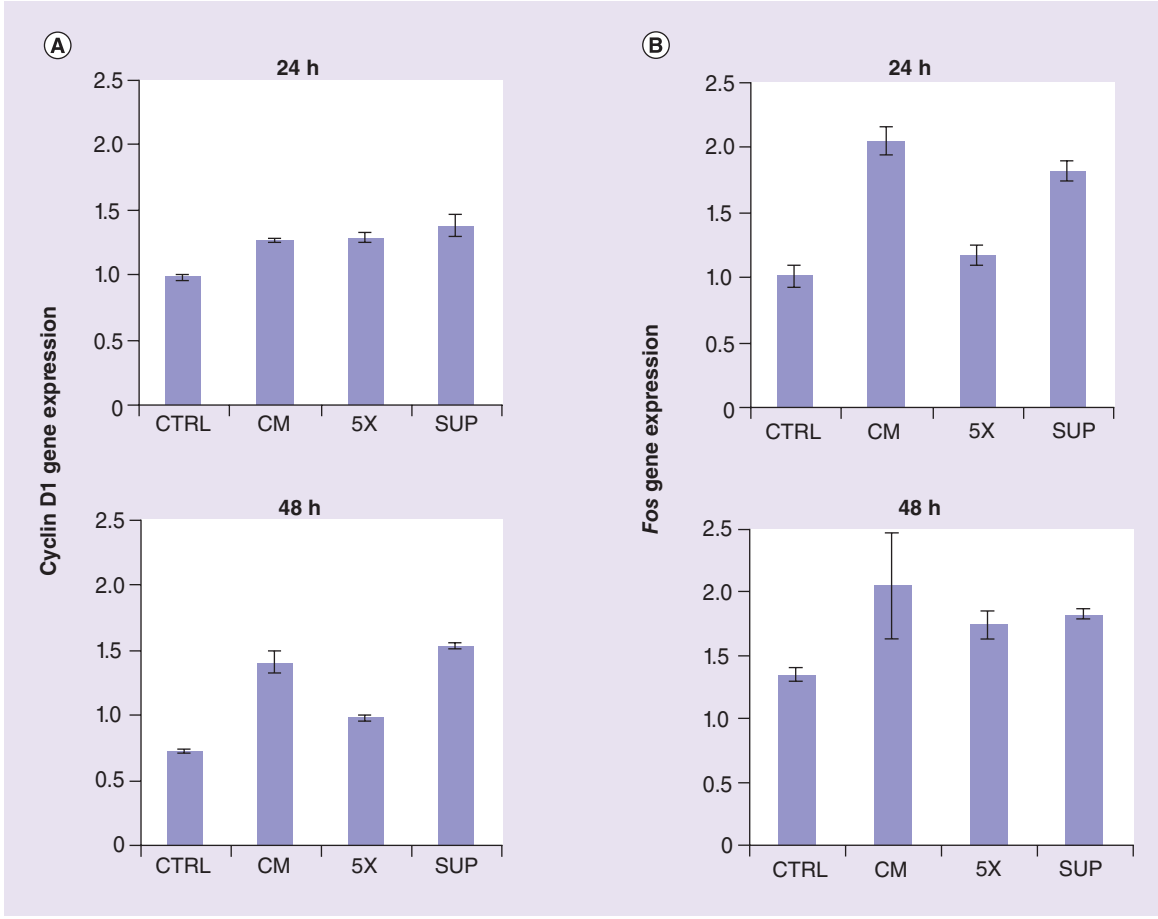

Figure 10. Selected renal cell-conditioned media promotes proliferation independently from secreted vesicles.
HK2 cells were cultured in selected renal cell (SRC)-CM for 24 and 48 h, and assayed by quantitative real-time PCR for cell cycle markers Cyclin D1 **(A)**, *FOS* **(B)**. Basal media was used as a negative CTRL. Vesicle-associated components of the media were separated from SRC-CM and concentrated by ultracentrifugation by a factor of 5 (5X). Vesicle-deplete CM was collected from the SUP. Error bars represent the standard error of the mean of three experimental replicates.
CM: Conditioned media; CTRL: Control; SUP: Supernatant.

express genes and/or proteins of numerous therapeutically relevant cytokines and growth factors, including PDGF-ββ, VEGF, NGF, GDNF, the matrix metalloproteinases MMP-1, MMP-9, TIMP-1 and MCP-1, which have been shown to mediate such paracrine effects [37].

Here, we have characterized progressive NF-κB activation and interstitial inflammation during development of etiology in the 5/6N_x model from 1 to 8 weeks postsurgery. A time-dependent increase in expression and nuclear localization of NF-κB p65 was observed, particularly during chronic phases of disease progression (2–8 weeks postnephrectomy). At 6 weeks postnephrectomy, robust p65 nuclear localization was observed in tubular epithelial and glomerular cells indicating that those particular cellular compartments were subjected to cellular stressors (Figure 1A). SRC product potency prior to cell transplantation was evaluated by functional characterization of B2-associated megalin:cubilin-mediated albumin transport and GGT1 activity. These bioassays demonstrated that the expression of cubilin and GGT1 was associated with functionally active protein. Interference by RAP, an established competitive inhibitor of megalin:cubilin-mediated albumin transport and the observed lack of albumin uptake in nontubular B4 subpopulation [22] confirmed the specificity of albumin transport. Observed functional outcomes met previously established pass/fail criteria for SRC product release [38, 39] and SRC was therefore found acceptable for cell transplantation.

Transplanted SRC was observed to attenuate NF-κB activation and reduce macrophage and T-cell infiltration. As shown in Figure 2A, SRC-treated tissues displayed decreased p65 nuclear localization and reduced numbers of both $CD68^+$ and $CD3^+$ leukocytes, while B1/B5 (non-SRC cell control) treated animals resembled untreated disease state. Additionally, trans-

Table 5. Quantitative histological analysis of impact of selected renal cell and B1/B5 treatment of 5/6 nephrectomized rodents.

	Group	NF-κB-p65	CD3	CD68	Ki-67
Rat ID#					
199	1	1	1	0	0
200	1	1	1	1	0
201	1	1	1	1	0
183	2	3	4	4	2
188	2	2	4	3	2
193	2	3	4	4	4
169	3	2	2	2	3
174	3	2	2	2	3
159	3	3	3	3	1
171	3	3	4	3	2
181	3	1	2	2	3
168	4	3	3	2	2
182	4	3	3	3	2
195	4	2	4	2	3
Rat treatment					
Hemi-NX	1	(n = 3)			
$5/6N_x$	2	(n = 3)			
$5/6N_x$ + SRC	3	(n = 5)			
5/6 + B1/B5	4	(n = 3)			

Grade 0 (absent/normal): This score reflects a focal, multifocal or diffuse distribution in which approximately 0–5 cells are staining positive per high power field (HPF; 40×).
Grade 1 (minimal): This score reflects a focal, multifocal or diffuse distribution in which approximately 5–10 cells are staining positive per HPF (40×).
Grade 2 (mild): This score reflects a focal, multifocal or diffuse distribution in which approximately >10–25 cells are staining positive per HPF (40×).
Grade 3 (moderate): This score reflects a focal, multifocal or diffuse distribution in which approximately >25–40 cells are staining positive per HPF (40×).
Grade 4 (marked): This score reflects a focal, multifocal or diffuse distribution in which approximately >40 cells are staining positive per HPF (40×).

planted SRC promotes tubular cell proliferation in the $5/6N_x$ model. SRC treatment specifically increased the number of $Ki67^+$ proliferating cells specifically in the tubular epithelia (Figure 2A & Table 5). This compartment-specific proliferation may be a direct indicator of therapeutic outcome: epithelial proliferation leads to replenishment of renal function, while interstitial proliferation leads to fibrosis. Given that proliferation occurs in a compartment-specific manner (Figure 2A & Table 5), increase in proliferation in SRC-treated kidneys is primarily in renal epithelium and not interstitium. Consistent with models described in [40,41], the simplest explanation of these data is that these proliferative cells are endogenous tubular epithelial cells that have been stimulated by SRC to divide and migrate to the sites of cellular injury and fibrosis.

Multiple established biomarkers of renal inflammation and injury may potentially be interrogated to evaluate the disease condition. As discussed in [38,39], expression of the kidney injury marker KIM1 is currently being leveraged as a potency marker and release criterion metric for SRC in ongoing Phase I clinical trials. Secretomic profiling of SRC has identified additional biomarkers potentially relevant for monitoring progress of renal disease. These include: α1MG, β2MG, calbindin, clusterin, CTGF, Cystatin C, GST-α, NGAL, osteopontin, TFF3, TIMP-1, VEGF, ANG2, PDGF-ββ, ICAM, MCP-1, MMP-9, PAI-1, RANTES, TIMP-1, GRO-α, IL6, MMP-1, bNGF, FN, TGF-β1, TNF-α [37]. However, for the purposes of the current study, CCL2 and CCL5 were selected because of their critical role in the NF-κB signaling pathway. Transplanted SRC reduced presence of CCL5 in the ZSF1 model of DN. By 35 weeks of age, obese rats demonstrated more robust NF-κB activation compared with 18-week-old obese rats,

reflecting the progressive nature of DN (Figure 3A). Unlike the 5/6N$_x$ model (Figure 1A), we did not observe robust NF-κB activation in glomerular cells at early or late time points (Figure 3A). Western analysis confirmed that expression and nuclear localization of p65 increased in obese rats over time (Figure 3B). Increased NF-κB activation and interstitial inflammation were consistent observations between the surgical model (5/6N$_x$) and genetic model (obese *ZSF1*) of CKD [42,43]. As we observed that injection of SRC ameliorated chronic inflammation in the 5/6N$_x$ model, we hypothesized that these cells would prove efficacious in attenuating renal inflammation in the ZSF1 model as well. As noted in the 5/6N$_x$ study, CCL2 expression was unaltered as a result of SRC injection (Figure 4A). However, CCL5 moderately increased over time as disease state progressed and this rate was attenuated in SRC-injected animals (Figure 4B).

CM from human SRC can attenuate NF-κB activation *in vitro* independent of vesicle-mediated cell signaling. While delivery of rat SRC to chronically diseased kidneys induced long-term benefits, there is limited evidence for SRC engraftment upon implantation *in vivo* [21–23]. These observations notwithstanding, induction of a regenerative response index representing a composite protein expression biomarker reflective of stem and progenitor cell bioactivity is increased in 5/6N$_x$ model upon injection of SRC [29]. Together, these data suggest that SRC leverage indirect, paracrine mechanisms to mediate observed functional outcomes [37], consistent with other studies on MOA of cell-based therapies in acute/chronic rodent models of renal disease [44–51]. To test this hypothesis *in vitro*, CM from human SRC cultures was collected to determine the capacity for attenuating NF-κB activation as well as enhancing cellular proliferation in target cell types.

An important contribution to the transition of animal studies to clinical trials is the availability of *in vitro* assays that are predictive for an *in vivo* response. To this end, EMT of renal epithelial tubular cell populations is believed to play a significant role in the development of tubulointerstitial fibrosis during the progression of CKD [52,53]. Cytokines including TGF-β1 have been shown to recapitulate EMT within populations of tubular epithelial cells [53,54] and TGF-β1-induced EMT of the human primary tubular epithelial cell line HK2 is now a well-established model system to evaluate the impact of small molecule and protein factors on EMT [54,55]. CM derived from SRC was observed to attenuate TGF-β1-induced EMT in HK2 cells [37]. HRMC are pericytes derived from the peripheral, capillary loop-associated vasculature found within the glomerular tufts. HRMC may potentially function to establish mesangial ECM, internalization of plasma components and regulation of hormonal elements associated with control of the vasculature. Uncontrolled growth of HRMC, and therefore, of HRMC-derived mesangial matrix, may manifest in multiple aspects of glomerulonephritis, glomerulosclerosis and nephropathies. Given that synthesis of mesangial matrix by HRMC is a function of externally applied signaling factors, HRMC are commonly regarded as model platforms for fibrosis secondary to CKD [56–59]. In the current manuscript, commercially available HRMC were used as surrogates for host-response tissues in the *in vitro* assays since mesangial cells express PAI-1 in injured/diseased kidneys [25–27,56–61]. We note also that the use of TGF-β1 and TNF-α to mimic *in vitro* renal disease and treatment options is well established in the literature [56–59]. Concentration–effect curves and time-course evaluations have also been extensively reported in the literature, for an example please see [60]. Assay conditions used in the current manuscript are based on those previously established in the literature [56–60].

As a functional test of the CM in the context of kidney disease, we designed an *in vitro* assay using the human proximal tubule cell line HK2 as a surrogate for responding host cells. Nuclear shuttling of p65 was inhibited by SRC-CM (Figure 6). To identify bioactive component(s) of SRC-CM responsible for NF-κB and PAI-1 attenuation capacity, media was subjected to ultracentrifugation at 200,000 g. This vesicle-rich media was unable to attenuate NF-κB activity (Figure 8A), showing that NF-κB suppressor(s) contained within SRC-CM are not directly associated with secreted vesicles and that the bioactive component is smaller than 5 kDa. Proliferation was assayed by evaluation of the expression of the cell cycle regulators CyclinD1 and FOS, both markers of cell cycle regulation [62]. Although it remains possible that the components (<5 kDa) that induce tubular epithelial cell proliferation are the same as those which attenuate NF-κB activation, we have no data currently to confirm this point. Given the low molecular weight (<5 kDa) of the bioactive factors, it is likely that these factors are small-molecule compounds or small peptides and not proteins. However, in the absence of further data, we cannot speculate regarding the identity of these compounds. Attenuation of the TGF-β-mediated signaling pathway regulating expression of PAI-1 is associated with soluble factors contained in vesicle rich CM (Figure 9A & B). Finally, direct comparison between vesicle-rich and vesicle-depleted SRC media shows proliferation is

enhanced in target epithelia by nonvesicular factors (Figure 10). A complete cataloging of miRNAs present in SRC-CM is the subject of a future manuscript [Basu *et al.* (2016), Manuscript in Preparation]. For the sake of clarity, we have chosen to focus in the current manuscript on miRNAs directly relevant to the PAI-1/NF-κB signaling pathway for which unambiguous functional data are available. On this basis, miR-449a was selected for further functional analysis. However, other relevant miRNAs identified in the current study and their RNA targets include: miR-30b-5p (both regulators of PAI-1), miR-21 (Pellino-1), miR-146a (IRAK/TRAF6), miR-124 and miR-151 (NF-κB). As predicted, transfection of synthetic miR-449a-reduced basal and TGF-β-induced expression of PAI-1 protein (compare lane 1 with lane 3, and lanes 2 and 4, Figure 9C). In addition to its role in regulation of PAI-1, miR-449a is well established as a potent inducer of cell death, cell cycle arrest and/or cell differentiation [34].

Our earlier studies have demonstrated that SRC can be identified within the implanted kidney at up to 3 months postimplantation, albeit at reduced frequency. In the 5/6N_x model leveraging male donors and female recipients, male SRC were detectable within the remnant kidney of the N_x female recipient host at 4 weeks after implant, as evidenced by visualization of PKH-26 dye-labeled cells within the parenchyma adjacent to the injection site. Retention of donor cells at the 3-month time point was verified in frozen tissue sections by FISH with rat Y/12 chromosome probes, confirming the presence of male donor cells in tubular and peritubular regions, predominantly localized within the corticomedullary zone. Finally, detection of the male-specific *SRY* gene by PCR in serial tissue sections supported the Y-chromosome FISH findings, demonstrating that the majority of SRY^+ donor-derived DNA persisted in the cortical/corticomedullary junction zone at an estimated frequency of 1:33,333 cells. SRY^+ DNA was found less frequently in the medullary zone and no SRY^+ DNA was detected in the papillary/pelvic zone suggesting that SRY^+ cells are retained preferentially within the CMJ zone [22].

The ZSF1 model leveraged SRC labeled with SPIO for whole organ detection by MRI and fluorescence microscopy following intrarenal transplantation into the anterior pole of the left kidney in obese diabetic ZSF1-recipient rats. MRI revealed a region of negative contrast at the anterior pole of the kidney where the cells were injected. These data are consistent with whole organ fluorescent imaging highlighting the injection site and iron-conjugated rhodamine located at the upper cortex of the anterior pole. Sectioning of the whole kidney indicated a bolus of iron–rhodamine-labeled cells by fluorescent detection and by Prussian-blue for iron migrating and distributing from the cortical injection site, confirming their presence in tubular and peritubular spaces of the cortex and medulla. In parallel with the qualitative MRI-based cell detection study, an *in vivo* study was performed to trace ZSF1 renal cells labeled with perfluorocarbon tracer Cell Sense DM-Red 19F by NMR. The robust detection of 19F-labeled cells at 3 and 24 h following implantation confirmed their early retention in the kidney and the diminished yet significant detection of 19F 7 days following the transplantation procedure. SRC retention was consistent with the detection of these cells observed in the 5/6N_x nephrectomy mass reduction model using both *SRY* gene detection and FISH for Y chromosome (male donor cell detection in female recipients), and cell-membrane PKH-26 dye-labeled studies [22, 23]. It remains unclear if continued or improved persistence of these cells would significantly improve the extent of immunomodulation.

Conclusion

To summarize, we have demonstrated in two models of CKD that robust NF-κB activation, PAI-1 expression and subsequent inflammation and fibrosis are common pathological outcomes despite their disparate etiologies. We confirm that a SRC cell-based approach can effectively promote resolution of CKD-related etiologies through influence on NF-κB signaling pathways in both disease models. An impact on TGF-β1 signaling is also suggested by the *in vitro* data but will require additional *in vivo* confirmation. Finally, we demonstrate both *in vitro* and *in vivo* that SRC specifically promotes proliferation of target tubular epithelial cells through secreted factors and in conjunction with effects on NF-κB activation and PAI-1 expression may attenuate advancement of CKD. Unequivocal proof of the existence of microvesicles in SRC-CM will require electron microscopic confirmation; such experiments are currently in progress.

Future studies on optimization of SRC-based renal cell therapy will include systematic dose-response analysis to identify optimal SRC dosage. To this end, a comparative evaluation of low dose (10^6 SRC) versus high dose (10^7 SRC) has been made and reported in [22]. Briefly, essentially identical and statistically significant stabilization of serum creatinine and BUN was observed from transplantation of both high and low doses of SRC in the 5/6N_x model, suggesting that 10^6 SRC may be acceptable for a rodent product prototype, greatly facilitating the manufacturing process. The potential impact of donor-specific dif-

ferences on SRC potency and bioactivity has thus far not been evaluated, in part because of the absence of a noninbred rodent model for CKD. Additionally, as SRC therapy is by definition autologous, the relevance of such studies to the SRC clinical program is minimal. Taken together, these studies extend and complement previous work on SRC-related MOA demonstrating mobilization of host-derived stem and progenitor-associated markers in 5/6N_x rodent models of CKD in response to treatment with SRC [29]. Identification of putative MOA(s) establishes the foundation for potency assay development and implementation, critical for successful clinical translation of any biologic product candidate [38,39]. To this end, Phase I/II clinical trials of Neo-Kidney Augment, a SRC/hydrogel composite cell therapeutic for treatment of ESRD, have been initiated [63,64].

Future perspective

Identification of putative MOA(s) establishes the foundation for potency assay development and implementation, critical for successful clinical translation of any biologic product candidate. As we have discussed in [39,40], growth factors and miRNAs secreted by SRC may be directly incorporated into a battery of functional bioassays that taken together provide a quantitative index of product potency. The development of renal fibrosis during progressive onset of CKD may be modeled *in vitro* by the induction of an EMT event in certain populations of renal cells with TGF-β. Factors present in SRC-derived CM are capable of blocking or reversing this EMT event, which may be monitored quantitatively by PCR methods providing another index of SRC bioactivity [38, 39]. Finally, RegenMedTX LLC's Neo-Kidney Augment (NKA) is a SRC/hydrogel composite cell therapeutic currently undergoing Phase I/II clinical trials in Sweden and the USA (ClinicalTrials.gov identifier #NCT01846715 and NCT02008851) for patients with Type 2 diabetes and CKD [63, 64]. It is expected that clinical data derived from these trials will further refine our understanding of mechanistic pathways associated with SRC therapeutic bioactivity.

Financial & competing interests disclosure

The authors declare an equity and intellectual property interest in Tengion, Inc., Assets of Tengion Inc. have since been acquired by RegenMedTX, LLC. The authors have no other relevant affiliations or financial involvement with any organization or entity with a financial interest in or financial conflict with the subject matter or materials discussed in the manuscript apart from those disclosed.

No writing assistance was utilized in the production of this manuscript.

Ethical conduct of research

The authors state that they have obtained appropriate institutional review board approval or have followed the principles outlined in the Declaration of Helsinki for all human or animal experimental investigations. In addition, for investigations involving human subjects, informed consent has been obtained from the participants involved.

Executive summary

Molecular characterization of rodent chronic kidney disease models

- Progressive NF-κB activation and interstitial inflammation are features in the development of chronic kidney disease in the 5/6 nephrectomy (5/6N_x) model.

Selected renal cell mechanism of action, 5/6N_x model

- Transplanted selected renal cell (SRC) attenuate NF-κB and PAI-1 activation and reduce macrophage and T-cell infiltration in the 5/6 nephrectomy model.
- Transplanted SRC promote tubular cell proliferation in 5/6N_x rats.

SRC mechanism of action, ZSF model

- Transplanted SRC attenuate NF-κB signaling and PAI-1 expression in ZSF1 model of diabetic nephropathy.

Effect of SRC-derived conditioned media

- Conditioned media (CM) from human SRC can attenuate NF-κB activation *in vitro* independent of vesicle-mediated cell signaling.

Role of vesicular component of SRC-derived CM

- Secreted vesicles in CM from rat and human SRC can attenuate PAI-1 expression *in vitro*; bioactivity is mediated in part by miRNAs.

Role of nonvesicular component of SRC-derived CM:

- Nonvesicle components of SRC-CM induce tubular cell proliferation.

Clinical trials

- RegenMedTX LLC's Neo-Kidney Augment is a SRC/hydrogel composite cell therapeutic currently undergoing Phase I/II clinical trials in Sweden and the USA for patients with Type 2 diabetes and chronic kidney disease.

References

Papers of special note have been highlighted as:
• of interest; •• of considerable interest

1 U.S. Renal Data System. Costs of CKD and ESRD, Minneapolis, MN, USA (2007). www.usrds.org/2007/pdf/00_intro_07.pdf

2 Moudgil A, Bagga A. Evaluation and treatment of chronic renal failure. *Indian J. Pediatr.* 66, 241–253 (1999).

3 Annual Report of the U.S. Organ Procurement and Transplantation Network and the Scientific Registry of Transplant Recipients: Kidney Transplant Data 2008. Department of Health and Human Services, Health Resources and Services Administration, Healthcare Systems Bureau, Division of Transplantation, Rockville, MD; United Network for Organ Sharing, Richmond, VA; University Renal Research and Education Association, Ann Arbor, MI.

4 Tumlin J, Wali R, Williams W *et al.* Efficacy and safety of renal tubule cell therapy for acute renal failure. *J. Am. Soc. Nephrol.* 19, 1034–1040 (2004).

5 Togel F, Cohen A, Zhang P, Yang Y, Hu Z, Westenfelder C. Autologous and allogeneic marrow stromal cells are safe and effective for the treatment of acute kidney injury. *Stem Cells Dev.* 18, 475–485 (2009).

6 Westenfelder C. Protective actions of administered mesenchymal stem cells in acute kidney injury:relevance to clinical trials. *Kidney Int.* (Suppl. 1), 103–106 (2011).

7 Humphreys BD, Bonventre JV. Mesenchymal stem cells in acute kidney injury. *Annu. Rev. Med.* 59, 311–325 (2008).

8 Basu J, Ludlow JW. Developmental engineering the kidney: leveraging principles of morphogenesis for renal regeneration. *Birth Defects Res. C. Embryo Today* 96, 30–38 (2012).

9 Yokoo T, Fukui A, Ohashi T *et al.* Xenobiotic kidney organogenesis from human mesenchymal stem cells using a growing rodent embryo. *J. Am. Soc. Nephrol.* 17, 1026–1034 (2006).

10 Kim SS, Gwak SJ, Han J *et al.* Kidney tissue reconstruction by fetal kidney cell transplantation: effect of gestation stage of fetal kidney cells. *Stem Cells* 25, 1393–1401 (2007).

11 Marshall D, Dilworth MR, Clancy M, Bravery CA, Ashton N. Increasing renal mass improves survival in anephric rats following metanephros transplantation. *Exp. Physiol.* 92, 263–271 (2007).

12 Patschan D, Plotkin M, Goligorsky MS. Therapeutic use of stem and endothelial progenitor cells in acute renal injury: ça ira. *Curr. Opin. Pharmacol.* 6, 176–183 (2006).

13 Chade AR, Zhu X, Lavi R *et al.* Endothelial progenitor cells restore renal function in chronic experimental renovascular disease. *Circulation* 119, 547–557 (2009).

14 Prodromidi EI, Poulsom R, Jeffery R *et al.* Bone marrow-derived cells contribute to podocyte regeneration and amelioration of renal disease in a mouse model of Alport syndrome. *Stem Cells* 24, 2248–2455 (2006).

15 Kirpatovskii VI, Kazachenko AV, Plotnikov EY *et al.* Experimental intravenous cell therapy of acute and chronic renal failure. *Bull. Exp. Biol. Med.* 143, 160–165 (2007).

16 Sagrinati C, Ronconi E, Lazzeri E, Lasagni L, Romagnani P. Stem-cell approaches for kidney repair: choosing the right cells. *Trends Mol. Med.* 14, 277–285 (2008).

17 Basu J, Ludlow JW. Platform technologies for tubular organ regeneration. *Trends Biotechnol.* 28, 526–533 (2010).

18 Basu J, Ludlow JW. Tissue engineering of tubular and solid organs: an industry perspective. In: *Advances in Regenerative Medicine.* Wislet-Gendebien S (Ed.). InTech Open Publishers, Rijeka, Croatia (2011).

19 Guo JK, Cantley LG. Cellular maintenance and repair of the kidney. *Annu. Rev. Physiol.* 72, 357–376 (2010).

20 Lin F, Moran A, Igarashi P. Intrarenal cells, not bone marrow derived cells, are the major source for regeneration in postischemic kidney. *J. Clin. Invest.* 115, 1756–1764 (2005).

21 Bruce AT, Guthrie KI, Kelley R. *Ex vivo* culture and separation of functional renal cells. *Methods Mol. Biol.* 1001, 53–64 (2013).

22 Kelley R, Werdin ES, Bruce AT *et al.* Tubular enriched subpopulation of primary renal cells improves survival and augments kidney function in a rodent model of chronic kidney disease. *Am. J. Physiol. Renal Physiol.* 299(5), F1026–F1039 (2010).

•• **First demonstration of selected renal cell (SRC) functionality in preclinical rodent model.**

23 Kelley R, Bruce A, Spencer T *et al.* A population of selected renal cells augments renal function and extends survival in the ZSF1 model of progressive diabetic nephropathy. *Cell Transplant.* 22, 1023–1039 (2013).

•• **First demonstration of SRC functionality in preclinical diabetic rodent model.**

24 Border WA, Noble NA. Transforming growth factor beta in tissue fibrosis. *N. Engl. J. Med.* 331, 1286–1292 (1994).

25 Eddy AA, Fogo AB. Plasminogen activator inhibitor-1 in chronic kidney disease: evidence and mechanisms of action. *J. Am. Soc. Nephrol.* 17, 2999–3012 (2006).

26 Seo JY, Park J, Yu MR, Kim YS, Ha H, Lee HB. Positive feedback loop between plasminogen activator inhibitor-1 and transforming growth factor-beta1 during renal fibrosis in diabetes. *Am. J. Nephrol.* 30, 481–490 (2009).

27 Liu Y. Renal fibrosis: new insights into the pathogenesis and therapeutics. *Kidney Int.* 69, 213–217 (2006).

28 Liu BC, Zhang L, Lv LL, Wang YL, Liu DG, Zhang XL. Application of antibody array technology in the analysis of urinary cytokine profiles in patients with chronic kidney disease. *Am. J. Nephrol.* 26, 483–490 (2006).

29 Genheimer CW, Ilagan RM, Spencer T *et al.* Molecular characterization of the regenerative response induced by intra-renal transplantation of selected renal cell in a rodent model of chronic kidney disease. *Cells Tissues Organs* 196, 374–384 (2012).

30 Bilan VP, Salah EM, Bastacky S *et al.* Diabetic nephropathy and long-term treatment effects of rosiglitazone and enalapril in obese ZSF1 rats. *J. Endocrinol.* 210, 293–308 (2011).

31 Tofovic SP, Jackson EK. Rat models of the metabolic syndrome. *Methods Mol. Med.* 86, 29–46 (2003).

32 ImageJ. http://imagej.nih.gov/ij/

33 Mirbase. www.mirbase.org

34 Lizé M, Klimke A, Dobbelstein M. MicroRNA-449 in cell fate determination. *Cell Cycle* 10, 2874–2882 (2011).

35 Aboushwareb T, Egydio F, Straker L, Gyabaah K, Atala A, Yoo JJ. Erythropoietin producing cells for potential cell therapy. *World J. Urol.* 26, 295–300 (2008).

36 Caplan AI, Correa D. The MSC: an injury drugstore. *Cell Stem Cell* 9, 11–15 (2011).

37 Basu J, Genheimer CW, Rivera EA *et al.* Functional evaluation of primary renal cell/biomaterial neo-kidney augment prototypes for renal tissue engineering. *Cell Transplant.* 20, 1771–1790 (2011).

• **Systematic profiling of character and function of SRC.**

38 Basu J, Ludlow JW. Cell-based therapeutic products: potency assay development and application. *Regen. Med.* 9, 497–512 (2014).

•• **First clear and systematic proposal for potency assay development of clinical cell therapy products.**

39 Guthrie K, Bruce A, Sangha N, Rivera E, Basu J. Potency evaluation of tissue engineered and regenerative medicine products. *Trends Biotechnol.* 31, 505–514 (2013).

•• **First clear and systematic proposal for potency assay development of clinical tissue-engineered products.**

40 Humphreys BD. Genetic tracing of the epithelial lineage during mammalian kidney repair. *Kidney Int. Suppl.* 1(3), 83–86 (2011).

41 Humphreys BD, Valerius MT, Kobayashi A *et al.* Intrinsic epithelial cells repair the kidney after injury. *Cell Stem Cell* 2, 284–291 (2008).

•• **Demonstration of role of host-derived tubular epithelial cells for mediating kidney repair.**

42 Ninichuk V, Khandoga AG, Segerer S *et al.* The role of interstitial macrophages in nephropathy of Type 2 diabetic db/db mice. *Am. J. Pathol.* 170, 1267–1276 (2007).

43 Tapmeier TT, Fearn A, Brown K *et al.* Pivotal role of $CD4^+$ T cells in renal fibrosis following ureteric obstruction. *Kidney Int.* 78, 351–362 (2010).

44 Villanueva S, Carreño JE, Salazar L *et al.* Human mesenchymal stem cell derived from adipose tissue reduce functional and tissue damage in a rat model of chronic renal failure. *Clin. Sci.* 125, 199–210 (2013).

45 Menke J, Iwata Y, Rabacal WA *et al.* CSF1 signals directly to renal tubular epithelial cells to mediate repair in mice. *J. Clin. Invest.* 119, 2330–2342 (2009).

46 Cheng K, Rai P, Plagov A *et al.* Transplantation of bone-marrow derived MSCs improves *cis*-platinum induced renal injury through paracrine mechanisms. *Exp. Mol. Pathol.* 94, 466–473 (2013).

47 Bagul A, Frost JH, Drage M. Stem cells and their role in renal ischemia reperfusion injury. *Am. J. Nephrol.* 37, 16–29 (2013).

48 Gatti S, Bruno S, Deregibus MC *et al.* Microvesicles derived from human adult mesenchymal stem cells protect against ischemia-reperfusion induced acute and chronic kidney injury. *Nephrol. Dial. Transplant.* 26, 1474–1483 (2011).

49 Yamaleyeva LM, Guimaraes-Souza NK, Krane LS *et al.* Cell therapy with human renal cell cultures containing erythropoietin positive cells improves chronic kidney injury. *Stem Cells Transl. Med.* 1, 373–383 (2012).

50 Guimarães ET, Cruz Gda S, Almeida TF *et al.* Transplantation of stem cells obtained from murine dental pulp improves pancreatic damage, renal function and painful diabetic neuropathy in diabetic type I mouse model. *Cell Transplant.* 22(12), 2345–2354 (2012).

51 Du T, Cheng J, Zhong L *et al.* The alleviation of acute and chronic kidney injury by human Wharton's jelly-derived mesenchymal stromal cells triggered by ischemia-reperfusion injury via an endocrine mechanism. *Cytotherapy* 14, 1215–1227 (2012).

52 Humphreys BD, Lin S, Kobayashi L *et al.* Fate tracing reveals the pericyte and not epithelial origin of myofibroblasts in kidney fibrosis. *Am. J. Pathol.* 176, 85–97 (2009).

53 Okada H, Inoue T, Suzuki H, Strutz F, Neilson EG. Epithelial–mesenchymal transformation of renal tubular epithelial cells *in vitro* and *in vivo*. *Nephrol. Dial. Transplant.* 15, 44–46 (2000).

54 Dudas PL, Argentieri RL, Farrell FX. BMP-7 fails to attenuate TGF-β1-induced epithelial-to-mesenchymal transition in human proximal tubule epithelial cells. *Nephrol. Dial. Transplant.* 24, 1406–1416 (2009).

55 Hills CE, Al-Rasheed N, Willars GB, Brunskill NJ. C-peptide reverses TGF-beta1-induced changes in renal proximal tubular cells: implications for treatment of diabetic nephropathy. *Am. J. Physiol. Renal Physiol.* 296, F614–F621 (2009).

56 Rodriguez-Barbero A, L'Azou B, Cambar J, Lopez-Novoa JM. Potential use of isolated glomeruli and cultured mesangial cells as *in vitro* models to assess nephrotoxicity. *Cell Biol. Toxicol.* 16, 145–153 (2000).

57 Zeisberg M, Maeshima Y, Mosterman B, Kalluri R. Renal fibrosis. Extracellular matrix microenvironment regulates migratory behavior of activated tubular epithelial cells. *Am. J. Pathol.* 160, 2001–2008 (2001).

58 Stockand JD, Sansom SC. Regulation of filtration rate by glomerular mesangial cells in health and diabetic renal disease. *Am. J. Kidney Dis.* 29, 971–981 (1977).

59 Grond J, Weening JJ. Mesangial cell injury, glomerulosclerosis, and therapeutic intervention. *Contrib. Nephrol.* 81, 229–239 (1990).

60 Kanalas JJ, Hopfer U. Effect of TGF-beta 1 and TNF-alpha on the plasminogen system of rat proximal tubular epithelial cells. *J. Am. Soc. Nephrol.* 8, 184–192 (1997).

61 Rerolle JP, Hertig A, Nguyen G *et al.* Plasminogen activator inhibitor type 1 is a potential target in renal fibrosis. *Kidney Int.* 58, 1841–1850 (2000).

62 Brown JR, Nigh E, Lee RJ *et al.* Fos family members induce cell cycle entry by activating cyclin D1. *Mol. Cell. Biol.* 18, 5609–5619 (1998).

63 Clinical trials database. http://clinicaltrials.gov/ct2/show/NCT01846715

64 Clinical trials database. http://clinicaltrials.gov/ct2/show/NCT02008851

Review

Pharmacogenomics

The role of pharmacogenetics and advances in gene therapy in the treatment of diabetic retinopathy

Diabetic retinopathy (DR) and its complications such as diabetic macular edema continue to remain a major cause for legal blindness in the developed world. While the introduction of anti-VEGF agents has significantly improved visual outcomes of patients with DR, unpredictable response, largely due to genetic polymorphisms, appears to be a challenge with this therapy. With advances in identification of various genetic biomarkers, novel therapeutic strategies consisting of gene transfer are being developed and tested for patients with DR. Application of pharmacogenetic principles appears to be a promising futuristic strategy to attenuate diabetes-mediated retinal vasculopathy. In this comprehensive review, data from recent studies in the field of pharmacogenomics for the treatment of DR have been provided.

First draft submitted: 27 July 2015; **Accepted for publication:** 25 November 2015; **Published online:** 25 January 2016

Keywords: diabetic retinopathy • gene therapy • genomic markers • HLA • linkage • mutation • pharmacogenomics • polymorphism • VEGF mutation • viral vectors

Aniruddha Agarwal[1], Sally A Ingham[2], Keegan A Harkins[3], Diana V Do[1,3] & Quan Dong Nguyen*[,1,3]

[1]Ocular Imaging Research & Reading Center (OIRRC), Stanley M. Truhlsen Eye Institute, University of Nebraska Medical Center, South 42nd Street & Emile St, Omaha, NE 68198, USA

[2]College of Medicine, University of Nebraska Medical Center, South 42nd Street & Emile St, Omaha, NE 68198, USA

[3]Stanley M. Truhlsen Eye Institute, University of Nebraska Medical Center, South 42nd Street & Emile St, Omaha, NE 68198, USA

*Author for correspondence:
Tel.: +1 402 559 4276
Fax: +1 402 559 5514
quan.nguyen@unmc.edu

Diabetes has been recognized as a major public health problem of the 21st century. The number of people worldwide suffering from diabetes and its macro- and microvascular complications may reach more than 500 million by the year 2030. Diabetic retinopathy (DR) and its complications such as diabetic macular edema (DME) increase with the duration of the disease [1]. It is estimated that >60% of those diagnosed with Type 2 diabetes develop certain stage of retinopathy after 20 years [2–4].

Despite numerous breakthroughs in the development of novel pharmacological agents for DME in the last decade, a significant proportion of patients gain suboptimal vision. Anti-VEGF therapies and corticosteroids such as triamcinolone acetonide and fluocinolone acetonide are the mainstay in the treatment of DME in the present day [5]. However, evidence from large clinical trials such as the RISE and RIDE study suggests that with anti-VEGF therapy, <50% patients may show a significant improvement (≥3 lines visual acuity) with 0.3 mg ranibizumab [6]. It has been recently recognized that genetic influences, such as polymorphisms in the gene encoding VEGF, may play a role in determining the response to anti-VEGF therapy [7]. Thus, there remains a significant unmet need for novel, more effective therapies for DR and DME, beyond the anti-VEGF agents.

Intraocular genesis of therapeutic proteins that can treat DR and DME is now possible by ensuring local delivery of a gene using a suitable vector. Following early successes of gene therapy in patients with inherited retinal degenerations, trials on retinal vascular pathologies such as DR are being designed [8,9].

In this review, recent advances in the identification of genetic factors, which play a role in the pathogenesis and management of DR and DME, have been summarized. Contemporary pharmacogenetic principles

Future Medicine part of fsg

and novel gene therapies in development for DR that may enable clinician-scientists to achieve better visual results have been highlighted. In addition, a futuristic perspective for the treatment of DR has been presented.

Genetic factors in the pathogenesis of diabetic retinopathy

To date, the genetics behind DR has not been fully elucidated. Current research and meta-analyses focus on either HLA associations or single-gene variations (SNPs). Some authors have also used linkage analysis and genome-wide association studies (GWAS) in order to attempt to find associations between various genes, SNPs and DR [10]. Studies investigating the genetic factors that influence the manifestations of retinopathy have revealed HLA associations and SNPs that may contribute to initiation or promotion of the inflammatory cascade [11].

Human leukocyte antigen associations & linkage analysis

There are two main types of HLA proteins in the human body that correspond either to major histocompatibility complex class I or class II. Studies that have been performed on DR in type 1 and 2 diabetic patients focus on HLAs corresponding to major histocompatibility complex class II as these are the proteins that present antigens outside of the cell to T-lymphocytes. Self-antigens that are presented are suppressed by regulatory T cells. It is theorized that the pathology behind DR may be caused by the presentation of self-antigens by HLA molecules that is then not suppressed by regulatory T cells [12].

According to two different studies in two different populations of patients with Type 1 diabetes, HLA *DQB1*0201* was associated with susceptibility to proliferative diabetic retinopathy (PDR) (n = 46; 23 healthy controls and 23 patients with Type 1 diabetes) [13,14]. In Croatian patients, the *DQB1*0201* has a relative risk of 5.29 toward the development of PDR. Although *DQB1*0201* has the highest relative risk, in a study on patients with Type 1 diabetes (n = 425 families), it was found that the DR alleles *DRB1*0301* and *DRB1*0402* are also associated with PDR with a relative risk of 2.12 and 3.01, respectively [15].

Although these studies showed clear associations between *DQB1*0201* and DR, other studies did not show such relationships. A recent meta-analysis that pooled data from seven studies with 2707 patients with Type 1 diabetes and 7638 healthy controls, showed that with covariate-adjusted models, *DQB1*0201* was a significant protective factor for the presence of microvascular complications (including DR). This meta-analysis also showed that there was a higher frequency of *HLA-B62* allele among Type 1 diabetic patients with PDR compared with Type 1 diabetics without PDR [16].

Thus, linkage analysis may help in the identification of alleles that may predispose to development of more aggressive form of DR, resistant to conventional form of therapy.

SNPs identified using candidate gene studies

There have been many SNPs implicated in the development in DR, in a number of different genes. The main genes that have been studied are *VEGF*, *TGF-β1* and the *CEP125* gene [10]. In addition, SNPs in certain candidate genes that play a role in the pathogenesis of DR, such as aldose reductase [17], endothelial nitric oxide[18], receptor for advanced glycation end products [19] and erythropoietin [20] genes have been studied extensively in various ethnic groups.

Numerous SNPs have been studied in the *VEGF* gene. SNPs in *VEGF* gene and its polymorphisms are of particular interest because therapy of DR largely focuses on anti-VEGF drugs [21]. The VEGF gene is located on chromosome 6p21.3 and is highly polymorphic as demonstrated in previous studies [22–24]. While significant advances have been made in identifying these polymorphisms, there is indeed a need for continued research in confirming the role of these polymorphisms in patients with DR and DME.

In Asian populations, the *VEGF* +936C/T (rs3025039) polymorphism was found to have an odds ratio of 3.19 in the development of DR in patients with Type 1 diabetes. This SNP is found in the splicing region of the *VEGF* gene [25]. In Japanese and Slovenian populations, there is an association of the C-634-G (rs2010963) polymorphism (which is in the 5′-untranslated region) and an increased risk of developing DME and DR in patients with Type 2 diabetes [26,27]. Yet another SNP, -2578, this one in the promoter region, showed an association with the development of DR except in Caucasians with Type 1 diabetes [28].

The TGF-β signaling pathway is implicated in the development of DR. A meta-analysis that analyzed a total of five studies (three studies with 521 cases and 580 controls for –509C/T polymorphism and two studies with 268 cases and 340 controls for +869T/C(L10P) polymorphism) demonstrated that +869T/C polymorphism is a potential protective factor in the development of DR in patients with Type 2 diabetes [29]. The *CEP125* gene, which is expressed in the retina and involved in the TGF-β signaling pathway, has also been studied. The rs4865047 polymorphism was studied in the Wisconsin epidemiologic study of DR in patients with Type 1 diabetes (n = 469). This

study showed that the *CEP125* SNP was associated with severe DR [30].

The SNPs discussed above are currently the most studied SNPs, most found through GWAS. To date, there are only a small number of primary studies and meta-analyses that have been performed on these SNPs. Many of the analyses have conflicting results, showing that more research needs to be done in this area. It appears that there is a significant genetic risk in the development of DR, but it has yet to be fully elucidated.

Genome-wide association studies

Compared with candidate gene study for SNPs and HLA linkage studies, GWAS consist of high density sampling of all the common human gene variation. Therefore, GWAS are not limited by knowledge of specific genes and have the potential to discover biological effects of genes that have not been reported earlier. Using this concept, millions of common polymorphisms can be identified in the human genome in a given population [31]. GWAS have been employed successfully in complex diseases such as age-related macular degeneration (AMD), among others [32].

The challenge with GWAS is determining the significance of the observed genotypes. Very large sample sizes may be required to demonstrate a significant association. GWAS performed in Mexican (n = 103) [33], Caucasian (n = 973) [34] and Chinese (n = 849 [35] and n = 1007 [36]) ethnicities did not identify any loci that were genome-wide significant. In a recent study of a group of Japanese patients with Type 2 diabetes (n = 1986), only one SNP (rs9362054) was found to have borderline genome-wide significance [37]. Thus, GWAS is yet to provide significant results. Studies with much larger sample sizes, multiple ethnicities, and standardized patient and control population may help to provide significant results in the future [11].

Techniques of genotype assessments

Apart from candidate gene studies and GWAS, techniques such as DNA sequencing may enable identification of causative genetic factors for DR [31]. Sequencing of the whole exome can detect disease variants in complex polygenic diseases such as AMD, shedding light on previously lesser studied pathogenetic pathways such as the ubiquitin-proteasome pathway [38]. Such techniques appear to have a promising role in shedding further light on genetic loci that predispose individuals to DR [39].

Table 1 lists a summary of relevant genes that have been shown to have an association with the development of DR or severe disease among various ethnicities by candidate gene studies or GWAS.

Genetic basis of variations in treatment response

Treatment options for DR and DME include laser photocoagulation, intravitreal or periocular corticosteroids (such as intravitreal dexamethasone, triamcinolone acetonide and fluocinolone acetonide), and anti-VEGF agents [56]. Currently, periodic intravitreal injections of anti-VEGF agents such as bevacizumab, ranibizumab and aflibercept are the standard of care for management of DME owing to its favorable outcome [57,58]. Such therapy is aimed at antagonizing VEGF and its downstream effects.

However, clinical trials have demonstrated marked variation in response to anti-VEGF therapy in DME. In the RISE study, 44.8% of patients gained >3 lines on EDTRS chart at 24 months with 0.3 mg ranibizumab, while 34% patients receiving 0.3 mg ranibizumab demonstrated an improvement of >3 lines on ETDRS chart in the RIDE study [6]. In both trials, there were few patients that showed loss of >15 letters, in other words, six of 250 patients in RISE and seven of 252 patients in RIDE study. The BOLT study employing intravitreal injection of bevacizumab to treat DME demonstrated that there was >3 line improvement (ETDRS) in visual acuity in only 39% of patients [59]. In the DA VINCI Study using intravitreal aflibercept for DME, 34% of the patients showed the significant level of visual acuity improvement at the study end point [60]. Thus, there is a large variation in the response to anti-VEGF therapy among patients with DME.

Based on the therapeutic response to anti-VEGF agents, patients may be termed either as responders or incomplete/nonresponders [10,61,62]. There appears to be significant differences in the genetic makeup and protein expression patterns between these two categories of patients. Among patients with DR, more than 100 genes may have altered expression, either upregulation or downregulation, resulting in suboptimal response to anti-VEGF therapy [63]. In addition, patients with reduced response to anti-VEGF therapy may demonstrate differences in cellular proteins, such as transcription factors (e.g., NF-κβ) [61,64] and cytokines (e.g., TGF-β) [65,66] compared with patients who show a favorable response. Variation of treatment response may also be attributed to differences in the intraocular expression of VEGFR (e.g., VEGFR2), which may be modulated by a number of molecular targets [67].

Thus, the relationship between intraocular VEGF bioactivity and its relationship to the levels of other cellular proteins in patients with DR appears to be complex and largely controlled by epigenetic and genetic influences [61]. Further research in this direction may expand our knowledge regarding the precise mechanisms of individual variations in treatment response.

Table 1. Summary of genes (other than *VEGF*) identified using various techniques associated with diabetic retinopathy.

Susceptible gene	Gene product	Population	Disease association	Number of subjects†	Ref.
Candidate gene studies					
ACE	Angiotensin-converting enzyme	Chinese	NPDR	145 (Type 2 DM)	[40]
AGTR1	Angiotensin II receptor, type 1	Romanian	DR and nephropathy	250 (Type 2 DM)	[41]
AR	Aldose reductase	Caucasian–Brazilian	PDR	579 (Type 2 DM)	[42]
CFH	Complement factor H	Chinese	NPDR	552 (Type 2 DM)	[43]
CHN2	Chimerin 2	Taiwanese	NPDR	719 (Type 2 DM)	[44]
EL	Endothelial lipase	Caucasian–French	PDR	396 (Type 2 DM)	[45]
eNOS	Endothelial nitric oxide synthase	Caucasian–French	Severe NPDR and PDR	200 (Type 1 DM)	[46]
EPO	Erythropoietin	American and Australian	PDR	518 (Type 1 and 2 DM)	[47]
MCP-1	Monocyte chemoattractant protein	Japanese	PDR	3802 (Type 2 DM)	[48]
MTHFR	Methylenetetrahydrofolate reductase	Turkish, Chinese and Japanese	NPDR and PDR, and diabetic neuropathy	860 (Type 2 DM)	[49–51]
OPG	Osteoprotegerin	Slovenian	NPDR	645 (Type 2 DM)	[52]
RAGE	Receptor for advanced glycation end products	Chinese and Malaysians	NPDR	711 (Type 2 DM)	[53,54]
SELP	P-selectin	Caucasian	NPDR	2691 (Type 2 DM)	[55]
Genome-wide association studies					
AKT3/ZNF238	Serine/threonine kinase	Caucasian	PDR and DME	2829 (Type 1 DM)	[34]
CEP162	Long noncoding RNA (lncRNA)	Japanese	NPDR and PDR	837 (Type 2 DM)	[37]
HS6ST3	Heparan sulfate 6-O-sulfotransferase 3	Chinese	NPDR and PDR	749 (Type 2 DM)	[35]
LRP2-BBS5	Megalin; gene involved in ciliogenesis	Chinese	PDR	2071 (Type 2 DM)	[36]
TBC1D4-COMMD6	Promoter region for GLUT4; downregulation of NF-κB	Chinese	PDR	2071 (Type 2 DM)	[36]
TINAG	Tubulointerstitial nephritis antigen	Mexican	Moderate to severe NPDR and PDR	281 (Type 2 DM)	[33]
PLXDC2/ ARHGAP22	Plexin domain-containing 2; Rho GTPase activating protein 2	Taiwanese	NPDR and PDR	749 (Type 2 DM)	[35]

†Indicates total number of subjects included in the studies cited in the table.
DM: Diabetes mellitus; DME: Diabetic macular edema; DR: Diabetic retinopathy; NPDR: Nonproliferative diabetic retinopathy; PDR: Proliferative diabetic retinopathy.

Gene therapies for diabetic retinopathy in development

With continually improving understanding of the pathogenesis of DR, several new approaches are being investigated to treat this disease. Novel approaches based on pharmacogenetic principles include gene therapy targeting various systems such as the renin–angiotensin, antioxidant and the complement system.

Although no human trials have been completed for gene therapy in DR yet, animal models have proven to be successful thus far [68]. The potential strategies for gene therapy in DR include either attenuation of pathogenic molecular targets that are upregulated, or increased production of protective molecules whose expression is abnormally low in DR. As evidenced by the exponential rise in the use of anti-VEGFs in the last decade, VEGF is a key factor that is upregulated in the pathogenesis of DR and is therefore, an obvious first target. On the other hand, antiangiogenic proteins that may be amenable to gene therapy include angiostatin, endostatin, K5 and kallistatin. Angiostatin has been shown to be decreased in diabetics. Its upregulation, however, was shown to decrease neovascularization in animal models [69,70]. Endostatin levels have been shown to inversely correlate with the severity of DR and VEGF levels [71,72]. K5 and kallistatin have been shown to decrease the formation of retinal neovascularization in a rat model [73,74].

VEGF gene therapy

Research into gene fragments that may serve as endogenous inhibitors to VEGF has led to the identification of the *sFlt-1* gene. sFlt-1 is a splice variant of VEGF receptor 1 and functions to bind free-circulating VEGF and PIGF. Thus, it serves to blunt the proangiogenic effects of VEGF [75].

In an oxygen-induced ischemic retinopathy rat model, lentiviral expression plasmids carrying sFlt-1 fragments showed significant inhibition of retinal neovascularization [76]. sFlt-1 has also been successfully transferred in a murine model using helper-dependent adenovirus (HD-Ad/s.Flt-1) resulting in regulated expression of

Table 2. Recombinant viral vectors in development for the treatment of diabetic retinopathy.

Recombinant vector	Expressed protein	Mechanism of action	Ref.
AAV2-sFlt-1 vector	VEGFR1	Inhibition of VEGF	[78,96]
Lenti.sFlt-1			[76]
HD-Ad/s.Flt-1	VEGFR1	Inhibition of VEGF	[77]
AAVrh.10BevMab	Bevacizumab	Long-term release of bevacizumab to suppress ocular neovascularization	[97]
AAV2-vasoinhibin	Vasoinhibin	Inhibition of angiogenesis (belongs to prolactin family)	[98]
AAV-ACE2/Ang-(1–7)	ACE2 and Ang-(1–7)	Reduction in retinal vascular leakage, acellular capillaries, inflammation and oxidative damage	[99]
AAV-sGFP-TatM013	Cell penetrating form of M013 protein (TatM013)	Blockade of IL-1β secretion	[100]
scAAV-GFAP-endostatin-FLAG and scAAV-HRSE-6XHRE-GFAP-endostatin-FLAG	Endostatin	Hypoxia-regulated or unregulated release of endostatin to inhibit angiogenesis	[101]
rAAV-angiostatin	Angiostatin	Reduction of vascular leakage and angiogenesis	[102]
AAV2/8-sCD59	CD59	Regulation of complement system	[68]
AAV2-GFP	PEDF	Inhibition of intraocular angiogenesis	[103]
rAAV2-CMV-hPEDF			[104]
rAAV-BDNF	BDNF	Increase in retinal ganglion cell population	[105]
rAAV2-NTF2	Nuclear transport factor 2	Promotes cytosolic functions that preserve blood–retinal–barrier functions	[106]
AAV-MnSOD	Mitochondrial superoxide dismutase	Reduction in reactive oxygen species damage	[91]
AAV-CAT	Catalase enzyme	Reduction in reactive oxygen species damage	[92]

AAV: Adeno-associated virus; Ang: Angiotensin; HD-Ad: Helper-dependent adenovirus; rAAV: Recombinant adeno-associated virus.

VEGF [77]. This potential therapeutic approach is being thoroughly evaluated for its clinical use in vascular retinal diseases such as neovascular AMD [78].

Renin–angiotensin system

ACE2 has been shown to increase diabetic complications when downregulated and be protective of these complications when upregulated [79]. Dysregulation of angiotensin II has been implicated in the pathogenesis of vascular growth, inflammation and fibrosis, by activation of angiotensin receptors, G-protein-coupled receptors, activation of reactive oxygen species, among other pathways [80,81]. Angiotensin II may behave as a proinflammatory cytokine and participate in various steps leading to pathological microvascular changes [82].

Several clinical trials of angiotensin II blockade in patients with diabetes have shown favorable results [83–85]. In mice models of DR, therapy with recombinant adeno-associated virus (AAV [AAV2-Ang-(1–7) and AAV-ACE2]) showed protective effect on the retina with decreased macrophage activation, prevention of basement membrane thickening and reduced overall oxidative damage [86].

Antioxidant system

In addition to modification of signaling pathways, patients with DR are known to have altered and mitigated genetic expression of antioxidant enzymes [87]. Recent studies have suggested that reactive oxygen species contribute to the pathogenesis of DR. Transgenic mice, which overexpress the antioxidants superoxide dismutase (SOD) and lipoic acid, were shown to decrease the progression of DR although with significant side effects [88,89]. Mitochondrial SOD (MnSOD) may play an important protective role in the retina preventing diabetes-induced abnormalities and microvascular changes [90].

More recently, studies have shown the efficacy of intravitreal gene therapy using AAV vectors with MnSOD and catalase in decreasing the progression of DR in mouse models [91]. When AAV-MnSOD was injected intravitreally in streptozotocin-induced diabetic rats, there was significant reduction in the apoptosis of retinal capillary cells and alleviation of damage to the retinal vascular endothelium. Similar protective effects may be expected after therapy with recombinant AAV containing the catalase gene (AAV-CAT) [92].

Intraocular complement system

Research has shown that normal human intraocular fluid contains factors that inhibit the activation of the complement system, especially the classical pathway. However, this complement regulatory activity can be blocked by monoclonal antibodies against membrane cofactor protein, decay-accelerating factor and CD59 [93]. In retinal vascular diseases such as DR, there may be aberrant activation of intraocular complement system, as demonstrated by deposition of CD5b-9 and C3d in the choriocapillaris [94]. Streptozotocin-induced diabetic rats demonstrate selective reduction in CD55 and CD59 in the wall of retinal vessels [95].

With this background, blockade of intraocular membrane attack complex formation and deposition has been attempted using gene therapy. Soluble membrane-independent form of CD59 (sCD59) can be delivered via gene therapy using AAV (AAV2/8-sCD59) in diabetic eyes. Further research is needed to explore this as a potential therapy for advanced DR.

In addition to the four major pathways mentioned above, recombinant vectors that express various other intracellular proteins have been prepared. Table 2 summarizes various viral vectors that have been tested in animal models for the treatment of diabetic retinopathy.

Epigenetic modifications & microRNAs

Epigenetic factors may play an important role in the pathogenesis of DR [39]. Epigenetic modifications can either silence or activate genetic loci without causing a change in the DNA sequence. These defects are potentially reversible but can remain stable [107]. The major epigenetic mechanisms that are considered to regulate gene expression include DNA methylation, histone modifications and noncoding RNA activity [108]. All of these mechanisms may be active in a hyperglycemic milieu found in diabetic patients.

Reduction in the methylation of the SOD2 [109] and matrix metalloproteinase (MMP9) [110] genes due to epigenetic modifications may be observed in patients with DR. Acetylation of retinal histone may also play a role in the pathogenesis of DR [111]. In addition, post-translational modification of proteins also appears to be relevant in DR. There are a number of miRNAs, including miR200b (a VEGF-regulating miRNA), that may control the post-transcriptional gene expression and thus, serve as an important potential mediator and biomarker of diabetic complications and response to conventional therapy [112,113]. Other miRNAs such as miR146, miR155, miR132 and miR-21 that are responsive to NF-κβ may be upregulated in diabetic patients [114].

Characterization of various epigenetic regulators may lead to development of novel pharmacological targets to prevent or treat diabetes and its microvascular complications such as DR.

Identification of genetic variants from clinical trials of diabetic retinopathy

Large, multicenter epidemiological studies and clinical trials provide a unique opportunity to assess the genetic

susceptibility of individuals of various ethnicities at risk for development of severe disease and/or suboptimal response to treatment. These subanalyses may help to identify candidate genes and their variations associated with poor retinal outcomes in DR. Previous epidemiological studies, such as the DCCT/EDIC study, have identified strong association between certain genes (e.g., *SOD1* and *ACE* genes) and severe nephropathy [115,116]. While there has been significant progress in the field of pharmacogenetics of diabetic nephropathy, further studies are needed to identify replicable genetic factors relevant to the pathogenesis of DR [117].

In order to expand the available knowledge regarding genetic biomarkers of DR, various clinical trials are being designed with an emphasis to evaluate genotypes of patients enrolled in the study. In addition, assay of intraocular cytokines may enable the clinicians to identify the expression patterns of certain genes in patients with DR. This may enable recognition of potential future therapeutic targets and provide the basis for development of novel pharmacological agents.

Conclusion & future perspective

Therapy with anti-VEGF agents has become the standard of care for the modern-day management of DME. However, ununiformed response to anti-VEGF agents and need for multiple injections are major limitations of this approach. Research in the field of pharmacogenomics has already led to the identification of several alterations in nucleic acids and other cellular proteins that may be associated with increased severity of DR and suboptimal response to conventional therapy.

As summarized above, during the past few years, significant advances have been made in the field of

Executive summary

Genetic factors associated with diabetic retinopathy

- There is increasing evidence in literature to illustrate the important role of pharmacogenetics in the treatment of diabetic retinopathy to ensure consistent response among the entire patient population.
- The phenotypical manifestations of diabetic retinopathy may depend upon the genetic composition of the individuals.
- A number of gene polymorphisms in the *VEGF*, *MTHFR*, *TGF-β1* and the *CEP125* gene have been extensively studied in large population cohorts.
- Certain human leukocyte antigen subtypes such as *DQB1*0201*, *DQB1*0301* and *DQB1*0402* have been implicated in the pathogenesis of severe forms of diabetic retinopathy in literature.
- Genome-wide association studies have provided preliminary evidence that genetic factors may play an important role in the pathological expression of the disease. However, further studies are required to establish significant associations.

Pharmacogenetics of treatment response

- In several, large pivotal clinical trials evaluating the role of anti-VEGF agents and corticosteroids, significant visual gain has been observed in less than 50% patients in the study cohorts.
- It is likely that mutations in certain genes such as the *VEGF* and the *VEGFR2* may render the angiogenic pathway resistant to treatment with anti-VEGF agents, resulting in a suboptimal response to therapy.

Gene therapies for diabetic retinopathy

- A number of potential gene therapies for diabetic retinopathy that are presently being evaluated in preclinical murine diabetic models have been summarized.
- From the literature, gene therapies targeting the major intraocular pathologic systems identified include the VEGF/sFtl-1, antioxidant pathway (superoxide dismutase), renin–angiotensin pathway and the complement system.
- Preliminary results after intraocular gene delivery using recombinant adenoviral vectors in streptozotocin-induced diabetic rats are promising and warrant further research with human subjects.
- Pharmacogenetic strategies targeting epigenetic modifications such as DNA methylation and histone acetylation may be of potential therapeutic benefit in diabetic retinopathy.
- Thus far, no serious ocular adverse events or genetic instability has been reported from trials of gene therapies for diabetic retinopathy.

Conclusion

- Extensive research has shown that a number of potential candidate genes and polymorphisms may be associated with diabetes and its microvascular complications such as retinopathy. However, further research is needed to establish the high-risk genotypes across different ethnicities.
- In the future, decision to treat patients with diabetic retinopathy with pharmacologic agents may be based upon the genotype of the individual.
- Advances in pharmacogenetics and pharmacogenomics related to diabetic retinopathy may contribute to the expansion of personalized gene therapies.

pharmacogenomics in DR. However, the role of several candidate genes is still a matter of investigation. With over 20,000 genes in the human genome, extensive research is needed to identify the at-risk alleles. Novel genetic analysis methods such as DNA sequencing that allow whole genome analysis have a major role to play in this task. Thus, in the next few years, it is likely that a number of genetic biomarkers associated with high-risk DR and DME may be identified. GWAS appears to be a promising technique to identify such genotypes in the population. Genome sequencing for DR may also find clinical applications. This may allow prediction of natural history of the disease, treatment response and may play a role in treatment decision-making. In the future, it may be possible to offer patients diagnosed with gene polymorphisms, such VEGF and VEGF receptor gene SNPs that affect the response to therapy, alternate treatment strategies. Therefore, rapid progress in the omics-based technologies may allow individualized treatment options for patients on the basis of their allelic patterns in future.

Improvements in the development of drug design and techniques of intracellular gene delivery have resulted in initiation of several preclinical and early clinical studies for various ocular diseases, including DR [118]. Gene therapy has thus far proven to be safe and feasible in animal models and in early clinical studies [119]. In the near future, gene therapy may become a part of routine clinical practice for DR. Further research in the field of pharmacogenetics and gene therapy is required to realize the full potential and limitations of this strategy.

Financial & competing interests disclosure

DV Do and QD Nguyen serve on the scientific advisory boards at Allergan, Genentech and Regeneron, and have received honoraria. DV Do chairs the Steering Committee for the VISTA Study. QD Nguyen chairs the Steering Committee for the RISE/RIDE Study. The University of Nebraska Center has received research funding support from Research to Prevent Blindness, Allergan, Genentech, and Regeneron, among others. The authors have no other relevant affiliations or financial involvement with any organization or entity with a financial interest in or financial conflict with the subject matter or materials discussed in the manuscript apart from those disclosed.

No writing assistance was utilized in the production of this manuscript.

References

Papers of special note have been highlighted as:
• of interest; •• of considerable interest

1 Klein BE. Overview of epidemiologic studies of diabetic retinopathy. *Ophthalmic Epidemiol.* 14(4), 179–183 (2007).

2 International Diabetes Federation. IDF Diabetes Atlas, (6th Edition) (2014). www.idf.org/diabetesatlas

3 Bourne RR, Stevens GA, White RA *et al.* Causes of vision loss worldwide, 1990–2010: a systematic analysis. *Lancet Glob. Health* 1(6), e339–e349 (2013).

4 Sanchez-Thorin JC. The epidemiology of diabetes mellitus and diabetic retinopathy. *Int. Ophthalmol. Clin.* 38(2), 11–18 (1998).

5 Agarwal A, Sarwar S, Sepah YJ, Nguyen QD. What have we learnt about the management of diabetic macular edema in the antivascular endothelial growth factor and corticosteroid era? *Curr. Opin. Ophthalmol.* 26(3), 177–183 (2015).

•• **Summarizes various learning lessons in the management of diabetic macular edema based on level I evidence from a number of multicenter, randomized clinical trials.**

6 Nguyen QD, Brown DM, Marcus DM *et al.* Ranibizumab for diabetic macular edema: results from 2 Phase III randomized trials: RISE and RIDE. *Ophthalmology* 119(4), 789–801 (2012).

•• **This is a landmark trial that provided evidence of the safety and efficacy of ranibizumab in the treatment of diabetic macular edema.**

7 El-Shazly SF, El-Bradey MH, Tameesh MK. Vascular endothelial growth factor gene polymorphism prevalence in patients with diabetic macular oedema and its correlation with anti-vascular endothelial growth factor treatment outcomes. *Clin. Experiment Ophthalmol.* 42(4), 369–378 (2014).

8 Samiy N. Gene therapy for retinal diseases. *J. Ophthalmic Vis. Res.* 9(4), 506–509 (2014).

9 Thompson DA, Ali RR, Banin E *et al.* Advancing therapeutic strategies for inherited retinal degeneration: recommendations from the monaciano symposium. *Invest. Ophthalmol. Vis. Sci.* 56(2), 918–931 (2015).

10 Agarwal A, Soliman MK, Sepah YJ, Do DV, Nguyen QD. Diabetic retinopathy: variations in patient therapeutic outcomes and pharmacogenomics. *Pharmacogenomics Pers. Med.* 7, 399–409 (2014).

11 Simo-Servat O, Hernandez C, Simo R. Genetics in diabetic retinopathy: current concepts and new insights. *Curr. Genomics* 14(5), 289–299 (2013).

12 Radha V, Rema M, Mohan V. Genes and diabetic retinopathy. *Indian J. Ophthalmol.* 50(1), 5–11 (2002).

13 Khazaee MH, Tavakol Afshari J, Khazaee B *et al.* HLA-DQB1 subtypes predict diabetic retinopathy in patients with type I diabetes mellitus. *Eur. J. Ophthalmol.* 19(4), 638–645 (2009).

14 Kastelan S, Tomic M, Salopek-Rabatic J *et al.* The association between the HLA system and retinopathy development in patients with Type 1 diabetes mellitus. *Coll. Antropol.* 37(Suppl. 1), 65–70 (2013).

15 Lipner EM, Tomer Y, Noble JA *et al.* HLA class I and II alleles are associated with microvascular complications of Type 1 diabetes. *Hum. Immunol.* 74(5), 538–544 (2013).

16 Sia C, Weinem M. The role of HLA class I gene variation in autoimmune diabetes. *Rev. Diabet. Stud.* 2(2), 97–109 (2005).

17 Abhary S, Hewitt AW, Burdon KP, Craig JE. A systematic meta-analysis of genetic association studies for diabetic retinopathy. *Diabetes* 58(9), 2137–2147 (2009).

18 Cheema BS, Kohli HS, Sharma R, Bhansali A, Khullar M. Endothelial nitric oxide synthase gene polymorphism and Type 2 diabetic retinopathy among Asian Indians. *Acta Diabetol.* 49(6), 481–488 (2012).

19 Hudson BI, Stickland MH, Futers TS, Grant PJ. Effects of novel polymorphisms in the rage gene on transcriptional regulation and their association with diabetic retinopathy. *Diabetes* 50(6), 1505–1511 (2001).

20 Tong Z, Yang Z, Patel S *et al.* Promoter polymorphism of the erythropoietin gene in severe diabetic eye and kidney complications. *Proc. Natl Acad. Sci. USA* 105(19), 6998–7003 (2008).

21 Dyer KH, Silva PS, Sun JK. Vascular endothelial growth factor gene polymorphisms and vitreous proteome changes in diabetic retinopathy. *Semin. Ophthalmol.* 28(5–6), 347–354 (2013).

22 Vincenti V, Cassano C, Rocchi M, Persico G. Assignment of the vascular endothelial growth factor gene to human chromosome 6p21.3. *Circulation* 93(8), 1493–1495 (1996).

23 Brogan IJ, Khan N, Isaac K *et al.*Novel polymorphisms in the promoter and 5' UTR regions of the human vascular endothelial growth factor gene. *Hum. Immunol.* 60(12), 1245–1249 (1999).

24 Stevens A, Soden J, Brenchley PE, Ralph S, Ray DW. Haplotype analysis of the polymorphic human vascular endothelial growth factor gene promoter. *Cancer Res.* 63(4), 812–816 (2003).

25 Han L, Zhang L, Xing W *et al.* The associations between VEGF gene polymorphisms and diabetic retinopathy susceptibility: a meta-analysis of 11 case-control studies. *J. Diabetes Res.* 2014, 805801 (2014).

26 Petrovic MG, Korosec P, Kosnik M *et al.* Local and genetic determinants of vascular endothelial growth factor expression in advanced proliferative diabetic retinopathy. *Mol. Vis.* 14, 1382–1387 (2008).

27 Awata T, Kurihara S, Takata N *et al.* Functional VEGF C-634G polymorphism is associated with development of diabetic macular edema and correlated with macular retinal thickness in Type 2 diabetes. *Biochem. Biophys. Res. Commun.* 333(3), 679–685 (2005).

28 Wang H, Cheng JW, Zhu LS *et al.* Meta-analysis of association between the -2578C/A polymorphism of the vascular endothelial growth factor and retinopathy in Type 2 diabetes in Asians and Caucasians. *Ophthalmic Res.* 52(1), 1–8 (2014).

29 Liu L, Jiao J, Wang Y *et al. TGF-β1* gene polymorphism in association with diabetic retinopathy susceptibility: a systematic review and meta-analysis. *PLoS ONE* 9(4), e94160 (2014).

30 Grassi MA, Tikhomirov A, Ramalingam S *et al.* Replication analysis for severe diabetic retinopathy. *Invest. Ophthalmol. Vis. Sci.* 53(4), 2377–2381 (2012).

31 Cho H, Sobrin L. Genetics of diabetic retinopathy. *Curr. Diab. Rep.* 14(8), 515 (2014).

• **Summarizes the key factors involved in the heretability of diabetic retinopathy and genetic polymorphisms associated with severe disease.**

32 Visscher PM, Brown MA, Mccarthy MI, Yang J. Five years of GWAS discovery. *Am. J. Hum. Genet.* 90(1), 7–24 (2012).

33 Fu YP, Hallman DM, Gonzalez VH *et al.* Identification of diabetic retinopathy genes through a genome-wide association study among Mexican–Americans from Starr County, Texas. *J. Ophthalmol.*doi:10.1155/2010/861291 (2010) (Epub ahead of print).

34 Grassi MA, Tikhomirov A, Ramalingam S *et al.*Genome-wide meta-analysis for severe diabetic retinopathy. *Hum. Mol. Genet.* 20(12), 2472–2481 (2011).

• **This meta-analysis provides information on several novel genetic loci associated with the pathophysiology of diabetic retinopathy based on evidence from genome-wide association studies.**

35 Huang YC, Lin JM, Lin HJ *et al.* Genome-wide association study of diabetic retinopathy in a taiwanese population. *Ophthalmology* 118(4), 642–648 (2011).

36 Sheu WH, Kuo JZ, Lee IT *et al.* Genome-wide association study in a chinese population with diabetic retinopathy. *Hum. Mol. Genet.* 22(15), 3165–3173 (2013).

37 Awata T, Yamashita H, Kurihara S *et al.* A genome-wide association study for diabetic retinopathy in a Japanese population: potential association with a long intergenic non-coding RNA. *PLoS ONE* 9(11), e111715 (2014).

38 Huang LZ, Li YJ, Xie XF *et al.* Whole-exome sequencing implicates UBE3D in age-related macular degeneration in east asian populations. *Nat. Commun.* 6, 6687 (2015).

39 Aboobakar IF, Allingham RR. Developments in ocular genetics: 2013 annual review. *Asia Pac. J. Ophthalmol. (Phila.)* 3(3), 181–193 (2014).

40 Liang S, Pan M, Hu N *et al.* Association of angiotensin-converting enzyme gene 2350 G/A polymorphism with diabetic retinopathy in chinese han population. *Mol. Biol. Rep.* 40(1), 463–468 (2013).

41 Manea SA, Robciuc A, Guja C, Heltianu C. Identification of gene variants in NOS3, ET-1 and RAS that confer risk and protection against microangiopathy in Type 2 diabetic obese subjects. *Biochem. Biophys. Res. Commun.* 407(3), 486–490 (2011).

42 Dos Santos KG, Canani LH, Gross JL *et al.* The -106CC genotype of the aldose reductase gene is associated with an increased risk of proliferative diabetic retinopathy in Caucasian–Brazilians with Type 2 diabetes. *Mol. Genet. Metabol.* 88(3), 280–284 (2006).

43 Wang J, Yang MM, Li YB *et al.* Association of *CFH* and *CFB* gene polymorphisms with retinopathy in Type 2 diabetic patients. *Mediators Inflamm.* 2013, 748435 (2013).

44 Chen M, Lin WR, Lu CH *et al.* Chimerin 2 genetic polymorphisms are associated with non-proliferative diabetic retinopathy in taiwanese Type 2 diabetic patients. *J. Diabetes Complications* 28(4), 460–463 (2014).

45 Arndt C, Leclercq I, Nazeyrollas P *et al.* Association of endothelial lipase Thr111Ile polymorphism with proliferative retinopathy in Type 2 diabetes patients. *Diabetes Metab.* 40(6), 452–458 (2014).

46 Taverna MJ, Sola A, Guyot-Argenton C *et al. eNOS4* polymorphism of the endothelial nitric oxide synthase

predicts risk for severe diabetic retinopathy. *Diabet. Med.* 19(3), 240–245 (2002).

47 Abhary S, Burdon KP, Casson RJ *et al.* Association between erythropoietin gene polymorphisms and diabetic retinopathy. *Arch. Ophthalmol.* 128(1), 102–106 (2010).

48 Katakami N, Matsuhisa M, Kaneto H *et al.* Monocyte chemoattractant protein-1 (*MCP-1*) gene polymorphism as a potential risk factor for diabetic retinopathy in Japanese patients with Type 2 diabetes. *Diabetes Res. Clin. Pract.* 89(1), e9–e12 (2010).

49 Yigit S, Karakus N, Inanir A. Association of *MTHFR* gene C677T mutation with diabetic peripheral neuropathy and diabetic retinopathy. *Mol. Vis.* 19, 1626–1630 (2013).

50 Maeda M, Yamamoto I, Fukuda M *et al. MTHFR* gene polymorphism is susceptible to diabetic retinopathy but not to diabetic nephropathy in Japanese Type 2 diabetic patients. *J. Diabetes Complications* 22(2), 119–125 (2008).

51 Sun J, Xu Y, Zhu Y, Lu H. Genetic polymorphism of methylenetetrahydrofolate reductase as a risk factor for diabetic nephropathy in chinese Type 2 diabetic patients. *Diabetes Res. Clin. Pract.* 64(3), 185–190 (2004).

52 Mankoc Ramus S, Kumse T, Globocnik Petrovic M, Petrovic D, Cilensek I. SNP rs2073618 of the osteoprotegerin gene is associated with diabetic retinopathy in slovenian patients with Type 2 diabetes. *Biomed Res. Int.* 2013, 364073 (2013).

53 Ng ZX, Kuppusamy UR, Iqbal T, Chua KH. Receptor for advanced glycation end-product (*RAGE*) gene polymorphism 2245G/A is associated with pro-inflammatory, oxidative-glycation markers and sRAGE in diabetic retinopathy. *Gene* 521(2), 227–233 (2013).

54 Zhang HM, Chen LL, Wang L *et al.* Association of 1704G/T and G82S polymorphisms in the receptor for advanced glycation end products gene with diabetic retinopathy in chinese population. *J. Endocrinol. Invest.* 32(3), 258–262 (2009).

55 Sobrin L, Green T, Sim X *et al.* Candidate gene association study for diabetic retinopathy in persons with Type 2 diabetes: the candidate gene association resource (CARE). *Invest. Ophthalmol. Vis. Sci.* 52(10), 7593–7602 (2011).

56 Bandello F, Casalino G, Loewenstein A *et al.* Pharmacological approach to diabetic macular edema. *Ophthalmic Res.* 51(2), 88–95 (2014).

57 Boyer DS, Hopkins JJ, Sorof J, Ehrlich JS. Anti-vascular endothelial growth factor therapy for diabetic macular edema. *Ther. Adv. Endocrinol. Metab.* 4(6), 151–169 (2013).

58 Patelli F, Radice P, Giacomotti E. Diabetic macular edema. *Dev. Ophthalmol.* 54, 164–173 (2014).

59 Rajendram R, Fraser-Bell S, Kaines A *et al.* A 2-year prospective randomized controlled trial of intravitreal bevacizumab or laser therapy (BOLT) in the management of diabetic macular edema: 24-month data: report 3. *Arch. Ophthalmol.* 130(8), 972–979 (2012).

•• **This multicenter clinical trial compares the efficacy of intravitreal bevacizumab and macular laser therapy in the management of eyes with diabetic macular edema.**

60 Do DV, Schmidt-Erfurth U, Gonzalez VH *et al.* The DA VINCI study: Phase 2 primary results of VEGF Trap-eye in patients with diabetic macular edema. *Ophthalmology* 118(9), 1819–1826 (2011).

•• **This landmark multicenter trial studied the efficacy of different dosing regimens of intravitreal aflibercept compared with macular laser therapy in the treatment of diabetic macular edema.**

61 Jain RK, Duda DG, Willett CG *et al.* Biomarkers of response and resistance to antiangiogenic therapy. *Nat. Rev. Clin. Oncol.* 6(6), 327–338 (2009).

62 Wykoff CC, Brown DM, Maldonado ME, Croft DE. Aflibercept treatment for patients with exudative age-related macular degeneration who were incomplete responders to multiple ranibizumab injections (TURF trial). *Br. J. Ophthalmol.* 98(7), 951–955 (2014).

63 Dabir SS, Das D, Nallathambi J, Mangalesh S, Yadav NK, Schouten JS. Differential systemic gene expression profile in patients with diabetic macular edema: responders versus nonresponders to standard treatment. *Indian J. Ophthalmol.* 62(1), 66–73 (2014).

• **This prospective study analyzed altered gene expression patterns in patients using microarray technique, providing insights into the possible signaling pathways associated with diabetic retinopathy.**

64 Choudhuri S, Chowdhury IH, Das S *et al.* Role of NF-κB activation and VEGF gene polymorphisms in VEGF up regulation in non-proliferative and proliferative diabetic retinopathy. *Mol. Cell. Biochem.* 405(1–2), 265–279 (2015).

65 Patel JI, Tombran-Tink J, Hykin PG, Gregor ZJ, Cree IA. Vitreous and aqueous concentrations of proangiogenic, antiangiogenic factors and other cytokines in diabetic retinopathy patients with macular edema: implications for structural differences in macular profiles. *Exp. Eye Res.* 82(5), 798–806 (2006).

66 Yang H, Huang Y, Chen X *et al.* The role of CTGF in the diabetic rat retina and its relationship with VEGF and TGF-β(2), elucidated by treatment with CTGFsiRNA. *Acta Ophthalmol.* 88(6), 652–659 (2010).

67 Yang Y, Yang K, Li Y *et al.* Decursin inhibited proliferation and angiogenesis of endothelial cells to suppress diabetic retinopathy via VEGFR2. *Mol. Cell. Endocrin.* 378(1–2), 46–52 (2013).

68 Adhi M, Cashman SM, Kumar-Singh R. Adeno-associated virus mediated delivery of a non-membrane targeted human soluble CD59 attenuates some aspects of diabetic retinopathy in mice. *PLoS ONE* 8(10), e79661 (2013).

69 Meneses PI, Hajjar KA, Berns KI, Duvoisin RM. Recombinant angiostatin prevents retinal neovascularization in a murine proliferative retinopathy model. *Gene therapy* 8(8), 646–648 (2001).

70 Spranger J, Hammes HP, Preissner KT, Schatz H, Pfeiffer AF. Release of the angiogenesis inhibitor angiostatin in patients with proliferative diabetic retinopathy: association with retinal photocoagulation. *Diabetologia* 43(11), 1404–1407 (2000).

71 Noma H, Funatsu H, Yamashita H *et al.* Regulation of angiogenesis in diabetic retinopathy: possible balance

between vascular endothelial growth factor and endostatin. *Arch. Ophthalmol.* 120(8), 1075–1080 (2002).

72 Funatsu H, Yamashita H, Noma H *et al.* Stimulation and inhibition of angiogenesis in diabetic retinopathy. *Jpn. J. Ophthalmol.* 45(6), 577–584 (2001).

73 Gao G, Shao C, Zhang SX, Dudley A, Fant J, Ma JX. Kallikrein-binding protein inhibits retinal neovascularization and decreases vascular leakage. *Diabetologia* 46(5), 689–698 (2003).

74 Zhang D, Kaufman PL, Gao G, Saunders RA, Ma JX. Intravitreal injection of plasminogen kringle 5, an endogenous angiogenic inhibitor, arrests retinal neovascularization in rats. *Diabetologia* 44(6), 757–765 (2001).

75 Shibuya M. VEGF-VEGFR signals in health and disease. *Biomol. Ther. (Seoul)* 22(1), 1–9 (2014).

76 Min Z, Qiang W, Benwen S, Bin L, Xinhua D. Lentivirus-mediated *sFlt-1* gene fragment transfer suppresses retinal neovascularization. *Curr. Eye Res.* 34(5), 401–410 (2009).

77 Lamartina S, Cimino M, Roscilli G *et al.* Helper-dependent adenovirus for the gene therapy of proliferative retinopathies: stable gene transfer, regulated gene expression and therapeutic efficacy. *J. Gene Med.* 9(10), 862–874 (2007).

78 Bainbridge JW, Mistry A, De Alwis M *et al.* Inhibition of retinal neovascularisation by gene transfer of soluble VEGF receptor sFlt-1. *Gene Ther.* 9(5), 320–326 (2002).

•• **Demonstrated a novel technique of *in vivo* VEGF inhibition using adeno-associated virus vector transfer of *sFlt-1* gene.**

79 Dhaunsi GS, Yousif MH, Akhtar S *et al.* Angiotensin-(1–7) prevents diabetes-induced attenuation in PPAR-γ and catalase activities. *Eur. J. Pharmacol.* 638(1–3), 108–114 (2010).

80 Marchesi C, Paradis P, Schiffrin EL. Role of the renin-angiotensin system in vascular inflammation. *Trends Pharmacol. Sci.* 29(7), 367–374 (2008).

81 Ruiz-Ortega M, Lorenzo O, Ruperez M *et al.* Role of the renin-angiotensin system in vascular diseases: expanding the field. *Hypertension* 38(6), 1382–1387 (2001).

82 Mezzano SA, Ruiz-Ortega M, Egido J. Angiotensin II and renal fibrosis. *Hypertension* 38(3 Pt 2), 635–638 (2001).

83 Chaturvedi N, Porta M, Klein R *et al.* Effect of candesartan on prevention (direct-prevent 1) and progression (direct-protect 1) of retinopathy in Type 1 diabetes: randomised, placebo-controlled trials. *Lancet* 372(9647), 1394–1402 (2008).

84 Chaturvedi N, Sjolie AK, Stephenson JM *et al.* Effect of lisinopril on progression of retinopathy in normotensive people with Type 1 diabetes. The euclid study group. Eurodiab controlled trial of lisinopril in insulin-dependent diabetes mellitus. *Lancet* 351(9095), 28–31 (1998).

85 Sjolie AK, Klein R, Porta M *et al.* Effect of candesartan on progression and regression of retinopathy in Type 2 diabetes (direct-protect 2): a randomised placebo-controlled trial. *Lancet* 372(9647), 1385–1393 (2008).

86 Li Q, Verma A, Zhu P *et al.* Gene therapy for diabetic retinopathy – targeting the renin-angiotensin system (2013). http://cdn.intechopen.com/pdfs-wm/43280.pdf

87 El-Bab MF, Zaki NS, Mojaddidi MA, Al-Barry M, El-Beshbishy HA. Diabetic retinopathy is associated with oxidative stress and mitigation of gene expression of antioxidant enzymes. *Int. J. Gen. Med.* 6, 799–806 (2013).

88 Kowluru RA, Kowluru V, Xiong Y, Ho YS. Overexpression of mitochondrial superoxide dismutase in mice protects the retina from diabetes-induced oxidative stress. *Free Radic. Biol. Med.* 41(8), 1191–1196 (2006).

89 Kowluru RA, Odenbach S. Effect of long-term administration of alpha-lipoic acid on retinal capillary cell death and the development of retinopathy in diabetic rats. *Diabetes* 53(12), 3233–3238 (2004).

90 Kanwar M, Chan PS, Kern TS, Kowluru RA. Oxidative damage in the retinal mitochondria of diabetic mice: possible protection by superoxide dismutase. *Invest. Ophthalmol. Vis. Sci.* 48(8), 3805–3811 (2007).

• **Provided early evidence of the role of epigenetics in the pathogenesis of diabetic retinopathy and the role of a mitochondrial enzyme, superoxide dismutase.**

91 Zhang L, Xia H, Han Q, Chen B. Effects of antioxidant gene therapy on the development of diabetic retinopathy and the metabolic memory phenomenon. *Graefes Arch. Clin. Exp. Ophthalmol.* 253(2), 249–259 (2015).

92 Liu Y, Tang L, Chen B. Effects of antioxidant gene therapy on retinal neurons and oxidative stress in a model of retinal ischemia/reperfusion. *Free Radic. Biol. Med.* 52(5), 909–915 (2012).

93 Sohn JH, Kaplan HJ, Suk HJ, Bora PS, Bora NS. Complement regulatory activity of normal human intraocular fluid is mediated by MCP, DAF, and CD59. *Invest. Ophthalmol. Vis. Sci.* 41(13), 4195–4202 (2000).

94 Gerl VB, Bohl J, Pitz S *et al.* Extensive deposits of complement C3d and C5b-9 in the choriocapillaris of eyes of patients with diabetic retinopathy. *Invest. Ophthalmol. Vis. Sci.* 43(4), 1104–1108 (2002).

95 Zhang J, Gerhardinger C, Lorenzi M. Early complement activation and decreased levels of glycosylphosphatidylinositol-anchored complement inhibitors in human and experimental diabetic retinopathy. *Diabetes* 51(12), 3499–3504 (2002).

96 Lai CM, Estcourt MJ, Himbeck RP *et al.* Preclinical safety evaluation of subretinal AAV2.sFlt-1 in non-human primates. *Gene Ther.* 19(10), 999–1009 (2012).

97 Mao Y, Kiss S, Boyer JL *et al.* Persistent suppression of ocular neovascularization with intravitreal administration of AAVrh.10 coding for bevacizumab. *Hum. Gene Ther.* 22(12), 1525–1535 (2011).

•• **Describes a novel therapeutic strategy of long-term *in vivo* VEGF inhibition using intraocular administration of bevacizumab-expressing gene.**

98 Ramirez M, Wu Z, Moreno-Carranza B *et al.* Vasoinhibin gene transfer by adenoassociated virus Type 2 protects against VEGF- and diabetes-induced retinal vasopermeability. *Invest. Ophthalmol. Vis. Sci.* 52(12), 8944–8950 (2011).

99 Verma A, Shan Z, Lei B *et al.* ACE2 and ANG-(1–7) confer protection against development of diabetic retinopathy. *Mol. Ther.* 20(1), 28–36 (2012).

100 Ildefonso CJ, Jaime H, Rahman MM *et al.* Gene delivery of a viral anti-inflammatory protein to combat ocular

inflammation. *Hum. Gene Ther.* 26(1), 59–68 (2015).

101 Biswal MR, Prentice HM, Dorey CK, Blanks JC. A hypoxia-responsive glial cell-specific gene therapy vector for targeting retinal neovascularization. *Invest. Ophthalmol. Vis. Sci.* 55(12), 8044–8053 (2014).

102 Shyong MP, Lee FL, Kuo PC *et al.* Reduction of experimental diabetic vascular leakage by delivery of angiostatin with a recombinant adeno-associated virus vector. *Mol. Vis.* 13, 133–141 (2007).

103 Haurigot V, Villacampa P, Ribera A *et al.* Long-term retinal PEDF overexpression prevents neovascularization in a murine adult model of retinopathy. *PLoS ONE* 7(7), e41511 (2012).

104 Yu H, Chen L, Jiang J. Administration of pigment epithelium-derived factor delivered by adeno-associated virus inhibits blood-retinal barrier breakdown in diabetic rats. *Mol. Vis.* 16, 2384–2394 (2010).

105 Gong Y, Chang ZP, Ren RT *et al.* Protective effects of adeno-associated virus mediated brain-derived neurotrophic factor expression on retinal ganglion cells in diabetic rats. *Cell. Mol. Neurobiol.* doi:10.1007/s10571-011-9779-x (2012).

106 Li B, Zhang HQ, Shi Y *et al.* Overexpression of nuclear transport factor 2 may protect against diabetic retinopathy. *Mol. Vis.* 15, 861–869 (2009).

107 Kowluru RA, Mishra M. Contribution of epigenetics in diabetic retinopathy. *Sci. China Life Sci.* 58(6), 556–63 (2015).

108 Kowluru RA, Santos JM, Mishra M. Epigenetic modifications and diabetic retinopathy. *Biomed Res. Int.* 2013, 635284 (2013).

109 Zhong Q, Kowluru RA. Epigenetic modification of SOD2 in the development of diabetic retinopathy and in the metabolic memory: role of histone methylation. *Invest. Ophthalmol. Vis. Sci.* 54(1), 244–250 (2013).

110 Zhong Q, Kowluru RA. Regulation of matrix metalloproteinase-9 by epigenetic modifications and the development of diabetic retinopathy. *Diabetes* 62(7), 2559–2568 (2013).

111 Zhong Q, Kowluru RA. Role of histone acetylation in the development of diabetic retinopathy and the metabolic memory phenomenon. *J. Cell. Biochem.* 110(6), 1306–1313 (2010).

112 Mastropasqua R, Toto L, Cipollone F *et al.*Role of microRNAs in the modulation of diabetic retinopathy. *Prog. Retin. Eye Res.* 43, 92–107 (2014).

113 Kato M, Castro NE, Natarajan R. Micrornas: potential mediators and biomarkers of diabetic complications. *Free Radic. Biol. Med.* 64, 85–94 (2013).

114 Silva VA, Polesskaya A, Sousa TA *et al.* Expression and cellular localization of microRNA-29b and RAX, an activator of the RNA-dependent protein kinase (PKR), in the retina of streptozotocin-induced diabetic rats. *Mol. Vis.* 17, 2228–2240 (2011).

115 Al-Kateb H, Boright AP, Mirea L *et al.* Multiple superoxide dismutase 1/splicing factor serine alanine 15 variants are associated with the development and progression of diabetic nephropathy: the Diabetes Control and Complications Trial/Epidemiology of Diabetes Interventions and Complications Genetics study. *Diabetes* 57(1), 218–228 (2008).

116 Boright AP, Paterson AD, Mirea L *et al.* Genetic variation at the *ACE* gene is associated with persistent microalbuminuria and severe nephropathy in Type 1 diabetes: the DCCT/EDIC Genetics Study. *Diabetes* 54(4), 1238–1244 (2005).

117 Hosseini SM, Boright AP, Sun L *et al.* The association of previously reported polymorphisms for microvascular complications in a meta-analysis of diabetic retinopathy. *Hum. Genet.* 134(2), 247–257 (2015).

118 Ginn SL, Alexander IE, Edelstein ML, Abedi MR, Wixon J. Gene therapy clinical trials worldwide to 2012 – an update. *J. Gene Med.* 15(2), 65–77 (2013).

• **Provides a comprehensive overview of progress being made in the clinical trials using gene therapy worldwide.**

119 Vandenberghe LH. What is next for retinal gene therapy? *Cold Spring Harb. Perspect. Med.* 5(10), a017442 (2015).